REPORT R-534 SEPTEMBER, 1971 UILU-ENG 71-2237

CSL COORDINATED SCIENCE LABORATORY

PARAMETRIC COEXCITATION OF ION-ACOUSTIC WAVES AND ELECTRON PLASMA WAVES BY A HIGH FREQUENCY ELECTRIC FIELD

DAVID WILLIAM STOWE

UNIVERSITY OF ILLINOIS - URBANA, ILLINOIS

"THIS DOCUMENT HAS BEEN APPROVED FOR PUBLIC RELEASE AND SALE; ITS DISTRIBUTION IS UNLIMITED."

PARAMETRIC COEXCITATION OF ION-ACOUSTIC WAVES AND ELECTRON PLASMA WAVES BY A HIGH FREQUENCY ELECTRIC FIELD

by

David William Stowe

This work was supported by the Joint Services Electronics Program (U. S. Army, U. S. Navy and U. S. Air Force) under Contract DAAB-07-67-C-0199.

Reproduction in whole or in part is permitted for any purpose of the United States Government.

This document has been approved for public release and sale; its distribution is unlimited.

PARAMETRIC COEXCITATION OF ION-ACOUSTIC WAVES AND ELECTRON PLASMA WAVES BY A HIGH FREQUENCY ELECTRIC FIELD

David William Stowe, Ph.D.
Department of Physics
University of Illinois at Urbana-Champaign, 1971

The basic theory of parametric coexcitation of ion-acoustic and electron plasma waves by a high frequency electric field is reviewed. Numerical calculations show that plasma-neutral collisions and steady state drift velocities have a significant influence on the interaction. Parametric excitation of ion-acoustic waves is observed experimentally in a helium dc discharge. The observations indicate that the radial density profile of the dc discharge modifies the parametric effect. In the absence of an applied field, unstable electron drift-excited ion-acoustic waves are experimentally observed. These waves are found to satisfy the dispersion relation for a plasma consisting of He^+ and He_2^+.

PARAMETRIC COEXCITATION OF ION-ACOUSTIC WAVES AND ELECTRON PLASMA WAVES BY A HIGH FREQUENCY ELECTRIC FIELD

BY

DAVID WILLIAM STOWE
B.S., University of Wisconsin, 1966
M.S., University of Illinois, 1968

THESIS

Submitted in partial fulfillment of the requirements
for the degree of Doctor of Philosophy in Physics
in the Graduate College of the
University of Illinois at Urbana-Champaign, 1971

Urbana, Illinois

ACKNOWLEDGEMENT

To Dr. Heinrich Böhmer, I express my genuine thanks for your earnest interest in my research as expressed by the numerous hours you spent teaching me physics, by your needed encouragement, and by your occasional prodding which kept this research progressing.

To Dr. Manfred Raether, I express my gratitude for your suggestion of this fruitful research and for your continued effort, guidance, and assistance in tackling this difficult problem.

I thank Dr. E. Atlee Jackson for many helpful discussions which have improved this work.

I also thank the men and women of the CSL staff who have consistently supported this work through their competent help, and I thank you especially for the times when your special assistance and consideration were required to get the job done.

I thank my typist, Velma Gadbury, for your excellent performance in typing this manuscript under fire.

To my wife and little girls, I am grateful for your unfailing support, patience and love during these trying times and I look forward to our future with expectation.

And to my parents, I thank you for fostering my respect for higher education, and for your continuous encouragement and interest in my work.

TABLE OF CONTENTS

		Page
I.	INTRODUCTION	1
	A. Introductory Parametric Excitation Theory	2
	B. Review of Theoretical and Experimental Studies	5
II.	THEORY OF PARAMETRIC EXCITATION	14
	A. Parametric Excitation Theory in an Infinite Homogeneous Plasma	14
	B. Numerical Solutions of the Dispersion Relation	22
III.	EXPERIMENTAL STUDY OF PARAMETRIC EXCITATION	42
	A. Experiment Design	42
	B. Experiment Observations	48
IV.	ION-ACOUSTIC WAVES IN THE HELIUM POSITIVE COLUMN	71
	A. Ion-Acoustic Theory for the Infinite Plasma	71
	B. Experimental Observations of Ion-Acoustic Waves in the Helium Positive Column	73
V.	SUMMARY OF RESULTS	83
	APPENDIX	85
	LIST OF REFERENCES	90
	VITA	93

I. INTRODUCTION

The resonant frequency of a classical oscillator may be parametrically excited if a parameter of the system is varied periodically with a frequency that is an appropriate multiple of the resonant frequency.[1] Parametric excitation of a system also requires that system losses due to damping are overcome by a minimum threshold variation of the variable parameter. In addition, in contrast with a driving force, a system cannot be parametrically excited unless small amplitude fluctuations exist in the system initially.

A plasma lends itself to a parametric interaction of a complex nature due to the existence of several normal modes in the plasma. When a time-dependent electric field is applied to the plasma as an externally controlled parameter, the modes of the plasma may be excited simultaneously or independently in a complex interaction that is related to the classical parametric resonance of a single mode oscillator.

The recent interest which has engulfed the study of parametric effects in a plasma is due to the many applications where strong high frequency electric fields are used in the presence of a plasma such as plasma diagnostics with microwaves, and in the study of propagation and scattering of electromagnetic radiation in laboratory plasmas and in the ionosphere. Since the parametric interaction may provide an effective means of coupling energy into a plasma, it has significant implications in the study of anomalous resistance, anomalous diffusion, and plasma heating by microwave and laser radiation.

This paper is concerned with a theoretical and experimental investigation of the specific resonance in which an electron plasma oscillation and ion-acoustic oscillation are parametrically excited in the plasma by a transverse electric field. A brief description of the parametric interaction and a summary of recent theoretical and experimental results are presented in the remainder of the Introduction. Section II includes theoretical considerations and numerical calculations based on the studies of Jackson[2] and Sanmartin.[3] Experimental results of a parametric excitation study in the positive column of a small diameter helium discharge are detailed in Section III. In Section IV supporting experimental data pertaining to self-excited ion-acoustic waves is presented. Section V is a brief resumé of results and important conclusions.

A. Introductory Parametric Excitation Theory

The detailed behavior of the parametric instability in a plasma depends upon the normal mode structure of the plasma. In the absence of a magnetic field, an infinite homogeneous plasma sustains two weakly damped modes, the electron plasma mode and the ion-acoustic mode. The high frequency electron plasma mode consists of long wavelength coherent longitudinal oscillations of electrons with a frequency $\omega \simeq \omega_{pe} \equiv (4\pi nq^2/m_e)^{1/2}$*. The low frequency ion-acoustic mode of the plasma has a phase velocity which is dispersionless, $v_{ia} = (\omega/k)_{ia} \simeq (KT_e/m_i)^{1/2}$, in analogy with acoustic

---

*The definition of all variables and expressions used in this paper are contained in the Appendix.

oscillations of a neutral gas. An ion-acoustic wave originates when the large inertia of the ions is opposed by a restoring force due to electron pressure. Typical ion-acoustic frequencies are of the order of $\omega \simeq (m_e/m_i)^{1/2}\omega_{pe}$.

The parametric effect in a plasma is studied theoretically by assuming the existence of a large sinusoidal electric field $\underset{\sim}{E}_o \cos\omega_o t$ in the plasma in addition to the self-consistent electric field $\underset{\sim}{E}$ arising from the charge distribution within the plasma. The behavior of the plasma is described by the set of collisionless Boltzmann or Vlasov equations, one equation for each plasma species:

$$\frac{\partial F_\sigma(\underset{\sim}{r},\underset{\sim}{v},t)}{\partial t} + \underset{\sim}{v}\cdot\frac{\partial F_\sigma(\underset{\sim}{r},\underset{\sim}{v},t)}{\partial \underset{\sim}{r}} + \frac{q_\sigma}{m_\sigma}(\underset{\sim}{E} + \underset{\sim}{E}_o\cos\omega_o t)\cdot\frac{\partial F_\sigma(\underset{\sim}{r},\underset{\sim}{v},t)}{\partial \underset{\sim}{v}} = 0. \qquad \text{(I-1)}$$

The distribution function F_σ is defined such that

$$\int F_\sigma(\underset{\sim}{r},\underset{\sim}{v},t)\,d\underset{\sim}{v} = n_\sigma(\underset{\sim}{r},t) \qquad \text{(I-2)}$$

where $n_\sigma(\underset{\sim}{r},t)$ is the number density of the σth component. The electric field $\underset{\sim}{E}$ is the self-consistent field determined from Poisson's equation

$$\nabla\cdot\underset{\sim}{E} = 4\pi\sum q_\sigma n_\sigma. \qquad \text{(I-3)}$$

Perturbation theory can be applied to Eq. (I-1) by assuming $F_\sigma = f_{o\sigma} + f_\sigma$ where $f_{o\sigma}$ is the equilibrium distribution function and f_σ is the perturbation. The equilibrium distribution satisfies

$$\frac{\partial f_{o\sigma}}{\partial t} + \frac{q_\sigma}{m_\sigma} \underset{\sim}{E}_o \cos(\omega_o t) \cdot \frac{\partial f_{o\sigma}}{\partial \underset{\sim}{v}} = 0. \tag{I-4}$$

The general solution to Eq. (I-4) is $f_{o\sigma} = f_{o\sigma}(\underset{\sim}{u})$ where

$$\underset{\sim}{u} = \underset{\sim}{v} - \frac{q_\sigma}{m_\sigma} \frac{\underset{\sim}{E}_o}{\omega_o} \sin\omega_o t. \tag{I-5}$$

The resultant linearized equation for f_σ is

$$\frac{\partial f_\sigma}{\partial t} + \underset{\sim}{v} \cdot \frac{\partial f_\sigma}{\partial \underset{\sim}{r}} + \frac{q_\sigma}{m_\sigma} \underset{\sim}{E}_o \cos(\omega_o t) \cdot \frac{\partial f_\sigma}{\partial \underset{\sim}{v}} + \frac{q_\sigma}{m_\sigma} \underset{\sim}{E} \cdot \frac{\partial f_{o\sigma}}{\partial \underset{\sim}{v}} = 0 \tag{I-6}$$

where E is subject to Poisson's equation

$$\nabla \cdot \underset{\sim}{E} = 4\pi \sum_\sigma q_\sigma \int f_\sigma d\underset{\sim}{v}. \tag{I-7}$$

Insight into the plasma mode coupling is gained from Eq. (I-6) by noting that perturbations in f_σ of frequency ω are coupled to perturbations of frequencies $\omega_o \pm \omega$ by the nonlinear term $(q_\sigma/m_\sigma)\ \underset{\sim}{E}_o \cos(\omega_o t) \cdot \partial f_\sigma / \partial \underset{\sim}{v}$. In particular, the relatively undamped high and low frequency modes of the plasma, ω_H and ω_L,* are coupled to components of frequency $\omega_o \pm \omega_H$ and $\omega_o \pm \omega_L$. As Jackson[2] points out, if ω_o is chosen so that $\omega_o - \omega_H = \omega_L$ (which also implies

*The modes of frequency ω_H and ω_L become the electron plasma and ion-acoustic modes, respectively, in the limit as $\underset{\sim}{E}_o \to 0$.

$\omega_o - \omega_L = \omega_H$), then strong mode-mode coupling can occur via the electric field. Consequently, when the frequency matching criterion is satisfied

$$\omega_H + \omega_L = \omega_o, \tag{I-8}$$

the modes may be parametrically coexcited provided the field strength is sufficient to overcome the loss mechanisms of the plasma.

B. Review of Theoretical and Experimental Studies

Theoretical studies of parametric resonance in a plasma fall primarily into two categories: kinetic theory and hydrodynamic theory. Among the kinetic treatments, Jackson[2] studies the parametric instability of an electron plasma wave coupled to an ion-acoustic wave, both of wave vector $\underset{\sim}{k}$, by a time-varying electric field ($\underset{\sim}{k}_o = 0$) of arbitrary intensity parallel to $\underset{\sim}{k}$:

$$\underset{\sim}{E}_o \cos \omega_o t, \quad \underset{\sim}{E}_o \parallel \underset{\sim}{k}.$$

He also studies the resonance which occurs when $\omega_o \simeq 2\omega_{pe}$ but finds that this instability is weaker than the first resonance and requires a spatial variation of $\underset{\sim}{E}_o$. Jackson substantiates the findings of DuBois and Goldman[4,5] which are based on a detailed quantum mechanical treatment of plasma interaction for a weak transverse pump field. DuBois and Goldman[6] also present a kinetic treatment of the 3 mode ($\omega_L, \omega_H, \omega_o$) excitation process with emphasis on the fluctuation spectrum. They note that physically there is no difference between longitudinal and transverse pump fields in the limit of infinite

wavelength. Sanmartin[3] develops essentially the same set of equations as Jackson[2] but only investigates them in detail for the non-oscillatory resonance (Reω=0) which originates from the field-induced streaming of electrons with respect to the ions.

In addition to parametric instability arising from velocity modulation of the plasma components, Ramazashvili[7] predicts coexcitation of ion-acoustic and plasma waves when an inhomogeneous plasma has a sufficiently large density gradient parallel to an externally applied time-varying field $\underset{\sim}{E}_o \cos\omega_o t$. In this case the applied field causes a periodic variation of the equilibrium density profile which, in turn, may excite electron plasma and ion-acoustic oscillations. This mechanism enables an unstable wave of wave vector $\underset{\sim}{k}$ to propagate across the applied field, i.e. $\underset{\sim}{k}\cdot\underset{\sim}{E}_o = 0$. Ramazashvili's treatment is limited to field strengths such that

$$\frac{q_\sigma}{m_\sigma}\frac{E_o}{\omega_o^2} \ll \frac{v_{T\sigma}}{\omega_o} \ll L \quad \text{for} \quad v_{T\sigma} = \left[\frac{KT_o}{m_\sigma}\right]^{1/2}$$

where L is the scale length of inhomogeneities of the equilibrium distribution function, $v_{T\sigma}/\omega_o$ is the distance travelled by the particle per oscillation, and $(q_\sigma/m_\sigma)E_o/\omega_o^2$ is the amplitude of the particle oscillation in the electric field. In a similar study Amano and Okamoto[8] investigate parametric effects in an inhomogeneous plasma including the effects of plasma neutral-collisions by a loss term

$$\left.\frac{\partial f}{\partial t}\right|_{\text{Collisions}} = -\nu_\sigma \left(f_\sigma - \frac{\int f_\sigma \, d\underset{\sim}{v}}{\int f_{o\sigma} \, d\underset{\sim}{v}} f_{o\sigma} \right) \qquad \text{(I-9)}$$

on the right side of the linearized Vlasov equation (I-6) in accord with the collision theory of Bhatnagar, Gross, and Krook[9]. Amano and Okamoto find that the threshold for parametric resonance is lowered substantially when large density gradients exist in the plasma parallel to $\underset{\sim}{E}_o$ and $\underset{\sim}{k}_{\text{excited}}$.

Hydrodynamic studies of the parametric resonance abound in the literature. However, these studies must be treated cautiously within the context of the present investigation. Jackson[10] shows that the hydrodynamic continuity and momentum equations* adequately describe plasma particle bunching, but do not account properly for the kinetic effect of particle trapping which may be of importance in the parametric excitation process.

Bunching occurs when plasma particles move across the potential troughs and hills of a plasma wave, alternatively gaining and losing kinetic energy. The resultant velocity modulation leads to a density modulation which, in turn, may enhance the wave energy. As opposed to bunching, linear particle trapping occurs when particles with velocities near the phase velocity of a plasma wave actually become trapped between two successive crests. Depending on the initial velocity of the particle relative to the wave, the particle may either relinquish energy to the wave or absorb energy from it. This

---

*These first two hydrodynamic moment equations are obtained by taking the zeroeth and first velocity moments of the linearized Vlasov equation (I-6).

energy exchange may result in growth of the plasma wave for an appropriate initial particle velocity distribution. Consequently, the truncated set of velocity-averaged moment equations does not properly account for linear particle trapping, because the trapping effect has its origin in the velocity distribution of the plasma particles.

Jackson[10] and Ichimaru[11] show that ion-acoustic waves may spontaneously become unstable when plasma ions and electrons have relative drift velocities sufficient to overcome damping losses. This instability originates predominantly from the particle trapping mechanism rather than bunching. As a result only kinetic theory adequately describes the instability. In the present experiment, we are interested in the parametric resonant process acting in conjunction with the ion-acoustic drift instability to drive the plasma unstable. Therefore, kinetic theory results are more appropriate for the present investigation of parametric effects. However, hydrodynamic theory does provide a convenient tractable set of equations for investigation of parametric effects in the absence of drift velocities.

The study of Krenz and Kino[12] is one of the first applications of parametric excitation theory to plasmas. Within the hydrodynamic approximation they predict theoretically and find experimentally an enhanced signal at ω_{pe} when a field is applied at $\omega_o \simeq 2\omega_{pe}$. Using a two-fluid hydrodynamic model, Silin[13] considers the parametric interaction in a cold plasma ($v_{Te}=v_{Ti}=0$) with a pump frequency $\omega_o \simeq \omega_{pe}/n$ where n is any integer. Lee and Su[14] investigate the parametric interaction for both transverse and longitudinal

fields. They also note that the usual ion-acoustic wave instability arising from the relative electron-ion drift can have a large effect on the parametric resonance due to the nonlinear mode coupling. Nishikawa[15] studies the general problem of parametric instability of two coupled damped oscillators. He then makes contact with the plasma[16] via the hydrodynamic equations including electron-neutral and ion-neutral collisions in the limit of weak pump fields. In addition to the parametric instability occurring for $\omega_H + \omega_L \simeq \omega_o$, Nishikawa was the first to report the existence of a non-oscillatory parametric resonance ($Re\omega=0$) which was verified later by Sanmartin[3].

Other parametric excitation processes are also considered in the literature. Sjölund and Stenflo[17] study the instability caused by the coupling of two external transverse waves to a longitudinal ion wave. Okutani[18] investigates parametric excitation of a plasma by varying the physical boundary of the plasma. Takeo[19] finds that a Mathieu equation describes parametric resonance for an externally applied electric field of frequency $\omega_o \simeq 2\omega_{pe}$ parallel to a density gradient. The excitation of low frequency transverse Alfvén waves propagating along a magnetic field are predicted by Montgomery and Harding[20] if the magnetic field contains a time varying component.

Among the experimental investigations, the work of Stern and Tzoar[21] is perhaps the most widely known. In their experiment an electric field was incident on a low pressure positive column of Hg with $\underset{\sim}{E}_o$ perpendicular to the discharge axis. Above a rather low power threshold, low frequency oscillations ω_L on the order of ion-acoustic frequencies were observed to onset. In

addition, oscillations at frequencies of $\omega_o \pm \omega_L$ were observed. These signals were believed to be manifestations of parametric excitation until a recent study by Mendel and Stern[22] showed the oscillations to be a dynamic relaxation process within the plasma. It was found that the incident rf energy heated the plasma and increased the density, altering the plasma properties to the point that most of the rf energy was reflected. Then the plasma cooled and the density decreased to the original level, allowing the dynamic cycle to periodically repeat itself. Mendel and Stern suggest that this mechanism is also responsible for the observations of Messiaen and Vandenplas[23] who observed low frequency oscillations of a Hg plasma when large pump powers were applied at the frequency of the main Tonks-Dattner resonance.* In a similar experiment Widner, Hsuan and Lonngren[24] observed low frequency oscillations which onset with pump power in a Hg discharge with the axis perpendicular to $\underset{\sim}{k}_o$ and $\underset{\sim}{E}_o$. Satellites of the excited frequency were also observed when the incident power was sufficiently large. The resonance occurred in a narrow density range for pump frequencies lying within the main Tonks-Dattner resonance. According to the succinct report by Kato and Yamagiwa[25] parametric coupling between ion plasma and ion-acoustic oscillations were observed in the "beam plasma" system

---

*In an infinite homogeneous plasma, the electron plasma mode manifests itself as a single weakly damped mode with a frequency $\omega_H \simeq \omega_{pe}$. However, when a plasma is subject to cylindrical boundary conditions as occur in a typical dc discharge, a series of discreet modes appear, the Tonks-Dattner resonances, with frequencies centered about ω_{pe}. Additional considerations are presented in Section III.

of a Hg vapor discharge. They reportedly observed enhancement of both frequencies when an rf field was applied to the plasma between parallel electrodes.

Several parametric excitation experiments have been performed in Q-machine plasmas. Wong, Goldman, Hai, and Rowberg[26] observed the parametric excitation of drift waves in potassium and cesium Q-machine plasmas by applying an rf voltage to a probe at twice the drift wave frequency. In a clever experiment Yadlowsky, Abrams, Ohe, and Lashinsky[27] modulated the electron temperature of their Q-machine plasma at twice the ion-acoustic frequency to parametrically excite ion-acoustic waves. They observed both parametric growth and damping depending upon the degree of temperature modulation. An interesting experiment by Dreicer, Henderson, and Ingraham[28] suggests the possibility of parametric excitation by a pump field of frequency $\omega_o \simeq \omega_{pe}$ in a potassium Q-machine plasma. They swept the frequency of an intense rf pump across the resonant frequency of a high-Q cavity which coaxially surrounded the plasma. Above a certain threshold field strength, the Q of the cavity decreased substantially, indicating enhanced absorption of rf power by the plasma. The authors suggest that the enhanced absorption is due to the parametric excitation of plasma oscillations which subsequently convect energy out of the cavity. Unfortunately no attempt was made to observe the low frequency oscillation spectrum to ascertain the existence of excited waves.

Several studies have involved excitation of the plasma at a frequency equal to one-half of the impressed frequency ω_o. Kato, Yoseli,

Kiyama, and Watanabe[29] applied an rf voltage to the anode of a Hg discharge to obtain a density modulation of their plasma. Resonant oscillations were observed at ω_{pe} and ω_{pi} when the modulation frequency was equal to $2\omega_{pe}$ and $2\omega_{pi}$ respectively. In a similar arrangement, Yoseli[30] excited oscillations at a frequency of ω_{pi} when an rf voltage of either $2\omega_{pi}$ or $2\omega_{pi}/3$ was applied. Both frequencies correspond to parametric instabilities of systems which are adequately described by the Mathieu equations.[31] Hiroe and Ikegami[32] reported excitation of the lower hybrid frequency $[\omega_{pi}^2 + \omega_{ci}^2]^{1/2}$ when the pump frequency was equal to $[\omega_{pe}^2 + \omega_{ce}^2]^{1/2}$ where $\omega_{c\sigma}$ is the cyclotron frequency of the σth component. Their experiment was performed in a Hg positive column passing through a waveguide in such a manner that the electric field was parallel to the discharge axis. A variable axial magnetic field was used to vary the cyclotron frequency and a threshold power level for onset of the oscillations was observed. Parametric excitation in the ionosphere has been reported by Wong and Taylor.[33] They observed sidebands in the Thomson back-scattering return of a high power radar pulse when a second signal of frequency $\omega_o \simeq \omega_{pe}$ was beamed at the ionosphere. The sidebands gave evidence of parametrically excited waves ranging in frequency from ω_{pe} to ω_{pi}.

In summary, the theory of parametric excitation of oscillations in an infinite plasma is well-established from the standpoint of kinetic theory and hydrodynamic theory. However, none of the treatments properly

account for the boundary conditions found in laboratory plasmas although several investigators have included the effect of an equilibrium density gradient. Experimental evidence of parametric instability is not convincing, particularly since the results of Stern and Tzoar[21] have been shown to be unrelated to parametric effects. Several investigators have reported enhancement of plasma oscillations when a time-varying pump field is applied to a plasma, but none of the studies has provided a quantitative comparison with theory. Perhaps the most convincing evidence of parametric effects in a plasma comes from the study of Yadlowsky et al.[27] but their mechanism for parametric excitation consists of temperature modulation rather than the application of an rf field.

II. THEORY OF PARAMETRIC EXCITATION

In this section an infinite set of equations is developed to describe the parametric coupling of ion-acoustic and plasma waves following the derivations of Jackson[2] and Sanmartin[3]. The equations are then extended to include the effects of collisional damping and relative drift of electrons and ions. Finally, the results of a numerical analysis of the parametric effect are presented, with plasma parameters chosen to simulate the positive column of a helium dc discharge.

A. Parametric Excitation Theory in an Infinite Homogeneous Plasma

In the Introduction the perturbed distribution function f_σ is found to obey the linearized Vlasov equation

$$\frac{\partial f_\sigma}{\partial t} + \underset{\sim}{v}\cdot\frac{\partial f_\sigma}{\partial \underset{\sim}{r}} + \frac{q_\sigma}{m_\sigma}\underset{\sim}{E}_o \cos\omega_o t\cdot\frac{\partial f_\sigma}{\partial \underset{\sim}{v}} - \frac{q_\sigma}{m_\sigma}\frac{\partial \varphi}{\partial \underset{\sim}{r}}\cdot\frac{\partial f_{o\sigma}}{\partial \underset{\sim}{v}} = 0, \tag{II-1}$$

where φ is subject to Poisson's equation

$$\frac{\partial^2 \varphi}{\partial r^2} = -4\pi\sum_\sigma q_\sigma \int f_\sigma d\underset{\sim}{v} \tag{II-2}$$

and

$$f_{o\sigma}(\underset{\sim}{u}) = f_{o\sigma}(\underset{\sim}{v} - \frac{q_\sigma}{m_\sigma}\frac{\underset{\sim}{E}_o}{\omega_o}\sin\omega_o t). \tag{II-3}$$

In the laboratory frame of reference each plasma component oscillates about its equilibrium position with a frequency ω_o. However, we can

move to the frame of reference oscillating with the σth species by the transformation:[3]

$$t = t, \quad \underset{\sim}{\rho}_\sigma = \underset{\sim}{r} + \underset{\sim}{\varepsilon}_\sigma \cos\omega_o t, \quad \underset{\sim}{u}_\sigma = \underset{\sim}{v} - \omega_o \underset{\sim}{\varepsilon}_\sigma \sin\omega_o t \tag{II-4}$$

where

$$\underset{\sim}{\varepsilon}_\sigma = \frac{q_\sigma}{m_\sigma} \frac{\underset{\sim}{E}_o}{\omega_o^2}.$$

Following this transformation, Eq. (II-1) becomes

$$\frac{\partial f_\sigma}{\partial t} + \underset{\sim}{u}_\sigma \cdot \frac{\partial f_\sigma}{\partial \underset{\sim}{\rho}_\sigma} - \frac{q_\sigma}{m_\sigma} \frac{\partial \varphi}{\partial \underset{\sim}{r}} \cdot \frac{\partial f_{o\sigma}}{\partial \underset{\sim}{u}_\sigma} = 0. \tag{II-5}$$

If we define

$$\varphi_{\underset{\sim}{k}} = \int \varphi(\underset{\sim}{r}) e^{-i\underset{\sim}{k}\cdot\underset{\sim}{r}} d\underset{\sim}{r} \text{ and } f_{\sigma\underset{\sim}{k}} = \int f_\sigma e^{-i\underset{\sim}{k}\cdot\underset{\sim}{\rho}_\sigma} d\underset{\sim}{\rho}_\sigma,$$

then the spatial Fourier transform of Eq. (II-5) in the reference frame oscillating with the σth species yields:

$$\frac{\partial f_{\sigma\underset{\sim}{k}}}{\partial t} + i\underset{\sim}{k}\cdot\underset{\sim}{u}_\sigma f_{\sigma\underset{\sim}{k}} - i \frac{q_\sigma}{m_\sigma} \varphi_{\underset{\sim}{k}} \exp(-i\underset{\sim}{k}\cdot\underset{\sim}{\varepsilon}_\sigma \cos\omega_o t)\, \underset{\sim}{k}\cdot\frac{\partial f_{o\sigma}}{\partial \underset{\sim}{u}_\sigma} = 0. \tag{II-6}$$

The corresponding Fourier transform of Poisson's Eq. (II-2) gives

$$k^2 \varphi_{\underset{\sim}{k}} = 4\pi \sum_\sigma q_\sigma \exp(i\underset{\sim}{k}\cdot\underset{\sim}{\varepsilon}_\sigma \cos\omega_o t) \int f_{\sigma\underset{\sim}{k}} d\underset{\sim}{u}_\sigma. \tag{II-7}$$

Elimination of $\varphi_{\underset{\sim}{k}}$ in Eqs. (II-6) and (II-7) yields

$$\frac{\partial f_{\sigma \underset{\sim}{k}}}{\partial t} + i\underset{\sim}{k}\cdot\underset{\sim}{u}_\sigma f_\sigma - \frac{4\pi i q_\sigma}{m_\sigma k^2}\,\underset{\sim}{k}\cdot\frac{\partial f_{o\sigma}}{\partial \underset{\sim}{u}_\sigma}\sum_\tau q_\tau \exp(i\underset{\sim}{k}\cdot\underset{\sim}{\varepsilon}_{\tau\sigma}\cos\omega_o t)\int f_{\tau \underset{\sim}{k}}\, d\underset{\sim}{u}_\tau = 0, \qquad \text{(II-8)}$$

where

$$\varepsilon_{\tau\sigma} = \varepsilon_\tau - \varepsilon_\sigma = -\varepsilon_{\sigma\tau}$$

A rigorous solution of Eq. (II-8) requires proper treatment of the initial value problem using the Laplace transform in time. Following Sanmartin[3], we define

$$f^m_{\sigma \underset{\sim}{k}} = \int_o^\infty dt\; f_{\sigma \underset{\sim}{k}} \exp(i(\omega + m\omega_o)t)$$

with $\mathrm{Im}\,\omega > 0$ for arbitrary m. Invoking the identity

$$\exp(ia\cos b) = \sum_p i^p J_p(a)\exp(ipb),$$

the Laplace transform of Eq. (II-8) is

$$f_{\sigma \underset{\sim}{k}}\Big|_{t=0} - i(\omega + m\omega_o - \underset{\sim}{k}\cdot\underset{\sim}{u}_\sigma) f^m_{\sigma \underset{\sim}{k}}$$

$$- \frac{4\pi i q_\sigma}{m_\sigma k^2}\,\underset{\sim}{k}\cdot\frac{\partial f_{o\sigma}}{\partial \underset{\sim}{u}_\sigma}\sum_\tau q_\tau \sum_p i^p J_p(\underset{\sim}{k}\cdot\underset{\sim}{\varepsilon}_{\tau\sigma})\int f^{m+p}_{\tau \underset{\sim}{k}}\, d\underset{\sim}{u}_\tau = 0. \qquad \text{(II-9)}$$

Since we are not interested in possible effects of the initial distribution function, the term $f_{\sigma \underset{\sim}{k}}\big|_{t=0}$ is neglected. Defining the quantity $A_\sigma^m = q_\sigma \int f_{\sigma \underset{\sim}{k}}^m d\underset{\sim}{u}_\sigma$ and integrating Eq. (II-9) with respect to $\underset{\sim}{u}_\sigma$, a homogeneous equation in the quantities A_σ^m is obtained:

$$A_\sigma^m + \frac{4\pi q_\sigma^2}{m_\sigma k^2} \int \frac{\underset{\sim}{k}\cdot \partial f_{o\sigma}/\partial \underset{\sim}{u}_\sigma}{\omega + m\omega_o - \underset{\sim}{k}\cdot\underset{\sim}{u}_\sigma} d\underset{\sim}{u}_\sigma \sum_\tau \sum_p i^p J_p(\underset{\sim}{k}\cdot\underset{\sim}{\varepsilon}_{\tau\sigma}) A_\tau^{m+p} = 0. \qquad \text{(II-10)}$$

But the usual linear susceptibility[11] of the component σ is just

$$\chi_\sigma(\omega) = \frac{4\pi q_\sigma^2}{m_\sigma k^2} \int \frac{\underset{\sim}{k}\cdot \partial f_{o\sigma}/\partial \underset{\sim}{u}_\sigma}{\omega - \underset{\sim}{k}\cdot\underset{\sim}{u}_\sigma} d\underset{\sim}{u}_\sigma \qquad \text{(II-11)}$$

so Eq. (II-10) may be expressed as

$$A_\sigma^m + \chi_\sigma(\omega+m\omega_o) \sum_\tau \sum_p i^p J_p(\underset{\sim}{k}\cdot\underset{\sim}{\varepsilon}_{\tau\sigma}) A_\tau^{m+p} = A_\sigma^m [1+\chi_\sigma(\omega+m\omega_o)]$$

$$+ \chi_\sigma(\omega+m\omega_o) \sum_{\tau\neq\sigma} \sum_n i^{n-m} J_{n-m}(\underset{\sim}{k}\cdot\underset{\sim}{\varepsilon}_{\tau\sigma}) A_\tau^n = 0. \qquad \text{(II-12)}$$

Since m is an arbitrary integer, we may restrict $\mathrm{Re}\omega < \omega_o/2$ without loss of generality. The normal modes of oscillation of the plasma are determined from Eq. (II-12) by equating the determinant of the coefficient matrix of the A_σ to zero. But in order to evaluate the determinant, it is necessary to truncate the infinite series in equation (II-12) after a finite number of terms.

Assuming a Maxwellian velocity distribution function for $f_{o\sigma}$, the susceptibility $\chi_\sigma(z)$[11] can be expressed as

$$\chi_\sigma(z) = \frac{k_{D\sigma}^2}{k^2} W\left(\frac{z}{kv_{T\sigma}}\right) \tag{II-13}$$

where

$$W(y) = -y^{-2} - 3y^{-4} - \ldots - (2n-1)!!y^{-2n} + i\left(\frac{\pi}{2}\right)^{1/2} py\, e^{-y^2/2} \tag{II-14a}$$

for $|y| >> 1$ where $y = \mathrm{Re}\, y + i\,\mathrm{Im}\, y$ and $p = 0$ for $\mathrm{Im}\, y > 0$,

$p = 1/2$ for $\mathrm{Im}\, y = 0$,

$p = 1$ for $\mathrm{Im}\, y < 0$,

and

$$W(y) = 1 - y^2 + \frac{y^4}{3} - \ldots + \frac{(-1)^{n+1} y^{2n+2}}{(2n+1)!!} + i\left(\frac{\pi}{2}\right)^{1/2} y \tag{II-14b}$$

for $|y| << 1$.

If $\omega_o >> \omega >> \gamma$ and $k/k_{De} << 1$, then $|\omega \pm m\omega_o|/(kv_{T\sigma}) >> 1$, $m \neq 0$, for both electrons and ions. Thus, keeping only the first term in the expansion (II-14a) and neglecting the small imaginary terms, the susceptibility $\chi_\sigma(\omega \pm m\omega_o)$ may be expressed as

$$\chi_\sigma(\omega \pm m\omega_o) \simeq \frac{-k_{D\sigma}^2}{k^2} \frac{(kv_{T\sigma})^2}{(\omega \pm m\omega_o)^2} \simeq -\frac{\omega_{p\sigma}^2}{(m\omega_o)^2}. \tag{II-15}$$

Consequently, $\chi_\sigma(\omega \pm m\omega_o)$ decreases proportionally to $1/m^2$ with increasing m, $m \neq 0$, for both electrons and ions, and the infinite summation (II-12) may be truncated at $m = \pm 1$ with reasonable accuracy. The resultant equations for a two component singly-charged electron-ion plasma are:

$$A_\sigma^o \epsilon_\sigma(\omega) + \chi_\sigma(\omega)[J_o A_\tau^o + iJ_1(A_\tau^1 + A_\tau^{-1})] = 0 \qquad \text{(II-16a)}$$

$$A_\sigma^{\pm 1} \epsilon_\sigma(\omega \pm \omega_o) + \chi_\sigma(\omega \pm \omega_o)[J_o A_\tau^{\pm 1} + iJ_1 A_\tau^o - J_2 A_\tau^{\pm 1}] = 0, \qquad \text{(II-16b)}$$

where $\epsilon_\sigma(\omega) = 1 + \chi_\sigma(\omega)$ and the argument of the Bessel functions is $\underset{\sim}{k} \cdot \underset{\sim}{\varepsilon}_{\tau\sigma}$. Near onset of parametric instability for a typical positive column plasma, $|\underset{\sim}{k} \cdot \underset{\sim}{\varepsilon}_{\tau\sigma}| \simeq 2 \times 10^{-3}$. Consequently, $J_2(\underset{\sim}{k} \cdot \underset{\sim}{\varepsilon}_{\tau\sigma}) \ll J_1(\underset{\sim}{k} \cdot \underset{\sim}{\varepsilon}_{\tau\sigma})$ and terms involving J_2 can be dropped with negligible error to give:

$$A_\sigma^o \epsilon_\sigma(\omega) + \chi_\sigma(\omega)[J_o A_\tau^o + iJ_1(A_\tau^1 + A_\tau^{-1})] = 0 \qquad \text{(II-17a)}$$

$$A_\sigma^{\pm 1} \epsilon_\sigma(\omega \pm \omega_o) + \chi_\sigma(\omega \pm \omega_o)[J_o A_\tau^{\pm 1} + iJ_1 A_\tau^o] = 0. \qquad \text{(II-17b)}$$

Jackson[2] has analytically evaluated Eqs. (II-17) for the 3-mode parametric instability of a two-component driftless Maxwellian distribution in the absence of collisions. In the limit $\omega_o \gg \omega_H$, he finds the frequency of the high and low frequency normal modes of the plasma to be:

$$\omega_{Ho}^2 = \omega_{pe}^2 + \omega_{pi}^2 + 3k^2 v_{Te}^2 - (1 - J_o^2 - J_1^2)\omega_{pi}^2 \qquad \text{(II-18A)}$$

$$\omega_{Lo}^2 = \omega_{pi}^2 [k^2/k_{De}^2 - (1 - J_o^2 - J_1^2)]. \qquad \text{(II-18B)}$$

In the limit $\omega_o \simeq \omega_H + \omega_L$, the frequencies (II-18) are modified further and the threshold electric field E_o for instability is found to be

$$\frac{E_o^2}{16\pi n K T_e} \simeq \frac{J_1^2(\underset{\sim}{k}\cdot\underset{\sim}{\varepsilon}_{ei})}{(k/k_{De})^2} = \left(\frac{\pi m_e}{2m_i}\right)^{1/2} \frac{\gamma_{Le}(\omega_H)}{\omega_H} \qquad \text{(II-19)}$$

where $\gamma_{Le}(\omega_H)$ is the linear Landau damping factor

$$\gamma_{L\sigma}(\omega) = \left(\frac{\pi}{8}\right)^{1/2} \omega \left(\frac{\omega}{k v_{T\sigma}}\right)^3 \exp\left(-\frac{\omega^2}{2k^2 v_{T\sigma}^2}\right). \qquad \text{(II-20)}$$

For a typical value of $\gamma_{Le}(\omega_H)/\omega_H \simeq 10^{-3}$ in an atomic helium plasma, the threshold requirement (II-19) becomes

$$E_o^2 = 9.17 \times 10^{-15}\, n T_e$$

for E_o in volts/cm, T_e in ^oK, and n in cm^{-3}.

In order to predict the behavior of a laboratory plasma more accurately, the equations (II-17) may be modified to include the effect of electron and ion drift velocities and plasma-neutral collisions. The effects of a drift velocity $\underset{\sim}{v}_{D\sigma}$ may be incorporated into the definition of the equilibrium distribution function $f_{o\sigma}$ by employing a drifted Maxwellian distribution. Mathematically, this alters the susceptibility χ_σ such that $\chi_\sigma(\omega)\big|_{Drift} = \chi_\sigma(\omega - \underset{\sim}{k}\cdot\underset{\sim}{v}_{D\sigma})$. To account for plasma-neutral collisions, the definition of the linear susceptibility is modified to include an effective collision frequency ν_σ when $\omega/(kv_{T\sigma}) >> 1$ in accord with Ichimaru[11]

$$\chi_\sigma(\omega)\big|_{Collisions} = \chi_\sigma(\omega) + \frac{i\nu_\sigma\omega_{p\sigma}^2}{\omega^2(\omega+i\nu_\sigma)}. \qquad \text{(II-21)}$$

The collision correction factor in equation (II-21) can also be obtained from the Bhatnagar, Gross, and Krook[9] collision term in equation (I-9) for the limiting case of small collision frequencies. In accord with Ichimaru[11] plasma neutral collisions may be neglected for $\omega/(kv_{T\sigma}) \lesssim 1$. Electron-ion and ion-electron collision frequencies[34] are proportional to $T_e^{-3/2}$ and are negligibly small due to the high electron temperatures occurring in dc discharges.

B. Numerical Solutions of the Dispersion Relation

With the preceeding additions to equations (II-14), we have a complete set of equations describing the parametric effect in a plasma, including the effects of collisional and Landau damping, and steady state drift velocities. However, Eqs. (II-17) contain nine dimensionless independent parameters:

$$\frac{k}{k_{De}}, \frac{\omega_{pe}}{\omega_o}, \underset{\sim}{k}\cdot\underset{\sim}{\varepsilon}_{ei}, \frac{m_e}{m_i}, \frac{T_e}{T_i}, \frac{\nu_e}{\omega_{pe}}, \frac{\nu_i}{\omega_{pi}}, \frac{v_{De}}{v_{Te}}, \text{ and } \frac{v_{Di}}{v_{Ti}}. \tag{II-22}$$

By restricting our study to the positive column of a cylindrical helium discharge, only 5 variables are found to be independent:

$$\frac{k}{k_{De}}, \frac{\omega_{pe}}{\omega_o}, \underset{\sim}{k}\cdot\underset{\sim}{\varepsilon}_{ei}, p, \text{ and } R, \tag{II-23}$$

where p is the neutral gas pressure and R is the radius of the plasma. The remaining variables in (II-22) may be determined with sufficient accuracy from the parameters (II-23) using experimental data on the helium discharge.[35-37]

For example, the temperature ratio Te/Ti and the dc electric field E_{pc} required to maintain a helium positive column may be determined from the product pR.[36] Then the plasma-neutral collision frequencies, ν_e/ω_{pe} and ν_i/ω_{pi}, can be determined from experimental data[35] if the density n and neutral temperature T_N is known. Finally, the plasma drift velocities

are related to E_{pc} by the mobility[37] μ_σ

$$\underset{\sim}{v}_{D\sigma} = \mu_\sigma \underset{\sim}{E}_{pc} \simeq q_\sigma/(m_\sigma \nu_\sigma) \underset{\sim}{E}_{pc}.$$

Consequently, the nine parameters (II-22) are reduced to the 5 independent parameters (II-23), substantially simplifying the task of comparing the predictions of equations (II-17) with experimental results.

The equations (II-17) including effects of Landau damping, collisional damping, and plasma drift have been numerically analyzed for a simulated atomic helium plasma. The results of this analysis are presented in the remainder of this section. The relevant parameters are expressed in terms of the neutral pressure p and radius R in addition to the pertinent dimensionless quantities (II-22). Solutions are obtained for the real and imaginary parts of the frequency $\omega_L + i\gamma_L$ for a preassigned value of the real wave vector $\underset{\sim}{k}$. Instability occurs when $\gamma_L > 0$. Solutions of the dispersion relation for complex $\underset{\sim}{k}$ as a function of real ω would provide a more accurate physical representation of the experiment, but these calculations were not performed due to their additional complexity.

When nonzero drift velocities are included in the calculations, the wave vector $\underset{\sim}{k}$ is assumed to lie in the direction of the electron drift velocity. The electric field $\underset{\sim}{E}_o$ is the applied field strength within the plasma and is also assumed to be parallel to $\underset{\sim}{k}$ and $\underset{\sim}{v}_{De}$. No corrections are made for the increased reflection of the applied external field when the plasma frequency ω_{pe} exceeds the applied frequency ω_o.

In Fig. 1 the numerical solution of the dispersion relation for the parametrically excited low frequency mode in a helium dc discharge is shown for several pump field intensities. In Fig. 2 the corresponding dispersion relation is shown for a driftless plasma. Since the inclusion of drift velocity alters the density at which parametric resonance occurs, the densities of the plasmas in Figs. 1 and 2 have been adjusted to optimize the parametric interaction. Otherwise, the plasmas differ only in drift velocity. The arrows in Figs. 1 and 2 denote the value of k/k_{De} at which the relative growth rate γ_R is maximum where γ_R is defined by

$$\gamma_R = \gamma_L\big|_{\text{Pump field applied}} - \gamma_L\big|_{\text{Pump field off}}. \qquad \text{(II-24)}$$

The group velocity $d\omega_L/dk$ of the excited waves shows an abrupt decrease near the center of the resonance in both simulated plasmas. For the large pump powers depicted in Figs. 1 and 2, the group velocity actually becomes negative, denoting a backward wave with energy propagation antiparallel to the phase velocity of the wave. As the pump power is decreased, the excited frequency deviates less from the unperturbed ion-acoustic frequency and eventually resonance occurs with $d\omega/dk$ remaining positive. The field intensities used in the present experiment are sufficiently low that no significant change in Re ω is predicted.

Figs. 1 and 2 also illustrate the effect of ion drift velocity. Since the excited low frequency waves propagate with a phase velocity $v_{ph} \simeq v_{ia}$ in the rest frame of the ions,[11] the frequency of these waves

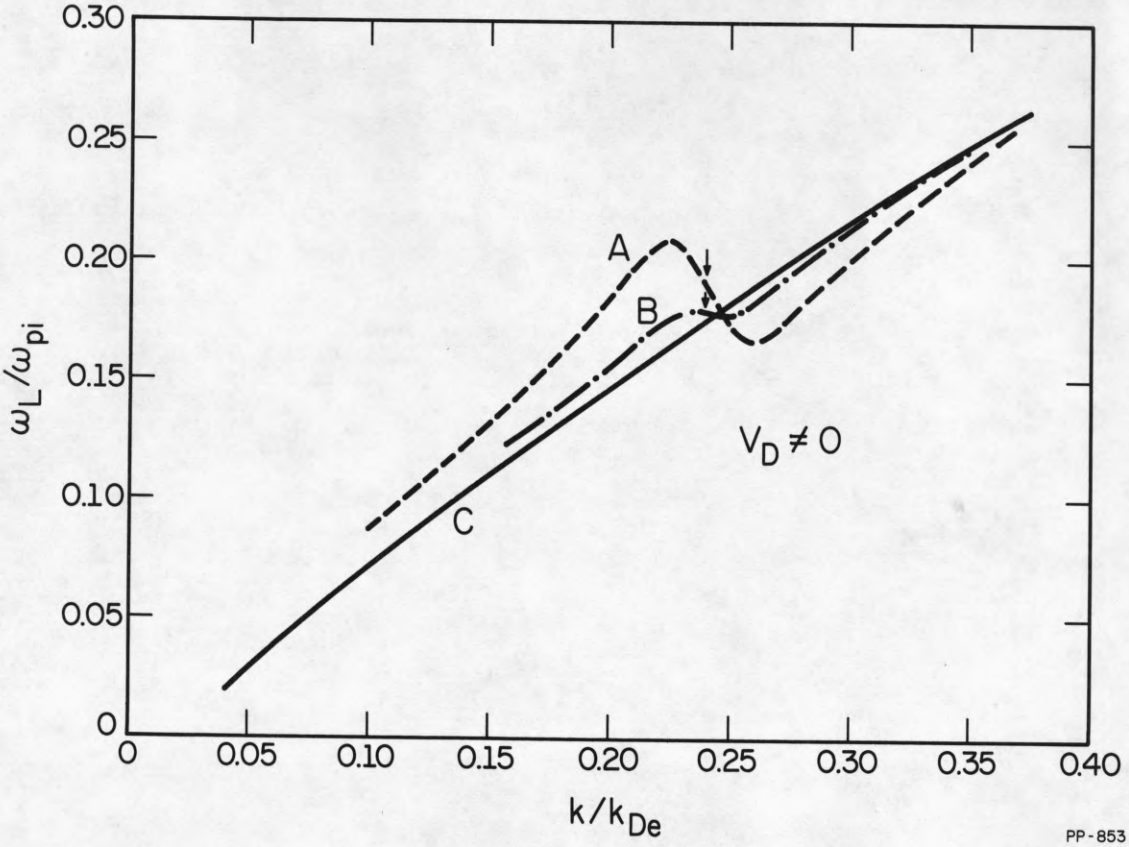

Fig. 1. Numerical solutions of the dispersion relation (II-17) for real $\underset{\sim}{k}$ in a helium positive column including drift velocity for several applied electric field strengths. Arrows indicate $(k/k_{De})_{Opt}$.

	$\frac{\omega_{pe}}{\omega_o}$	$\frac{v_{De}}{v_{Te}}$	$\frac{v_{Di}}{v_{Ti}}$	$\frac{\nu_e}{\omega_{pe}}$	$\frac{\nu_i}{\omega_{pi}}$	$\underset{\sim}{k}_{De} \cdot \underset{\sim}{\varepsilon}_{ei}$	$\frac{T_e}{T_i}$
A	1.02	.48	-4.1	.023	.058	.24	318.
B	"	"	"	"	"	.12	"
C	"	"	"	"	"	0.0	"

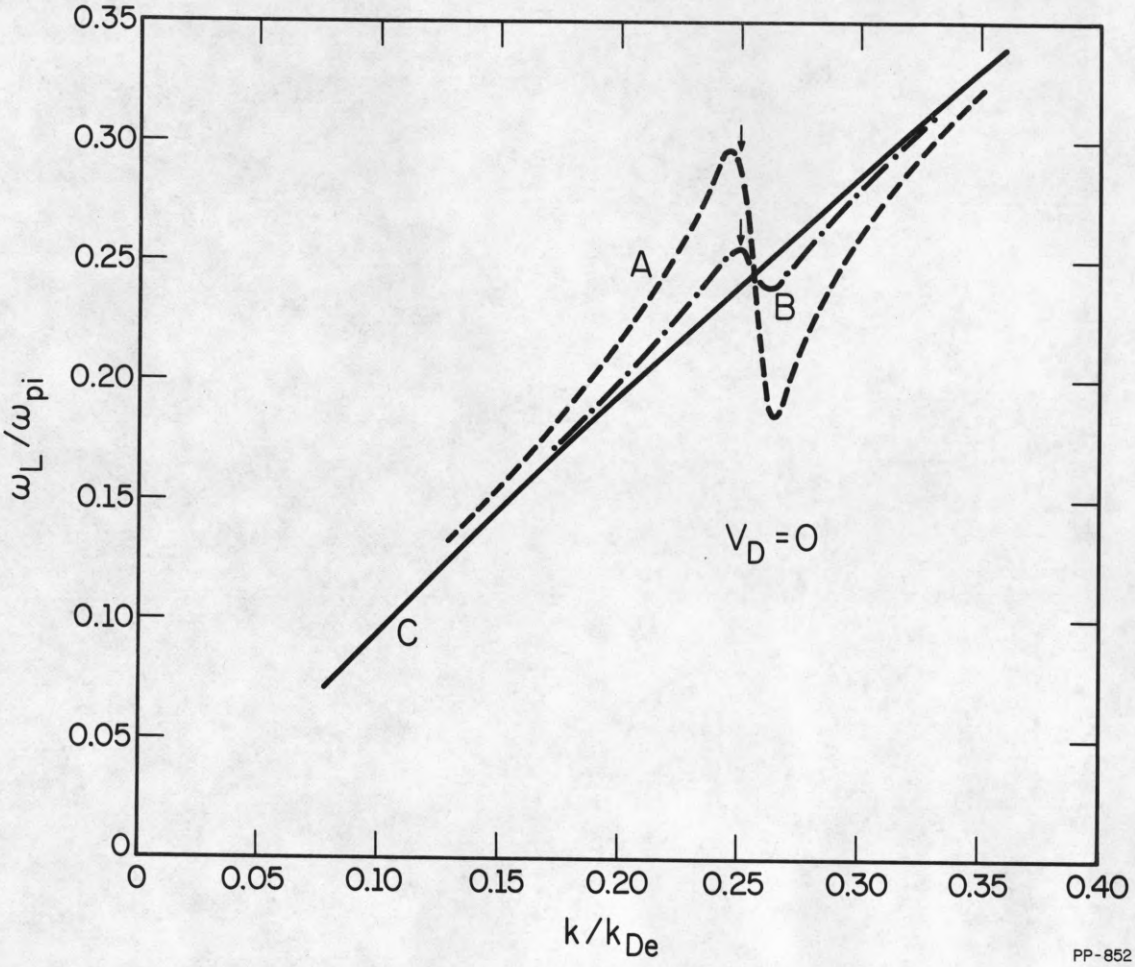

Fig. 2. Numerical solutions of the dispersion relation (II-17) for real $\underset{\sim}{k}$ in a driftless helium plasma for several applied electric field strengths. Arrows indicate $(k/k_{De})_{Opt}$.

	$\frac{\omega_{pe}}{\omega_o}$	$\frac{v_{De}}{v_{Te}}$	$\frac{v_{Di}}{v_{Ti}}$	$\frac{\nu_e}{\omega_{pe}}$	$\frac{\nu_i}{\omega_{pi}}$	$\underset{\sim}{k}_{De} \cdot \underset{\sim}{\varepsilon}_{ei}$	$\frac{T_e}{T_i}$
A	.90	0.0	0.0	.026	.065	.22	318.
B	"	"	"	"	"	.11	"
C	"	"	"	"	"	0.0	"

observed in the laboratory is Doppler shifted by

$$\omega_{Lab} = \underset{\substack{\text{rest}\\ \text{frame}}}{\omega_{Ion}} + \underset{\sim}{k}\cdot\underset{\sim}{v}_{Di} \qquad \text{(II-25)}$$

For ion drift velocities antiparallel to the wave phase velocity, the laboratory frequency is decreased (Fig. 1) relative to the driftless plasma (Fig. 2). The phase velocity of the waves in the laboratory becomes $v_{ph} = \omega_{Lab}/k = \omega_{pi}/k_{De} - v_{Di}$, and the resultant Doppler shift may lower the observed laboratory frequency by as much as 30%.

The normalized growth rate γ_L/ω_{pi} for the excited waves is displayed as a function of k/k_{De} in Fig. 3. The growth rate of the drifting plasma in the absence of an applied field (Fig. 3-1C) is large and positive (eventually peaking near $k/k_{De} \simeq .7$) due to the ion-acoustic instability arising from the relative electron-ion drift.[11] In contrast, the corresponding growth rate of the driftless plasma (Fig. 3-2C) is relatively constant and negative due primarily to ion-neutral collisional damping.

When a pump field E_o of frequency $\omega_o = 1.02\ \omega_{pe}$ is applied to the drifting plasma, a resonance occurs for k/k_{De} centered about a value of .24. The magnitude of the relative growth rate γ_R(II-24) is seen to be approximately proportional to E_o^2. In a second less pronounced resonance which is not shown in Fig. 3 for the drifting plasma, the growth rate attains a

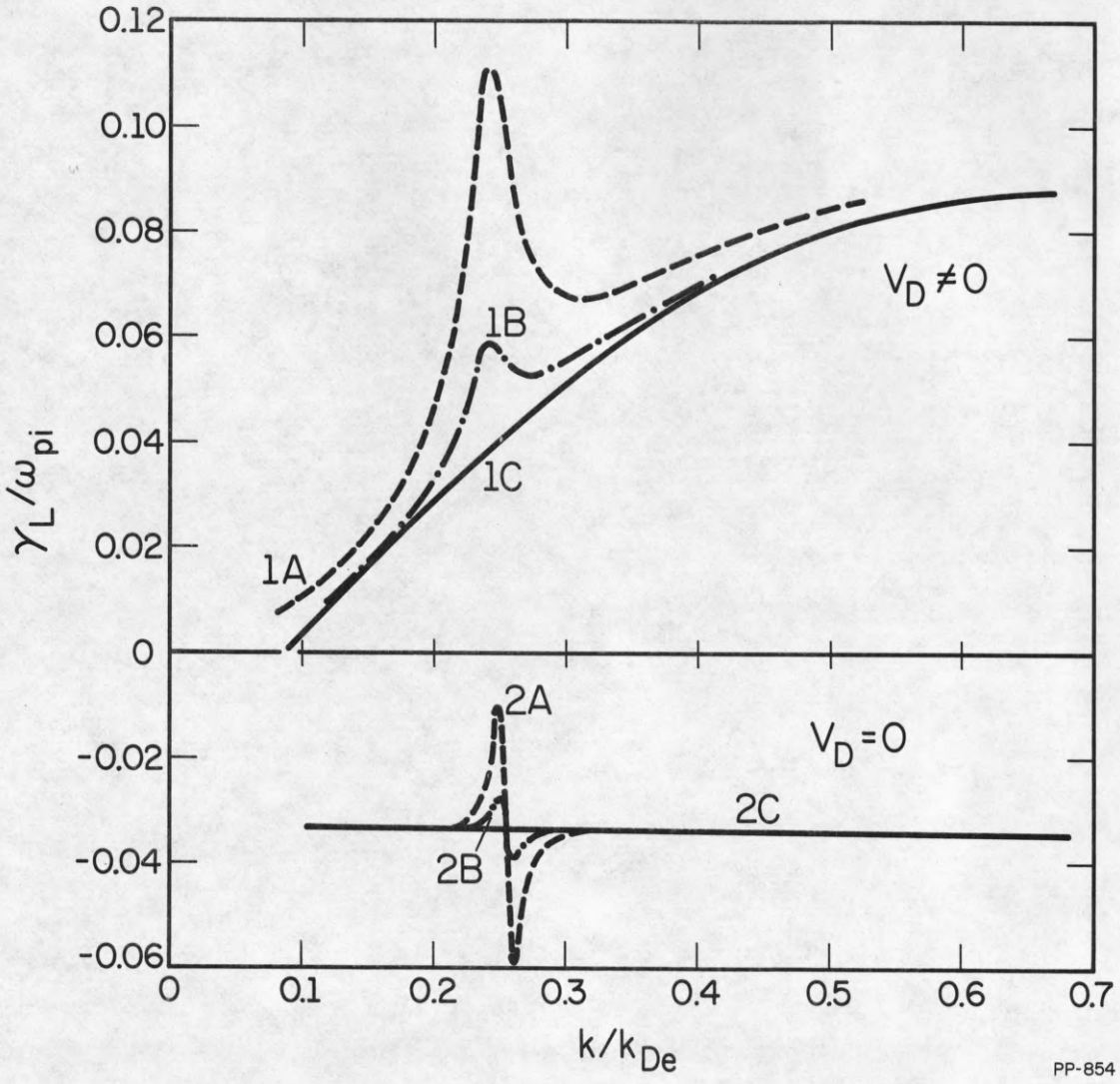

Fig. 3. Numerical solutions for the temporal growth rate as a function of wave number for the helium plasmas of Figs. 1 and 2 for several applied field strengths.

	$\frac{\omega_{pe}}{\omega_o}$	$\frac{v_{De}}{v_{Te}}$	$\frac{v_{Di}}{v_{Ti}}$	$\frac{\nu_e}{\omega_{pe}}$	$\frac{\nu_i}{\omega_{pi}}$	$\tilde{k}_{De} \cdot \tilde{\varepsilon}_{ei}$	$\frac{T_e}{T_i}$
1A	1.02	.48	-4.1	.023	.058	.24	318.
1B	"	"	"	"	"	.12	"
1C	"	"	"	"	"	0.0	"
2A	.90	0.0	0.0	.026	.065	.22	"
2B	"	"	"	"	"	.11	"
2C	"	"	"	"	"	0.0	"

minimum for $k/k_{De} < .05$. In contrast, the resonant maximum and minimum of the growth rate for the driftless plasma occur in a narrow range of k/k_{De} centered about .25 for $\omega_o = .90\ \omega_{pe}$.

The resonances are closer together in the driftless plasma than in the drifting plasma due to the frequency matching condition

$$\omega_H \pm \omega_L \simeq \omega_o. \tag{II-26}$$

For the nondrifting plasma,

$$\omega_H \simeq \omega_{pe}\left(1 + \frac{3}{2}\frac{k^2}{k_{De}^2}\right)^{1/2} \quad \text{and} \quad \omega_L \simeq \omega_{pi}\frac{k}{k_{De}} << \omega_{pe}.$$

It then follows from Eq. (II-26) that resonance occurs when

$$\frac{k}{k_{De}} \simeq \left(\frac{2}{3}\frac{\omega_o-\omega_{pe}}{\omega_{pe}}\right)^{1/2}\left(1 \mp \frac{\omega_L/2}{\omega_o-\omega_{pe}}\right).$$

Since $\omega_L << \omega_o$, the two resonances are only separated by

$$\frac{\Delta k}{k_{De}} \simeq -\omega_L\left[\frac{2/3}{\omega_{pe}(\omega_o-\omega_{pe})}\right]^{1/2}$$

in the driftless plasma.

In comparison, the high frequency mode of the drifting plasma as observed in the laboratory attains the frequencies

$$\omega_H \simeq \omega_{pe}\left(1 + \frac{3}{2}\frac{k^2}{k_{De}^2}\right)^{1/2} \pm kv_{De}.$$

Therefore, condition (II-26) indicates that the resonances of the drifting plasma are separated by

$$\frac{\Delta k}{k} \simeq k_{De}\, v_{De}\left[\frac{2/3}{\omega_{pe}(\omega_o - \omega_{pe})}\right]^{1/2}$$

for $\omega_L << kv_{De} < \omega_o$. Since kv_{De}/ω_{pe} ranges between .1 and .5 under typical experimental conditions, the separation of the resonances in $\underset{\sim}{k}$ space for the drifting plasma is appreciable. Due to the close proximity of the resonances in the driftless plasma, mutual cancellation of the resonances may occur. As a result, the isolated maximum of γ_R in the drifting plasma is more pronounced than the corresponding maximum in the driftless plasma.

In addition to separating the parametrically excited resonances, the electron drift velocity tends to decrease the threshold field strength for parametric excitation by decreasing the damping of the background ion-acoustic oscillations. In fact, if the ion-acoustic waves are already unstable due to electron drift, no minimum field strength is required for parametric excitation.

Plasma-neutral collisions also dramatically affect the parametric resonance as illustrated in Fig. 4. Curve C shows the growth rate for the driftless plasma of Fig. 2 with an applied field $\underset{\sim}{E}_o$ = 77.6 volts/cm. Curve A shows the same plasma without plasma-neutral collisions. The

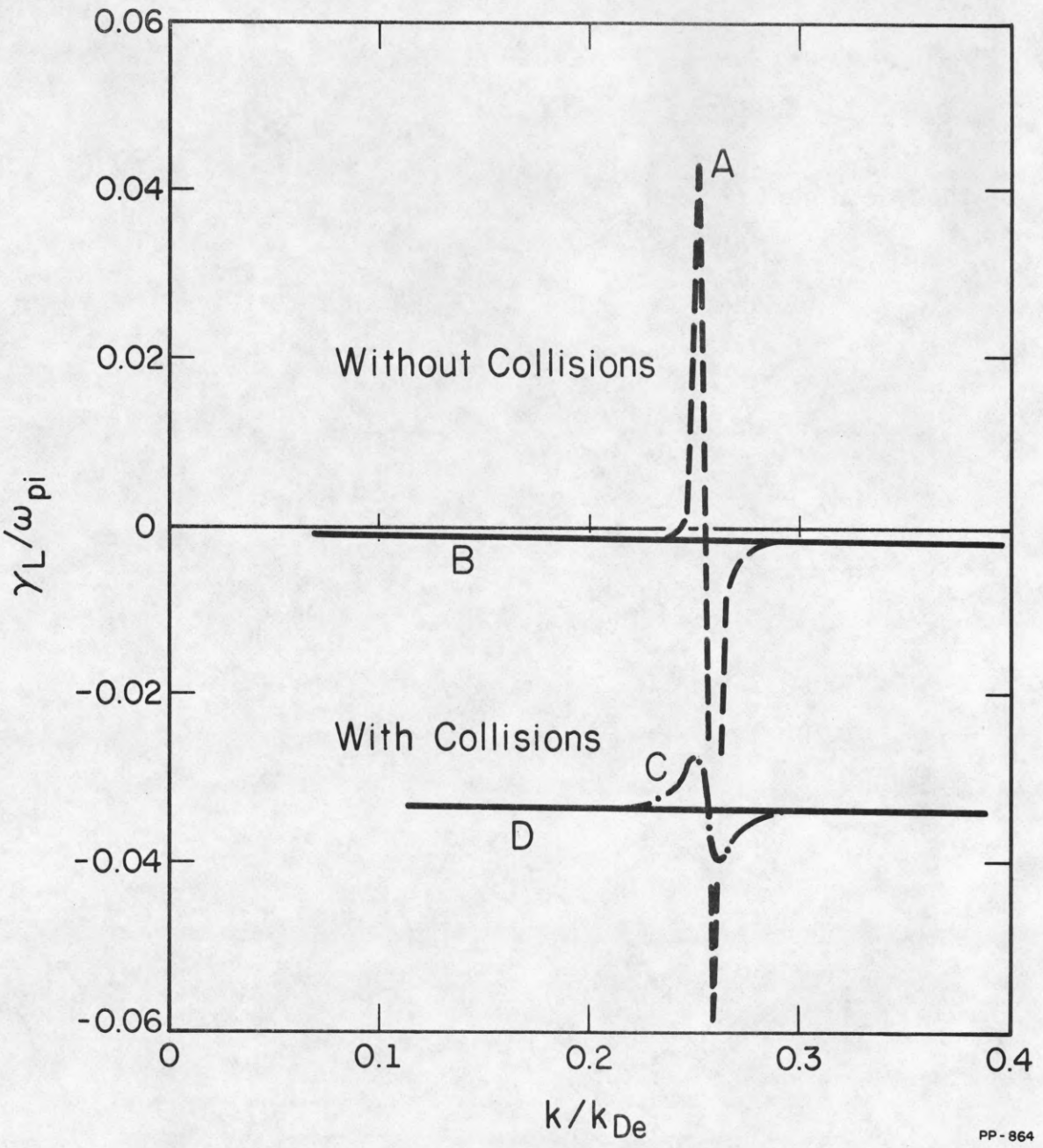

Fig. 4. Numerical solutions for the temporal growth rate as a function of wave number in a driftless helium plasma with and without collisions for a constant applied electric field.

	$\frac{\omega_{pe}}{\omega_o}$	$\frac{v_{De}}{v_{Te}}$	$\frac{v_{Di}}{v_{Ti}}$	$\frac{\nu_e}{\omega_{pe}}$	$\frac{\nu_i}{\omega_{pi}}$	$\underset{\sim}{k}_{De} \cdot \underset{\sim}{\varepsilon}_{ei}$	$\frac{T_e}{T_i}$
A	.90	0.0	0.0	0.0	0.0	.11	318.
B	"	"	"	"	"	0.0	"
C	"	"	"	.026	.065	.11	"
D	"	"	"	"	"	0.0	"

threshold field strength for parametric instability is affected by collisional damping in two ways. First, in the collisionless plasma, parametric instability occurs when the relative growth rate γ_R (II-24) exceeds the relatively small Landau damping rate of the undisturbed plasma (Fig. 4-B). However, when ion-neutral collisions are included, the relative growth rate at threshold must equal the collisional damping rate $\simeq \nu_i/2$ (Fig. 4-D), which may exceed the Landau damping rate by a factor of 30. Inclusion of collisional damping also increases the threshold field strength by lessening the effectiveness of the resonant mode coupling as seen by the large difference in relative growth rates between Curves A and C in Fig. 4. In addition, the range of resonant k/k_{De} is broadened slightly due to collisional effects.

Jackson's relationship (II-19) for parametric instability is applicable to the collisionless driftless plasma represented by Curves A and B in Fig. 4. Jackson's expression gives a value of 3.46 volts/cm for the threshold electric field compared to the numerical value of 4.49 volts/cm.

The relationship between the growth rate and frequency for parametrically excited waves is shown in Fig. 5 for the drifting plasma represented in Figs. 1 and 3. The strange loop in Curve A actually represents a spiral in the three dimensional space in which the k/k_{De} axis comes out of the page. Thus, although the same frequency may be linked to as many as three different growth rates, each value of k/k_{De} is paired to a unique frequency and growth rate. As the effectiveness of the parametric mode coupling is decreased (by decreasing the applied field strength, increasing

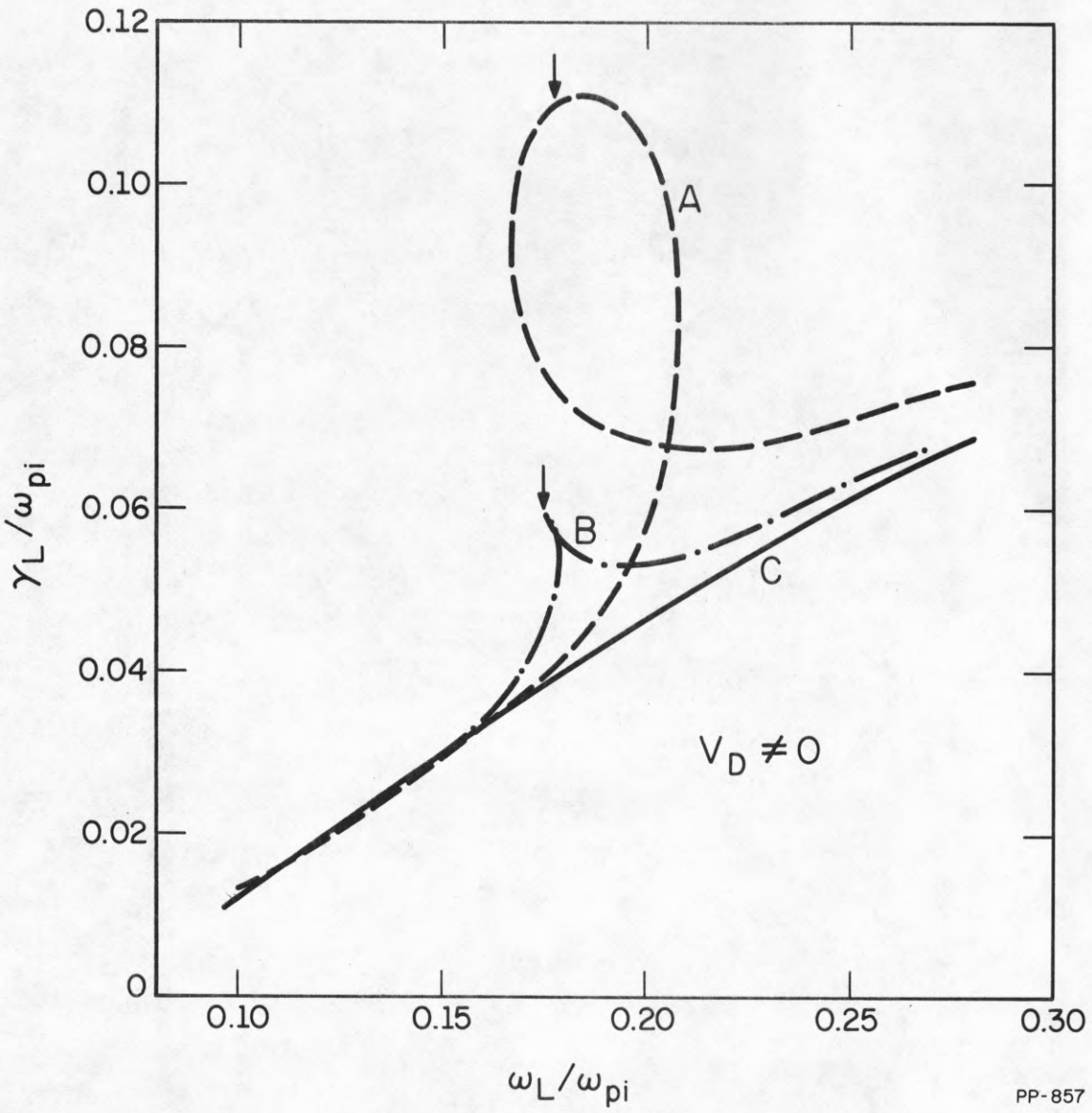

Fig. 5. Temporal growth rate versus frequency for the helium positive column of Fig. 1 for several applied electric field strengths. Arrows indicate $(\omega_L/\omega_{pi})_{Opt}$.

	$\frac{\omega_{pe}}{\omega_o}$	$\frac{v_{De}}{v_{Te}}$	$\frac{v_{Di}}{v_{Ti}}$	$\frac{\nu_e}{\omega_{pe}}$	$\frac{\nu_i}{\omega_{pi}}$	$\underset{\sim}{k}_{De} \cdot \underset{\sim}{\varepsilon}_{ei}$	$\frac{T_e}{T_i}$
A	1.02	.48	-4.1	.023	.058	.24	318.
B	"	"	"	"	"	.12	"
C	"	"	"	"	"	0.0	"

collision frequency, or changing ω_{pe}/ω_o to an off-resonant value), the loop becomes smaller and eventually disappears. The corresponding relationship for the driftless plasma is presented in Figs. 6 and 7. The arrows in Figs. 5-7 show the frequency at which the growth rate of the parametrically excited signal is maximum relative to the growth rate of the plasma in the absence of an applied field.

In the analysis to this point, the parametric interaction has been investigated as a function of k/k_{De} and ω_L/ω_{pi} while the density and pump frequency (and hence ω_{pe}/ω_o) were held constant. However, the character of the parametric resonance also changes if ω_{pe}/ω_o is varied. For example, if ω_{pe}/ω_o is increased, the value of k/k_{De} at parametric resonance decreases due to the frequency matching condition (I-8),

$$\omega_H + \omega_L \simeq \omega_{pe}\left(1 + \frac{3}{2}\frac{k^2}{k_{De}^2}\right)^{1/2} + kv_{De} + \omega_{pi}\frac{k}{k_{De}} - kv_{Di} \simeq \omega_o.$$

This variation of $(k/k_{De})_{Opt}$ with ω_{pe}/ω_o is shown in Fig. 8 for the driftless plasma of Fig. 2 and for a drifting plasma at two different pressures. The quantity $(k/k_{De})_{Opt}$ is defined as the value of k/k_{De} for which the relative growth rate γ_R attains its maximum. The sizeable electron drift velocity v_{De} is the cause of the large values of $(k/k_{De})_{Opt}$ for the drifting plasma relative to the driftless plasma. The increase of $(k/k_{De})_{Opt}$ with decreasing pressure in the drifting plasma is a manifestation of the corresponding

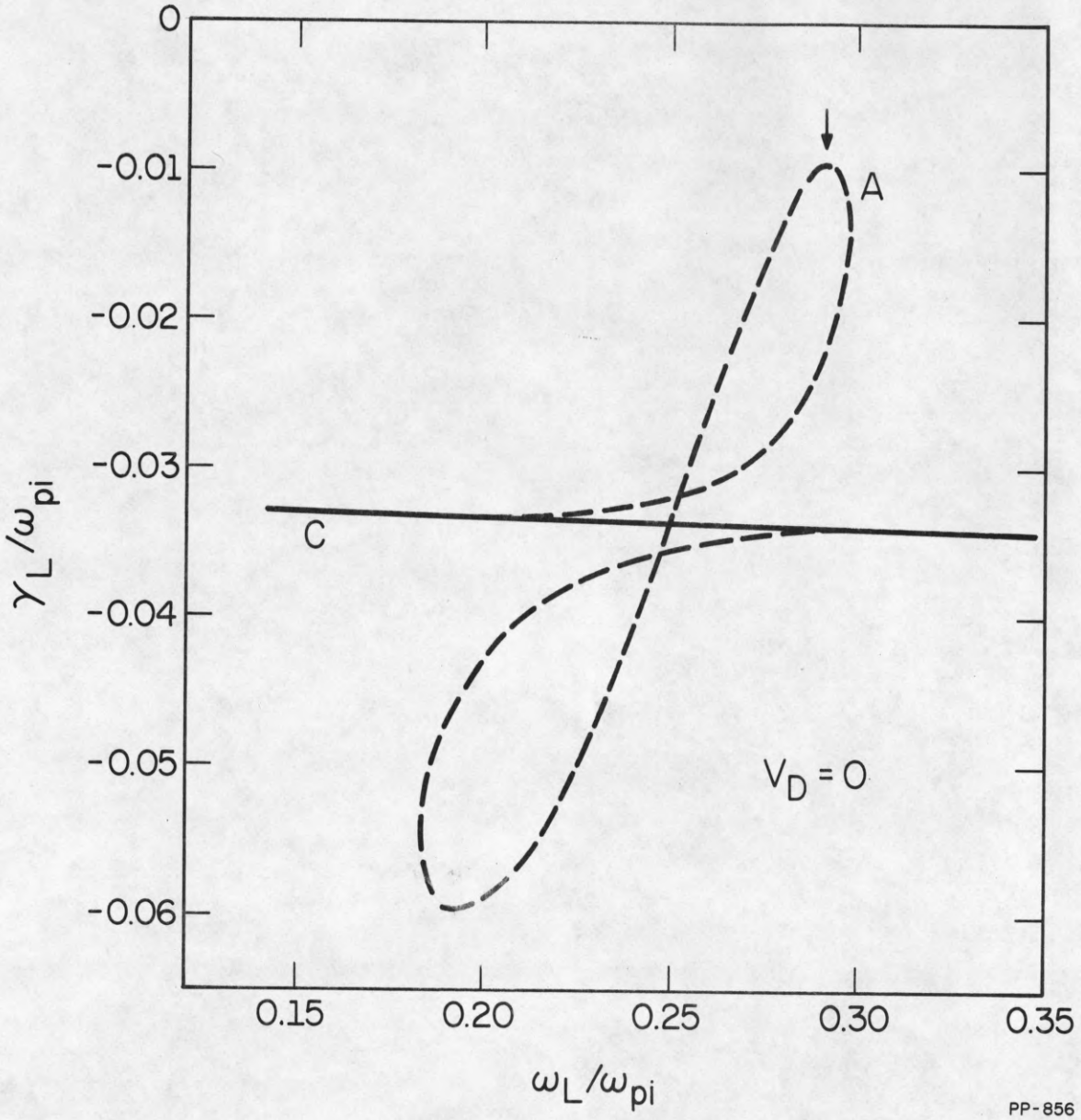

Fig. 6. Temporal growth rate versus frequency for the driftless helium plasma of Fig. 2. Arrow indicates $(\omega_L/\omega_{pi})_{Opt}$.

	$\frac{\omega_{pe}}{\omega_o}$	$\frac{v_{De}}{v_{Te}}$	$\frac{v_{Di}}{v_{Ti}}$	$\frac{\nu_e}{\omega_{pe}}$	$\frac{\nu_i}{\omega_{pi}}$	$\underset{\sim}{k}_{De} \cdot \underset{\sim}{\varepsilon}_{ei}$	$\frac{T_e}{T_i}$
A	.90	0.0	0.0	0.26	.065	.22	318.
C	"	"	"	"	"	0.0	"

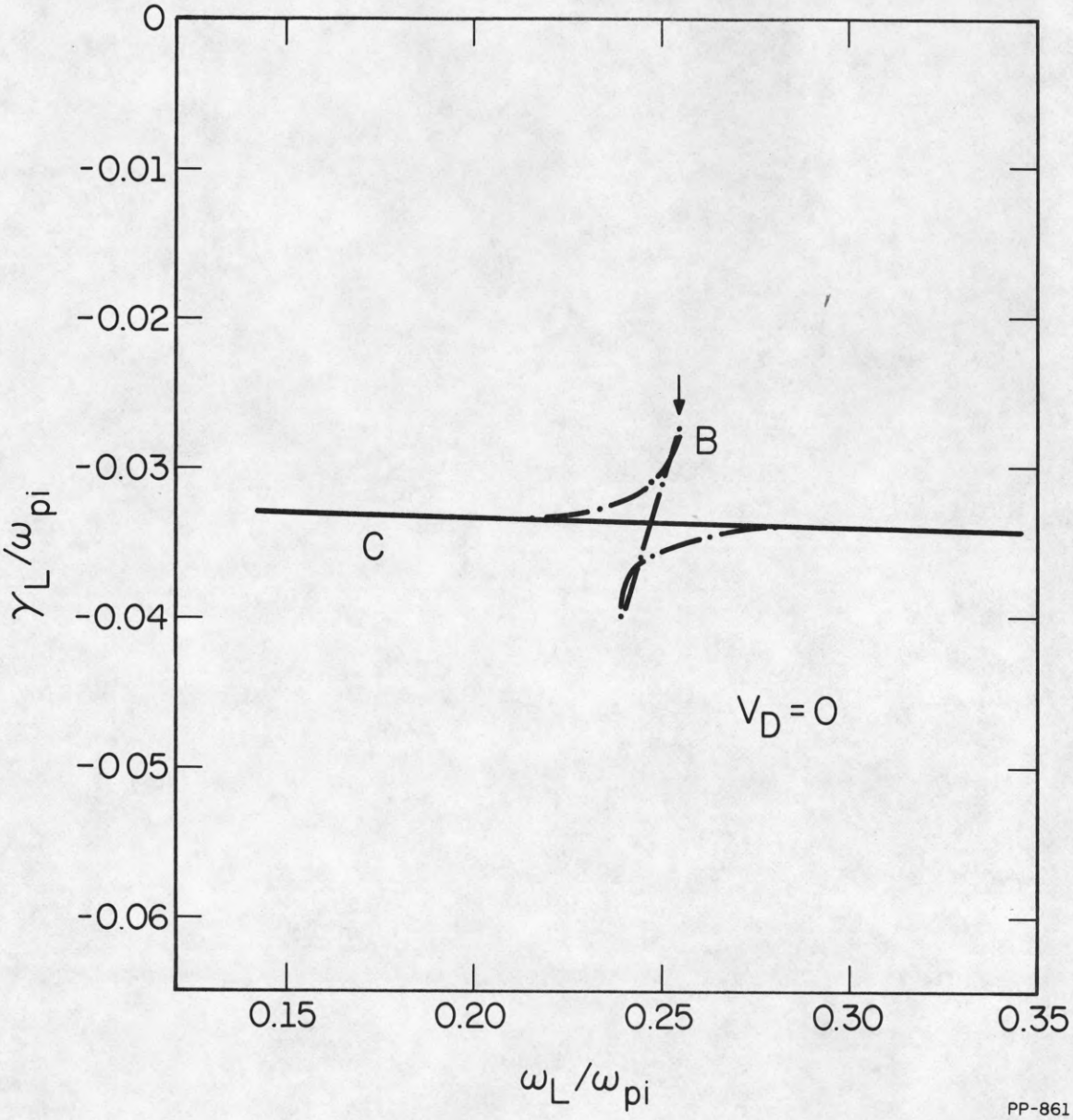

Fig. 7. Temporal growth rate versus frequency for the driftless helium plasma of Fig. 2. The arrow indicates $(\omega_L/\omega_{pi})_{Opt}$.

	$\frac{\omega_{pe}}{\omega_o}$	$\frac{v_{De}}{v_{Te}}$	$\frac{v_{Di}}{v_{Ti}}$	$\frac{\nu_e}{\omega_{pe}}$	$\frac{\nu_i}{\omega_{pi}}$	$\underset{\sim}{k}_{De} \cdot \underset{\sim}{\varepsilon}_{ei}$	$\frac{T_e}{T_i}$
B	.90	0.0	0.0	.026	.065	.11	318.
C	"	"	"	"	"	0.0	"

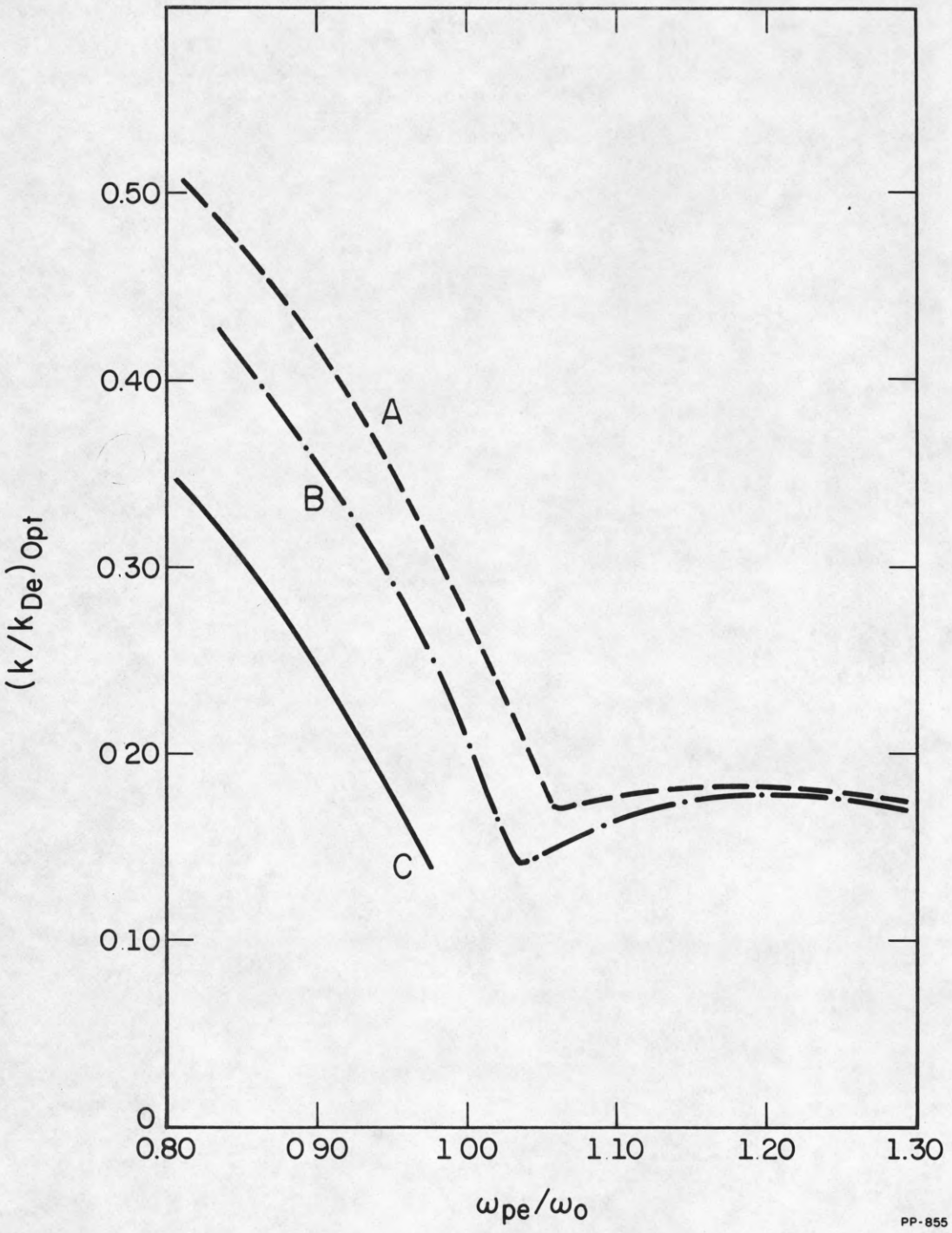

Fig. 8. Numerical values of $(k/k_{De})_{Opt}$ versus ω_{pe}/ω_o for a constant applied electric field in a helium positive column and in a driftless plasma.

	p	E_o	$\frac{v_{De}}{v_{Te}}$	$\frac{v_{Di}}{v_{Ti}}$	$\frac{\nu_e}{\omega_o}$	$\frac{\nu_i \omega_{pe}}{\omega_{pi} \omega_o}$	ε_{ei}	$\frac{T_e}{T_i}$
A	.10 torr	77.5 V/cm	.48	-4.1	.023	.059	.0015 cm	318.
B	.20 torr	"	.31	-2.9	.046	.092	"	255.
C	.10 torr	"	0.0	0.0	.023	.059	"	318.

increase in electron drift velocity due to a lower collision frequency. The sudden increase in $(k/k_{De})_{Opt}$ in Curves A and B for values of $\omega_{pe}/\omega_o > 1.05$ occurs in a region where the parametric resonance is very broad and weak. The corresponding variation of $(\omega/\omega_{pi})_{Opt}$ with ω_{pe}/ω_o is shown in Fig. 9 for the simulated plasmas of Fig. 8.

As ω_{pe}/ω_o is varied, the domain of frequencies involved in the parametric resonance also changes as seen in Fig. 10 where the relative growth rate is displayed as a function of frequency for a drifting plasma. As the plasma is detuned from the optimum density for parametric excitation, the relative growth rate decreases rapidly and the resonance broadens substantially, particularly if the density becomes larger than the optimum density.

Finally, the modification of the parametric resonance due to increasing pressure in the positive column is shown in Fig. 11. Collisional broadening and a weakening of the resonance are evident as the pressure is increased.

During the preparation of this thesis, a preprint by Freidberg and Marder[38] was obtained in which they present numerical solutions of the parametric effect based upon the kinetic formulation of Silin[13] for a collisionless driftless plasma. Under conditions of maximum parametric growth, our results agree with theirs within 5% for ω_{pe}/ω_o, within 15% for γ/ω_o, and within 25% for $\underset{\sim}{k}\cdot\underset{\sim}{\varepsilon}_{ei}$. Since Freidberg and Marder are interested in field strengths comparable to those obtained with lasers, they have retained higher order terms in Eq. (II-12) which were neglected in the present study.

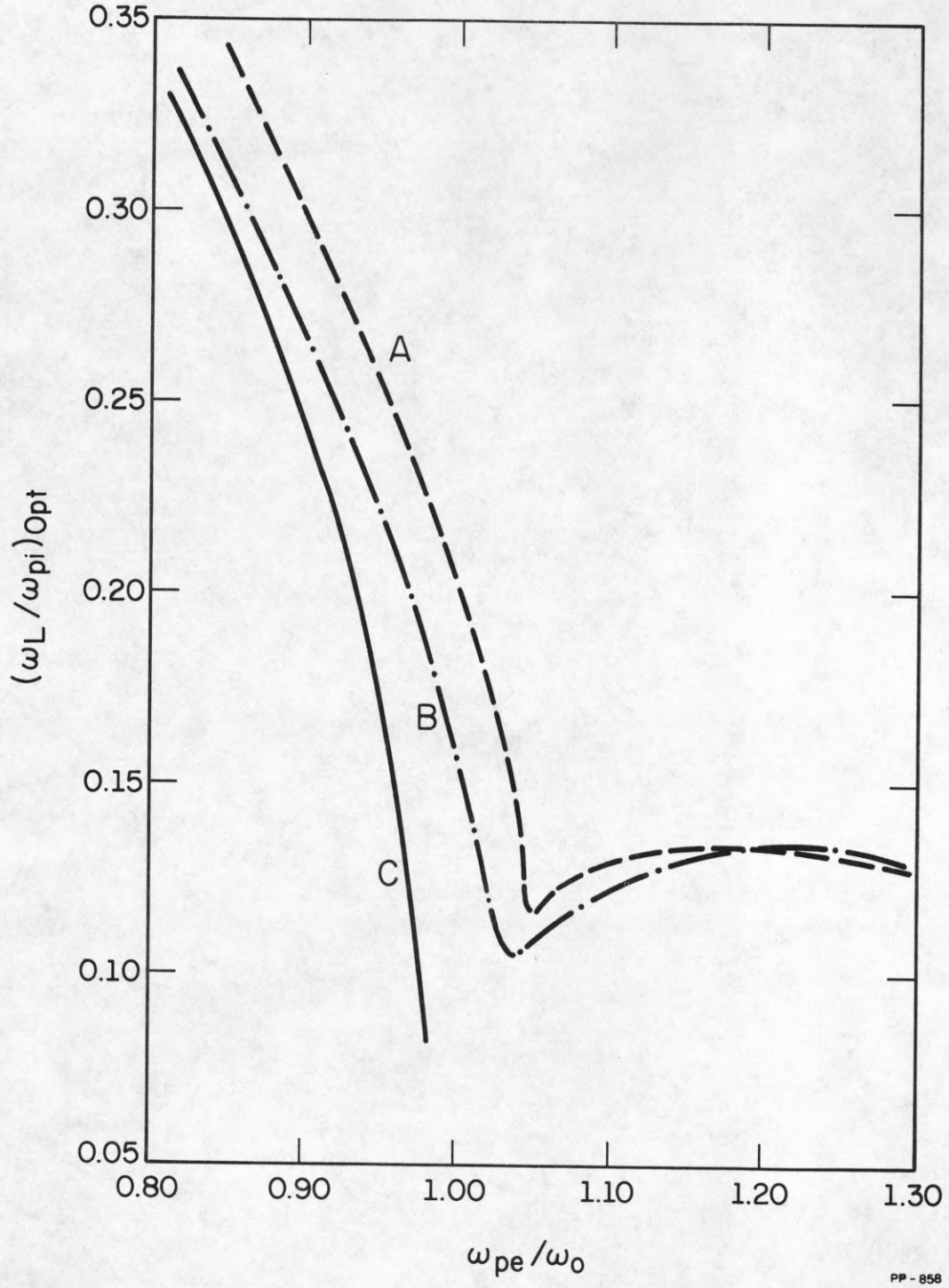

Fig. 9. Numerical values of $(\omega_L/\omega_{pi})_{Opt}$ versus ω_{pe}/ω_o for the conditions of Fig. 8.

	p	E_o	$\frac{v_{De}}{v_{Te}}$	$\frac{v_{Di}}{v_{Ti}}$	$\frac{\nu_e}{\omega_o}$	$\frac{\nu_i \omega_{pe}}{\omega_{pi} \omega_o}$	ε_{ei}	$\frac{T_e}{T_i}$
A	.10 torr	77.5 V/cm	.48	-4.1	.023	.059	.0015 cm	318.
B	.20 torr	"	.31	-2.9	.046	.092	"	255.
C	.10 torr	"	0.0	0.0	.023	.059	"	318.

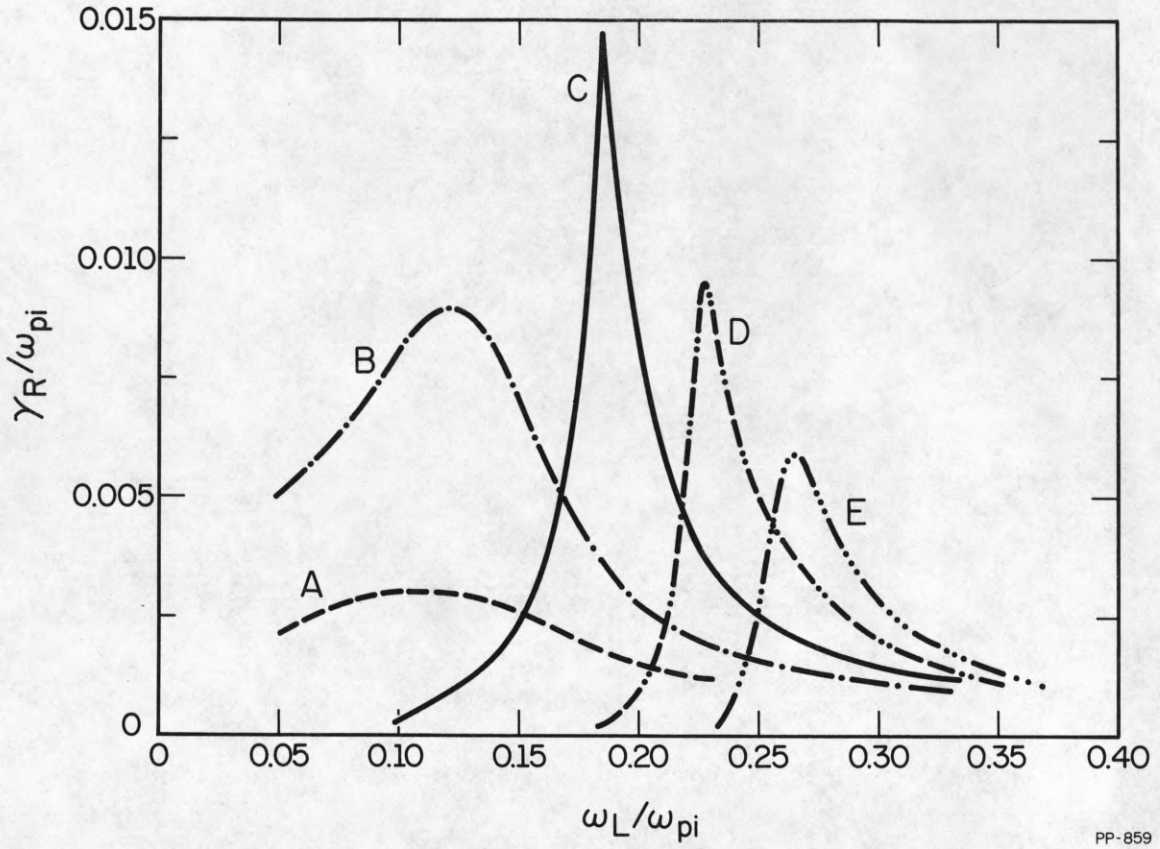

Fig. 10. Numerical solutions for the relative temporal growth rate as a function of frequency in a helium positive column for several values of ω_{pe}/ω_o for a constant applied electric field.

	p	E_o	$\frac{\omega_{pe}}{\omega_o}$	$\frac{v_{De}}{v_{Te}}$	$\frac{v_{Di}}{v_{Ti}}$	$\frac{\nu_e}{\omega_o}$	$\frac{\nu_i \omega_{pe}}{\omega_{pi} \omega_o}$	$k_{De} \cdot \varepsilon_{ei}$	$\frac{T_e}{T_i}$
A	.20 torr	77.5 V/cm	1.06	.31	-2.9	.048	.096	.12	255.
B	"	"	1.02	"	"	"	"	.12	"
C	"	"	.98	"	"	"	"	.13	"
D	"	"	.94	"	"	"	"	.14	"
E	"	"	.90	"	"	"	"	.14	"

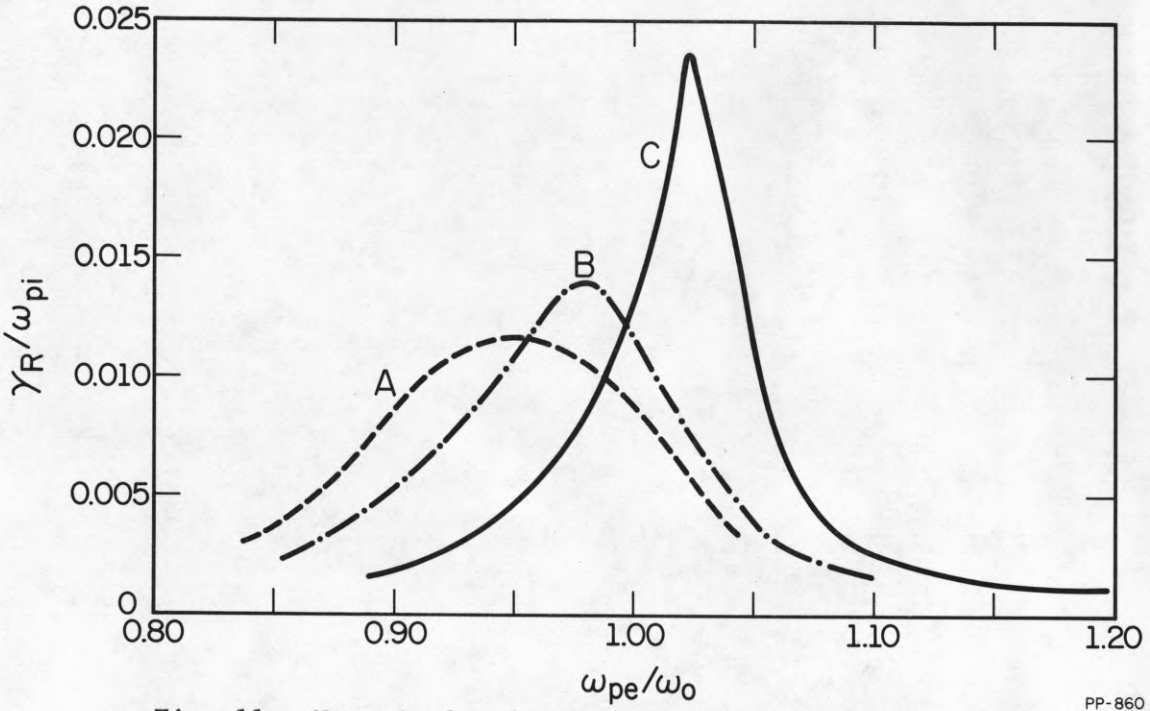

Fig. 11. Numerical solutions for the relative temporal growth rate as a function of ω_{pe}/ω_o in a helium positive column for various pressures with a constant applied pump field.

	p	E_o	$\frac{v_{De}}{v_{Te}}$	$\frac{v_{Di}}{v_{Ti}}$	$\frac{\nu_e}{\omega_o}$	$\frac{\nu_i \omega_{pe}}{\omega_{pi} \omega_o}$	ε_{ei}	$\frac{T_e}{T_i}$
A	.30 torr	77.5 V/cm	.23	-2.3	.068	.120	.0015 cm	226.
B	.20 torr	"	.31	-2.9	.046	.092	"	255.
C	.10 torr	"	.48	-4.1	.023	.059	"	318.

III. EXPERIMENTAL STUDY OF PARAMETRIC EXCITATION

In this section the parametric excitation of low frequency waves by an incident rf field in the positive column of a helium discharge is reported. The behavior of the excited waves is in basic agreement with the numerical solutions for the infinite plasma and the points of dissimilarity are believed to arise from inadequate theoretical treatment of the radial boundary conditions of the dc discharge.

A. Experiment Design

The basic configuration of the present experiment is shown in Fig. 12. The experiment is performed in the positive column of a dc discharge which is maintained by passing a current through a 0.96 cm i.d. quartz discharge tube filled with helium gas. A large positive voltage is applied to the copper anode by a current-regulated power supply with a range of operation from 20 mA to 200 mA. Free electrons are provided at the cathode by a hot filament operated in the emission-limited regime. Research grade helium gas is admitted to the plasma through a variable leak control valve near the anode and passes out of the system to a diffusion pump at the cathode. The system can be pumped out to a pressure only a factor of two above the ultimate diffusion pump pressure of 8×10^{-7} torr, so impurity levels in the plasma are believed to be negligible.

The techniques for excitation and detection of low frequency plasma waves is straightforward. The rf power for parametric excitation is applied through the TM_{010} mode of a 15cm diameter microwave cavity which is coaxial

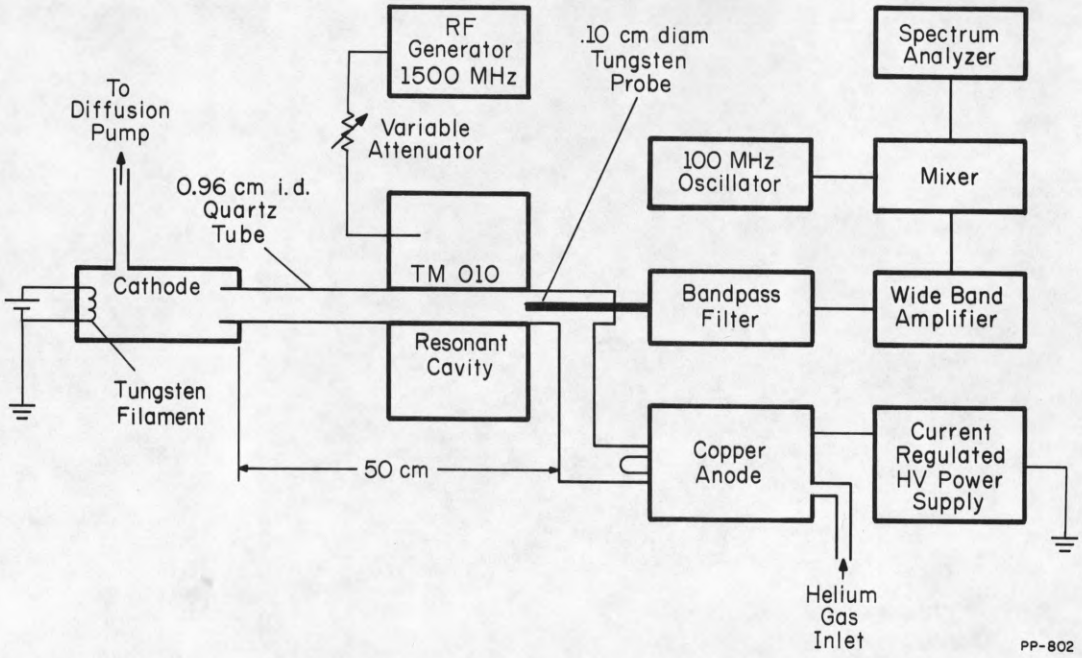

Fig. 12. Block diagram of the experimental arrangement.

with the axis of the discharge tube. The resonant frequency of the TM_{010} mode of the cavity is $\omega_o/2\pi \simeq 1.50$ GHz and a typical value of the Q of the cavity is 700. The electric field within the cavity is given by

$$\underset{\sim}{E}_{010} = E_o J_o(2x_{01} \frac{r}{D}) \hat{1}_z$$

where D is the cavity diameter and $\hat{1}_z$ is parallel to the axis of the discharge.

The source of the rf power is a 10 watt tunable oscillator, providing maximum field strengths of the order of 10 volts/cm at the center of the cavity. As the density of the plasma is varied, the effective dielectric constant within the cavity changes, resulting in a shift of the TM_{010} resonant frequency, which in turn, necessitates retuning of the power oscillator. However, this apparent inconvenience actually allows the determination of the plasma density within the cavity while the interaction is occurring. The slight change in ω_o due to retuning of the oscillator, $\Delta\omega_o/\omega_o < 0.3\%$, has a negligible effect on the parametric excitation process. The resonant cavity also acts as a filter, rejecting sideband frequencies emanating from the oscillator.

The voltage fluctuations of the excited low frequency waves are detected with a 0.10 cm tungsten probe which is parallel to the axis of the positive column and is facing the cathode. The detecting surface of the probe is positioned at the inside wall of the resonant cavity, and the probe is allowed to float at the floating potential of the plasma. The main length of the probe is insulated from the plasma.

Oscillations may also be detected by a loop encircling the plasma tube. The loop and the probe provide similar spectra with slight differences in relative intensities. The excited oscillations are frequently observed most easily with the coupling loop. The detected signal from the probe or loop is passed through a matched 10kHz to 20MHz bandpass filter followed by a sensitive video preamplifier with a noise figure of 4 db. The amplified signal is then converted to higher frequencies in a passive mixer by a 100MHz local oscillator signal. The resultant signal is displayed on a HP 851B spectrum analyzer with the option of recording the data on an x-y plotter. The initial bandpass filter rejects strong local FM stations which otherwise feed through the mixing network and confuse the observed spectrum.

Of the supporting diagnostic measurements, an accurate determination of electron density is the most essential in the study of parametric excitation. In the present experiment, the electron density is determined by measuring the shift in resonant frequency of the TM_{010} or TM_{020} modes of the 15 cm diameter microwave cavity. According to perturbation theory[39] for

$$\frac{\omega_{020}}{2\pi} = 3.51 \text{ GHz} >> \frac{\omega_{pe}}{2\pi} = 1.50 \text{ GHz},$$

the electron density n_o at the center of the discharge tube is given by

$$n_o = 2.02 \times 10^{15} \frac{\Delta\omega_{020}}{\omega_{020}} \text{ cm}^{-3} \qquad \text{(III-1)}$$

where a radial density profile* due to ambipolar diffusion is assumed:

$$n = n_o J_o(x_{01}\, r/R). \tag{III-2}$$

The density measurement is accurate within 15% including uncertainties due to inexact knowledge of the radial density profile.

The electron drift velocity v_{De} is determined directly from the discharge current I_{Dis} and the electron density profile, assuming the drift velocity is constant across the discharge tube

$$v_{De} \simeq \frac{I_{Dis}}{2\pi q \int_o^R n(r) r dr\, A_{Dis}} \tag{III-3}$$

where A_{Dis} is the discharge area. Since the drift velocity in a positive column remains constant at constant pressure, the discharge current and density are linearly related. However, the drift velocity does vary with pressure, as evidenced by the pressure dependence of the normalized discharge current I_{Dis}/n_o shown in Fig. 13. The accompanying curves for the numerically simulated plasma show good agreement with the experimental data.

Microwave cavity measurements can also be used to determine the electron-neutral collision frequencies since the change in Q of the resonant cavity is related to ν_e by[39]

---

*Experimental values of $\omega_{p\sigma}$ are calculated using the maximum value of the density n_o in the ambipolar diffusion profile.

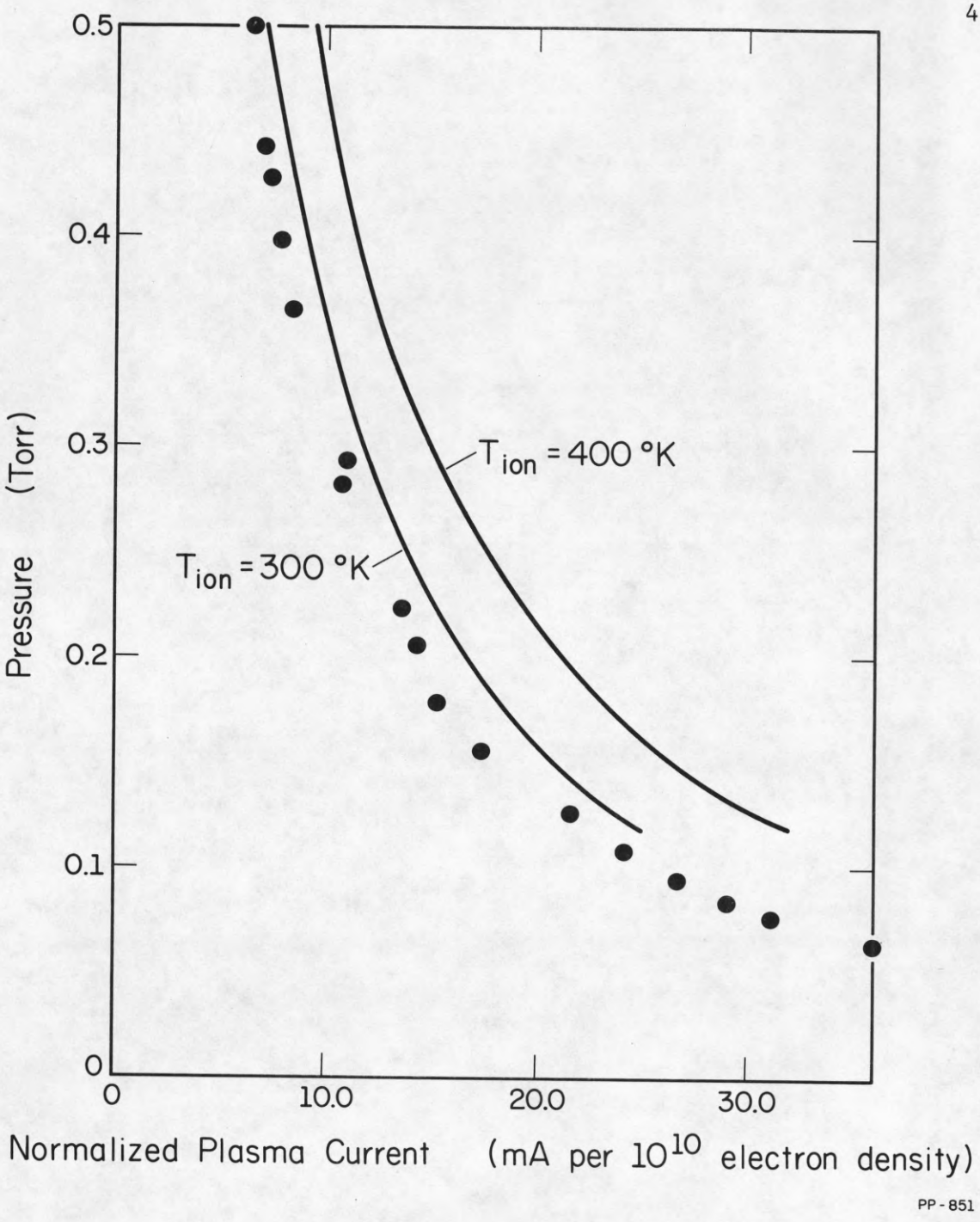

Fig. 13. Experimental and numerically simulated pressure dependence of the normalized plasma current for a .96 cm diameter helium positive column. The normalized plasma current is defined as the discharge current which results in a peak electron density $n_o = 10^{10}$ cm^{-3}.

$$\Delta\left(\frac{1}{Q}\right) \simeq \frac{2\nu_e}{\omega_{020}} \frac{\Delta\omega_{020}}{\omega_{020}}. \qquad \text{(III-4)}$$

In Fig. 14 the pressure dependence of the observed electron-neutral collision frequency is compared with the simulated values; excellent agreement is found.

Attempts to measure the electron temperature with a Langmuir probe[40] were discontinued because the probe appreciably disturbed the plasma. The electron temperature predicted by the plasma simulation (Section II) is believed to be correct within 20%. The temperature of the wall of the discharge tube provides an indication of the temperature of the helium gas which is assumed to be in thermal equilibrium with the ions. The wall temperature generally remains near $300^{\circ}K$, and increases somewhat with increasing discharge current and decreasing neutral gas pressures. The electron collision frequencies of Fig. 14 are compatible with ion temperature varying from $300^{\circ}K$ to $400^{\circ}K$.

The neutral gas number density is measured near the cathode with a Westinghouse 7903 ionization gauge which has been calibrated with a McCleod gauge. The pressure measurements are accurate within 20% of the true pressure.

B. Experiment Observations

When an rf field of frequency $\omega_o/2\pi \simeq 1.5$ GHz

($\omega_{pe}/\omega_o = 1 \Rightarrow n_o = 2.8 \times 10^{10} cm^{-3}$) is applied to the plasma, low frequency oscillations are parametrically excited for a limited range of densities. Figs. 15-17 show typical oscillation spectra with and without power at several densities and pressures. The intensity of the oscillations is

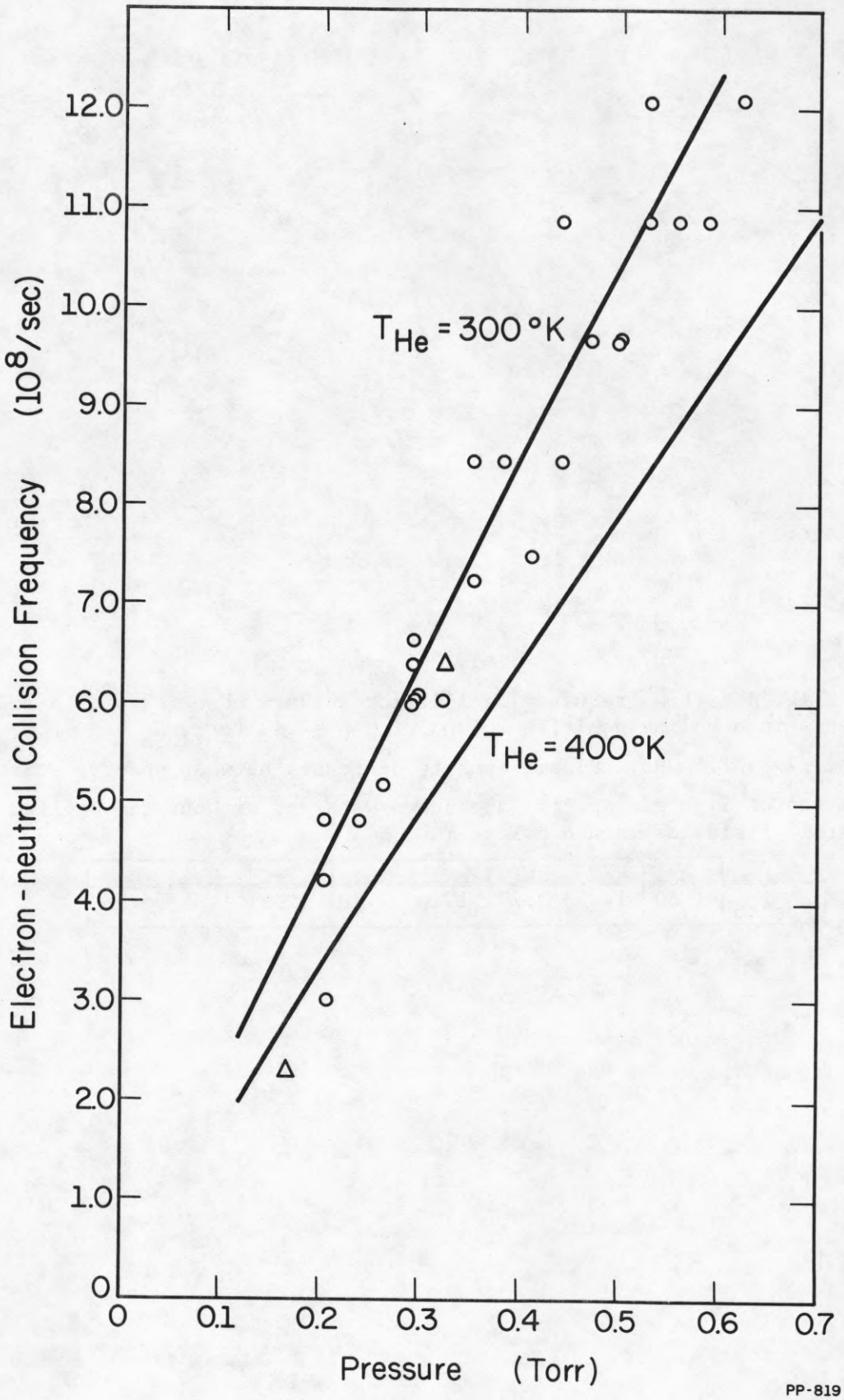
Electron-neutral Collision Frequency (10^8/sec)
12.0
11.0
10.0
9.0
8.0
7.0
6.0
5.0
4.0
3.0
2.0
1.0
0
0
0.1
0.2
0.3
0.4
0.5
0.6
0.7
Pressure (Torr)
T_He = 300 °K
T_He = 400 °K
PP-819

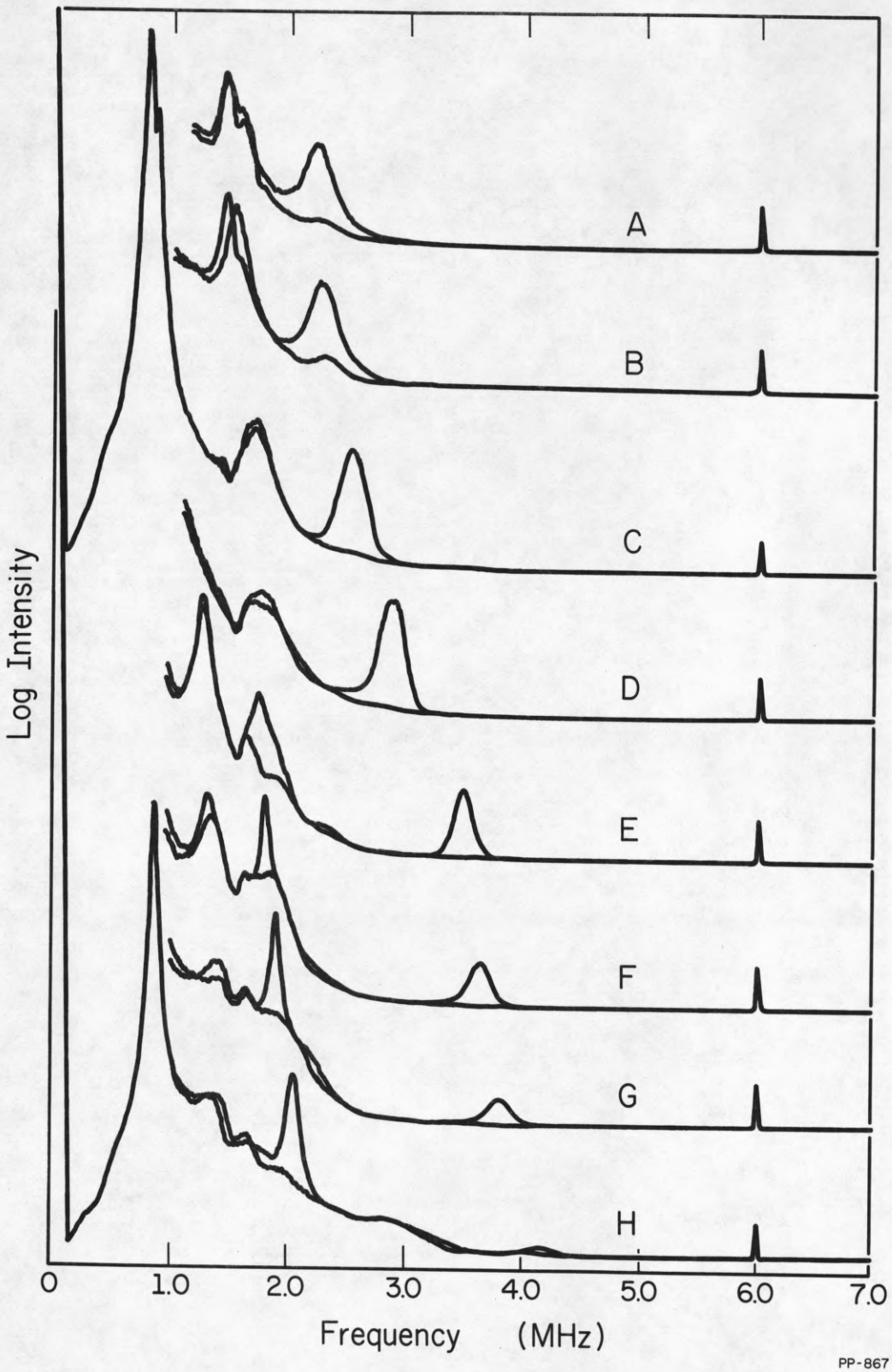
A
B
C
D
E
F
G
H
Log Intensity
0
1.0
2.0
3.0
4.0
5.0
6.0
7.0
Frequency (MHz)
PP-867

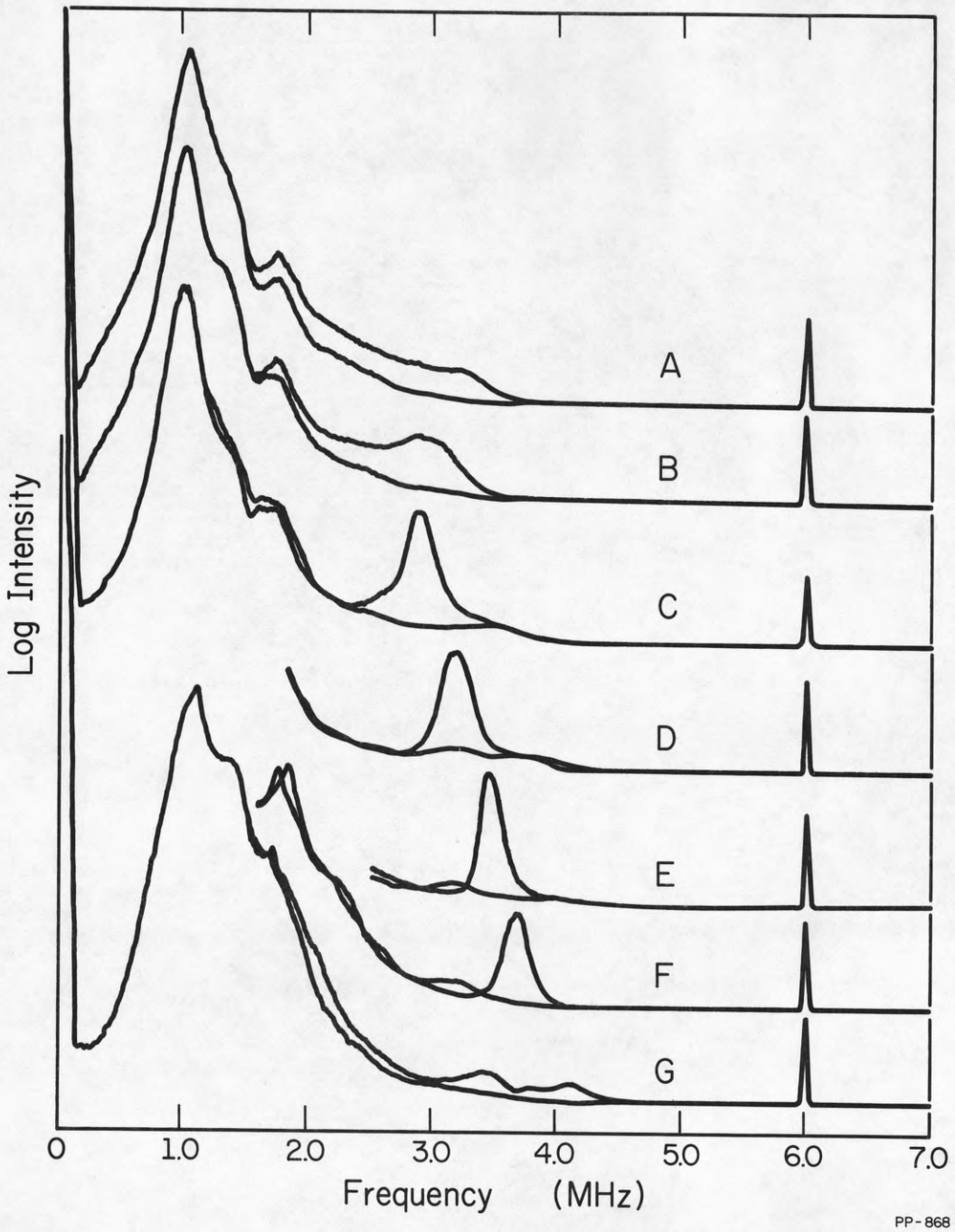

Fig. 16. Low frequency oscillation spectra observed with a loop antenna in a helium positive column with p = .15 torr, $E_o \simeq 3$ V/cm and $\omega_o/2\pi = 1.5$ GHz. Plasma density decreases between spectra starting from top of figure. Spectra are shown with and without the applied electric field for each density.

	A	B	C	D	E	F	G
ω_{pe}/ω_o	1.26	1.23	1.18	1.14	1.10	1.05	1.00

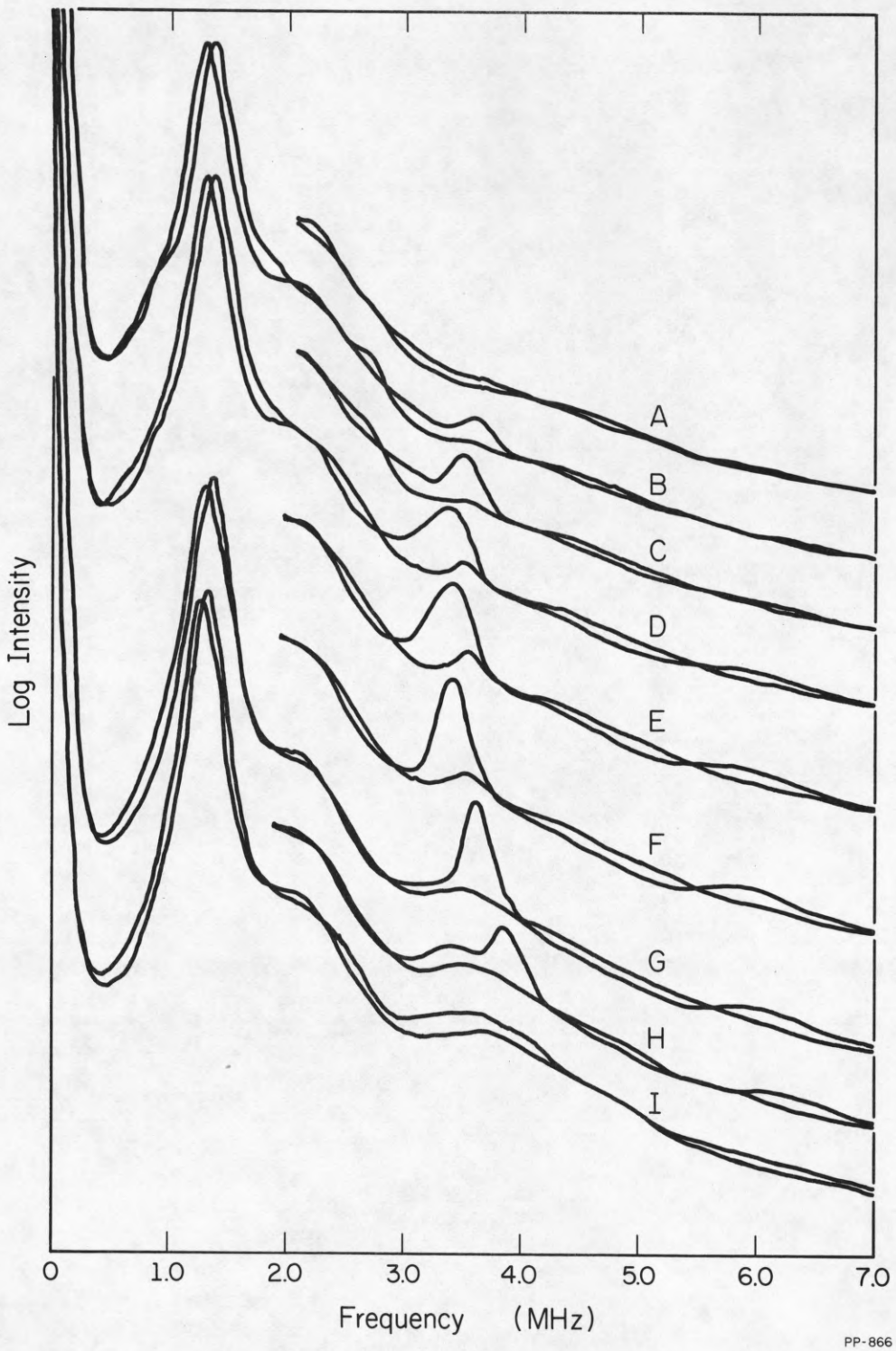

Fig. 17. Low frequency oscillation spectra observed with a floating probe in a helium positive column with p = .15 torr, $E_o \simeq 3$ V/cm, and $\omega_o/2\pi = 1.5$ GHz. Plasma density decreases between spectra starting from top of figure. Spectra are shown with and without applied power for each density.

	A	B	C	D	E	F	G	H	I
ω_{pe}/ω_o	1.30	1.27	1.24	1.21	1.18	1.15	1.12	1.08	1.05

displayed on a logarithmic scale as a function of frequency. Between data runs, the density is increased while keeping the pump frequency constant (other than retuning the oscillator to keep it at the resonant frequency of the cavity). The spectra in Figs. 15 and 16 were observed with a wire loop detector for pressures of 0.10 torr and 0.15 torr. Fig. 17 shows data obtained with a floating Langmuir probe for a pressure of 0.15 torr. The main parametric resonance occurs between 2 MHz and 5 MHz, decreasing in frequency as the density is increased toward the optimum density for parametric growth, n_{opt}. In Figs. 16 and 17 the resonance broadens appreciably and shifts to higher frequencies as the density is increased above n_{opt}. These general trends agree with our numerical study of parametric excitation (Figs. 9 and 10).

Before further discussion of the parametrically excited waves, several features of the low pressure positive column in the absence of an applied field should be noted. Due to large drift velocities and small collision frequencies, all of the waves observed in Figs. 15-17 are unstable. However, the oscillations do not resemble ion-acoustic oscillations which are characterized by a broad spectrum with intensity increasing to a maximum near $\omega/\omega_{pi} = .5$. In contrast, an irregular variation of intensity with frequency is observed, with several well-defined maxima, suggesting that discreet frequencies or eigenmodes of the system are excited. Similar spectra have been observed by Crawford [41] in a low pressure mercury vapor discharge. The existence of unstable eigenmodes in a positive column with a longitudinal magnetic field is predicted by Ewald, Crawford, and Self [42,43] when the effects of the radial boundary conditions are included. Two types

of weakly damped propagating waves are expected on the basis of hydrodynamic theory. Ion-acoustic waves propagate with a phase velocity $\omega/k_z \simeq v_{ia}$ parallel to the discharge (z) axis with a small off-axis $\underset{\sim}{k}$ vector. The second type of wave, propagating with $\omega/k_z >> v_{ia}$, is called an electron wave because it depends on electron dynamic effects ($m_e \neq 0$). This wave may be thought of as an ion-acoustic wave that propagates radially, and possibly azimuthally, with only a small component of $\underset{\sim}{k}$ parallel to the discharge axis. Although the electron drift velocity tends to decrease the damping rates of both types of waves, all the modes are found to be stable in the absence of a magnetic field. However, as discussed in the Introduction, the hydrodynamic equations underestimate the destabilizing effect of electron drift velocity for ion-acoustic waves. In analogy, radial ion-acoustic waves, and possibly electron waves, may be less stable than predicted by Ewald et al.,[42,43] perhaps becoming unstable due solely to sufficiently large electron drift velocities.

Thus, the discreet eigenmodes observed in Figs. 15-17 are probably unstable radial ion-acoustic waves or electron waves which are confined to a narrow range of radial wave vectors k_R by the radial boundary conditions. If an acoustic-like dispersion relation is valid for these waves

$$\omega \simeq \frac{\omega_{pi}}{k_{De}} (k_R^2 + k_z^2)^{1/2} \qquad \text{(III-5)}$$

and if k_R is of the order of k_z, then the influence of k_z on the frequency is decreased. Thus, an oscillation may be limited to a narrow frequency range if the radial wave vector is dominant. An alternative explanation of the

eigenmodes in Figs. 15-17 is that discreet oscillations originate in processes[44] near the cathode or discharge tube constrictions and propagate through the positive column as weakly damped ion-acoustic or electron waves. In either case, the mode structure of the positive column suggests that parametric excitation of ion-acoustic or electron waves of arbitrary order may occur. With these considerations in mind, we observe that Curves A-D of Fig. 15 show an excited peak at 2 MHz in addition to the main resonance occurring above 3 MHz. Additional peaks are observed occasionally, often coalescing (Fig. 15-C) with an unstable eigenmode of the system as the density is varied. This behavior suggests that a weakly damped eigenmode is parametrically driven over the threshold for instability by the applied field. In contrast, the parametric coupling to the predominant resonance in Figs. 15-17 is sufficiently strong to cause instability even though these oscillations do not appear to be associated with a natural instability of the system without power. Since several modes of various radial and azimuthal order exist within the positive column, simultaneous parametric excitation of several frequencies is not unexpected.

In addition to parametric excitation, two other power dependent effects should be considered. First, the applied pump field alters the equilibrium velocity distribution. When typical fields of $\simeq$ 3 volts/cm are applied to the plasma, the average density increases by 5% to 10% with a corresponding decrease in drift velocity for a current regulated plasma.*

*For constant I_{Dis}, the relationship $\Delta v_{De}/v_{De} = -\Delta n/n$ is obtained by a straightforward application of Eq. (III-3).

The electron temperature also increases proportionately. However, these changes actually tend to stabilize ion-acoustic oscillations (and possibly radial ion-acoustic and electron waves, as well) because

$$\gamma_{ia} \sim n^{1/2} v_{De}/v_{Te}.$$

In Figs. 15-17 the small power dependent changes observed in the off-resonant portions of the spectra probably result from these slight alterations in the equilibrium distribution.

In a second mechanism, oscillations can be excited in the plasma if the time-averaged pump power varies periodically with a frequency of the order of ion-acoustic frequencies. If the rf power is applied through a resonant microwave cavity, these dynamic relaxation oscillations are easily recognized as follows. Mendel and Stern[22] show that relaxation oscillations occur when the applied field increases the density and temperature of the plasma to the point where the applied field is totally reflected by the plasma. But if the density increases within a microwave cavity, the resonant frequency shifts and the rf power is reflected by the cavity long before the properties of the plasma itself are altered sufficiently to reflect the radiation. Thus, dynamic oscillations can only occur if the rf power is rejected periodically by the cavity itself. But the frequency of such oscillations must then depend upon the Q of the cavity because the cavity Q determines the admissable increase in plasma density before the rf power is reflected. When the cavity Q is altered in the present experiment, there is no change in the parametrically excited oscillations.

In Figs. 18 and 19 experimental and numerical values of the excited frequency at maximum intensity are displayed as a function of ω_{pe}/ω_o. The similarity between the curves indicates that the parametrically excited waves are indeed ion-acoustic waves. The fact that the observed frequency shift with ω_{pe}/ω_o is smaller than the calculated shift for the infinite plasma can be explained if the excited waves have a radial dependence and obey the dispersion relation (III-5). Since the radial wave vector k_R must remain fixed due to the radial boundary conditions of the positive column, the frequency matching condition

$$\omega_L(k_R,k_z) + \omega_H(k_R,k_z) = \omega_o \qquad \text{(III-6)}$$

must be satisfied solely by variation in k_z for a constant density. However, for a given change in ω_{pe}/ω_o with a resultant change in k_z, the radial ion-acoustic frequency

$$\omega \simeq \frac{\omega_{pi}}{k_{De}} (k_R^2 + k_z^2)^{1/2}$$

will shift less than the infinite plasma ion-acoustic frequency

$$\omega \simeq \frac{\omega_{pi}}{k_{De}} k_z .$$

The existence of a radial component of the parametrically excited oscillations may also account for the increased sensitivity of the coupling loop relative to the Langmuir probe as mentioned in Section III-A.

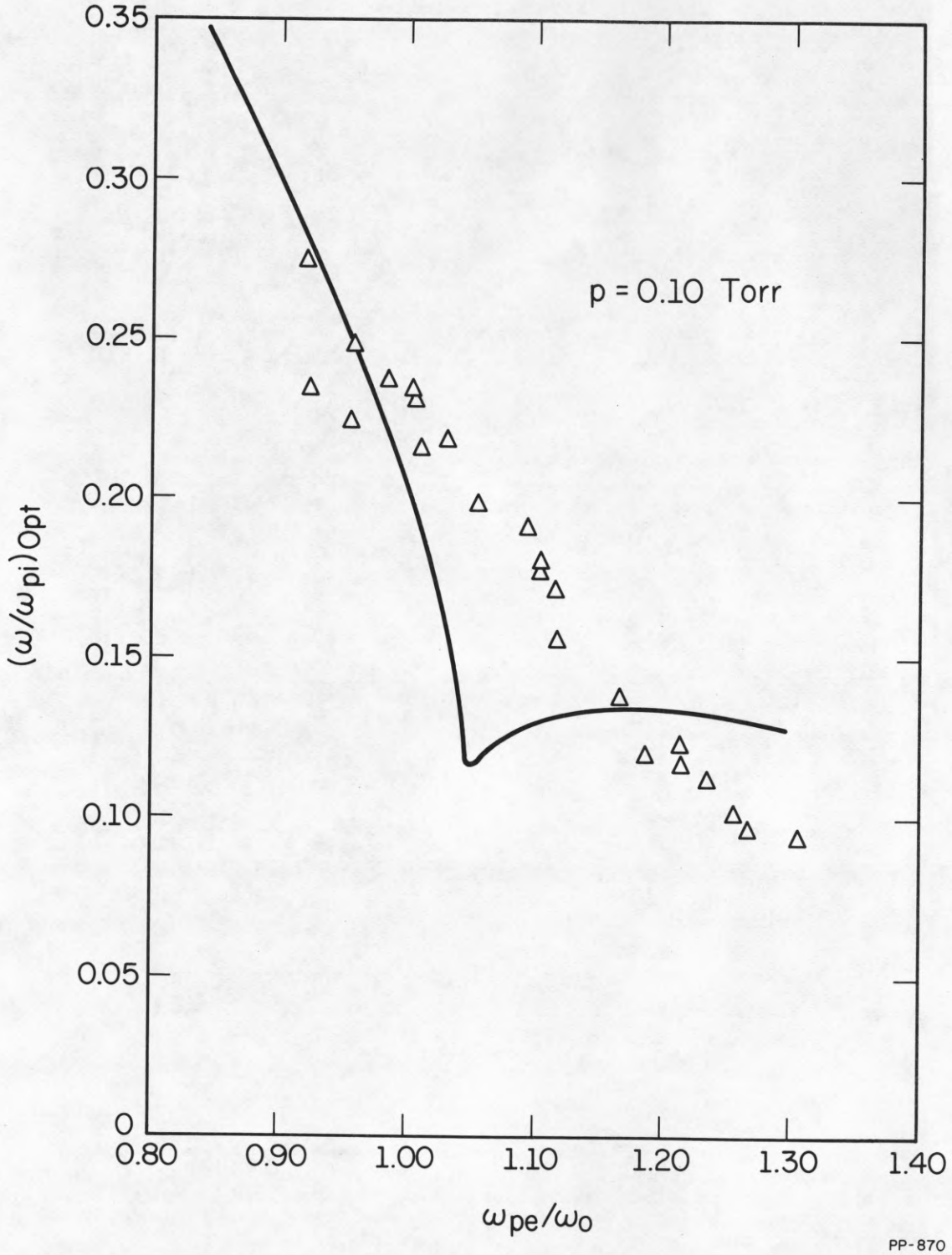

Fig. 18. Observed values [Δ] and calculated values [solid line] of $(\omega/\omega_{pi})_{Opt}$ versus ω_{pe}/ω_{o} for the data of Fig. 15.

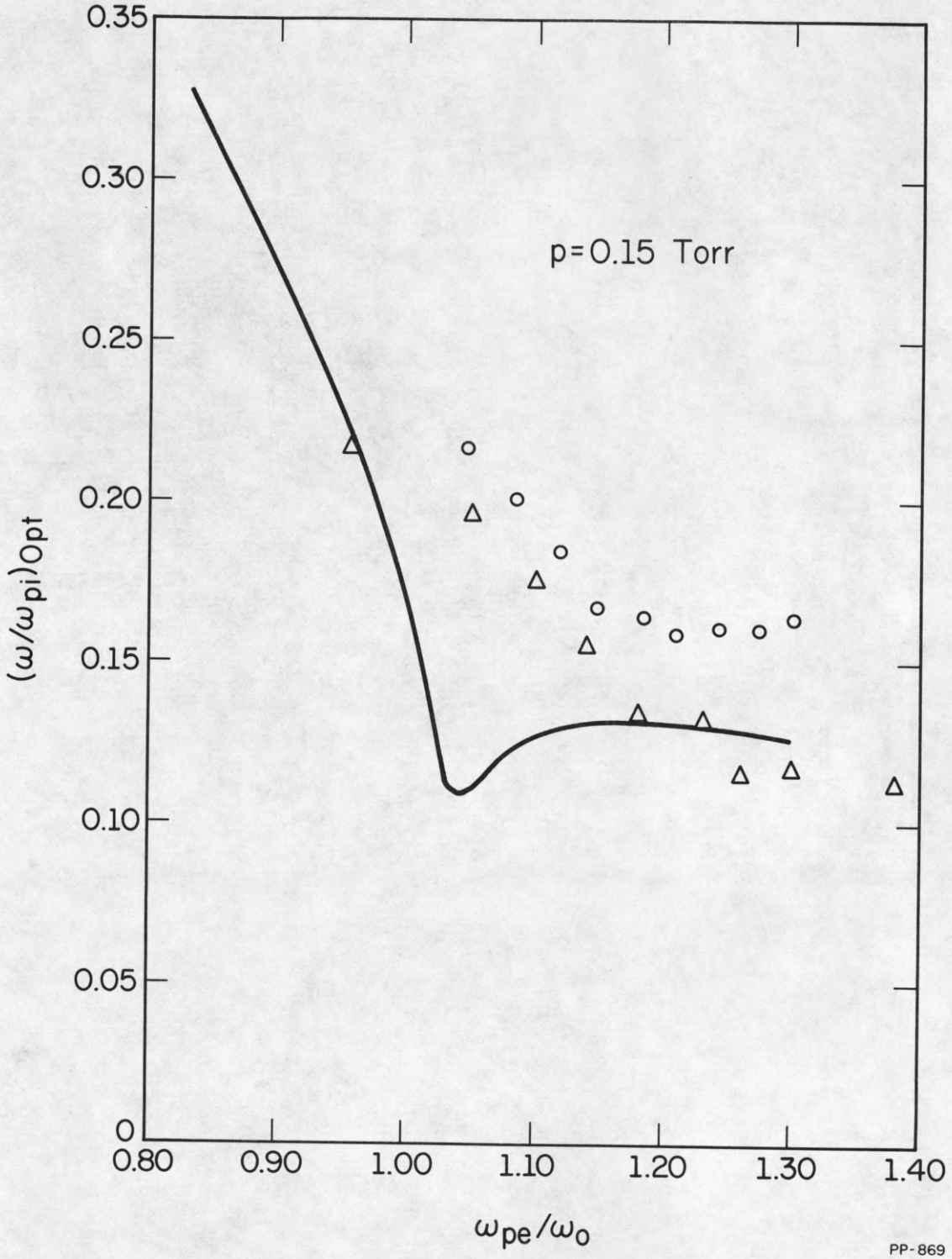

Fig. 19. Observed values and calculated values [solid line] of $(\omega/\omega_{pi})_{Opt}$ versus ω_{pe}/ω_{o}. Δ: data of Fig. 16. o: data of Fig. 17.

The fact that the dispersion relation is solved numerically for real $\underset{\sim}{k}$ rather than real ω does not account for the discrepancy between the observed and calculated frequencies, because the observations are made near onset of the instability ($\gamma = 0$). In this limit, the results for the spatial and temporal growth rates are equal.

Figs. 18 and 19 also show that the observed frequency of the resonance changes very little with pressure as expected from the numerical results shown in Fig. 9. The frequency differences between the observed probe data and loop data in Fig. 19 do not arise from an intrinsic difference between the response of the detectors. Instead, the plasma conditions, varying within the limits of our experimental error, evidently changed sufficiently between the two sets of data to favor the excitation of different order modes.

The logarithm of the maximum wave intensity relative to the background plasma noise is proportional to the relative spatial growth rate. However, the spatial growth rate β_L can be related to the effective temporal growth rate γ_L by the approximation

$$\gamma_L \simeq v_{group} \cdot \beta_L$$

where $v_{group} = \partial\omega_L/\partial k$ and $\gamma << \omega_L$. Using this approximation, the observed and calculated values of the effective relative temporal growth rates are shown in Figs. 20 and 21 for the spectra of Figs. 15-17. The growth rates are normalized to unity. At both pressures the growth rate attains a well-defined maximum at an optimum value of ω_{pe}/ω_o. The observed value of $(\omega_{pe}/\omega_o)_{opt}$ increases with decreasing pressure, in agreement with our numerical calculations. However, the observed value of $(\omega_{pe}/\omega_o)_{opt}$ is 15% higher than the predicted value for both pressures. This discrepancy is large compared to a maximum experimental error in ω_{pe}/ω_o of 5% to 10%.

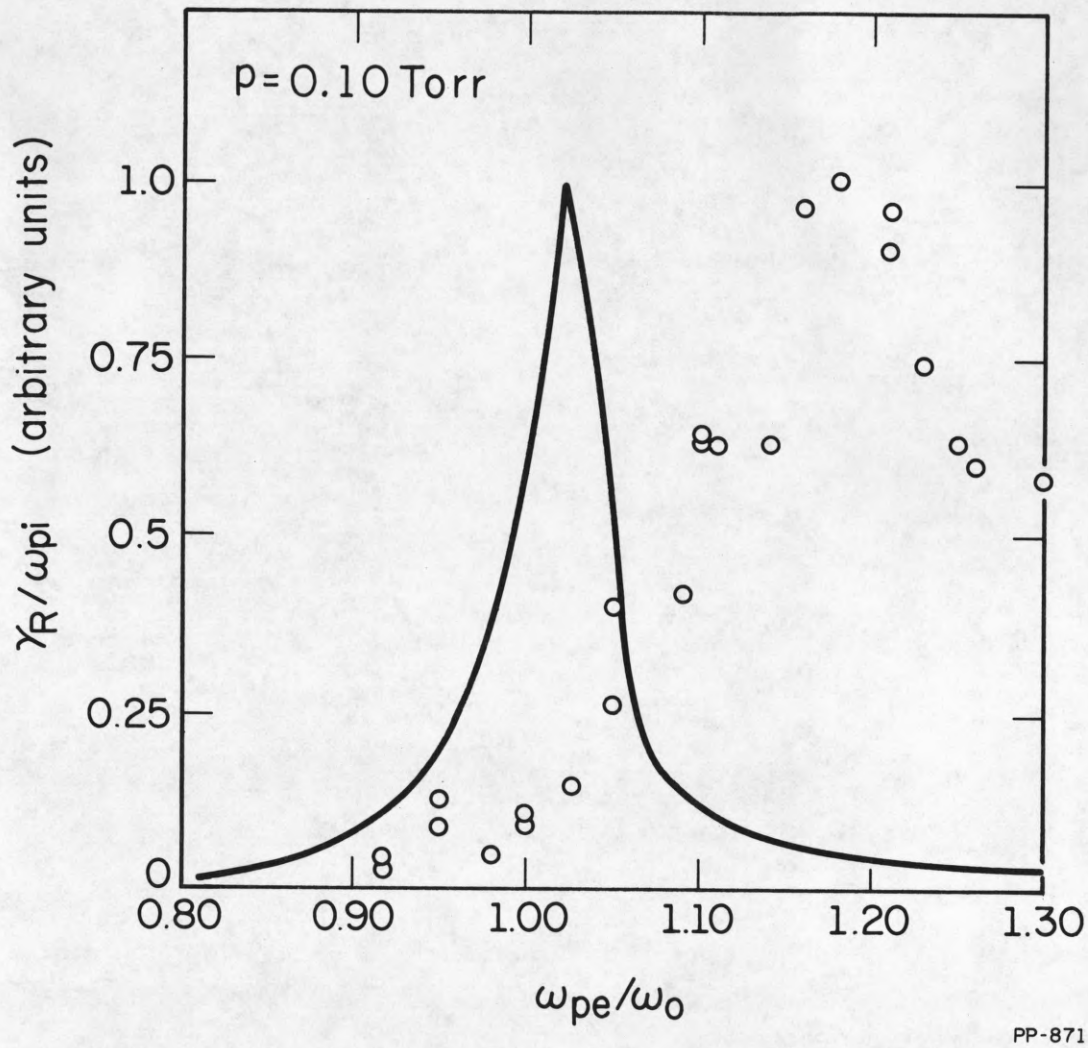

Fig. 20. Observed values [o] and calculated values [solid line] of the relative growth rate versus ω_{pe}/ω_o for the data of Fig. 15.

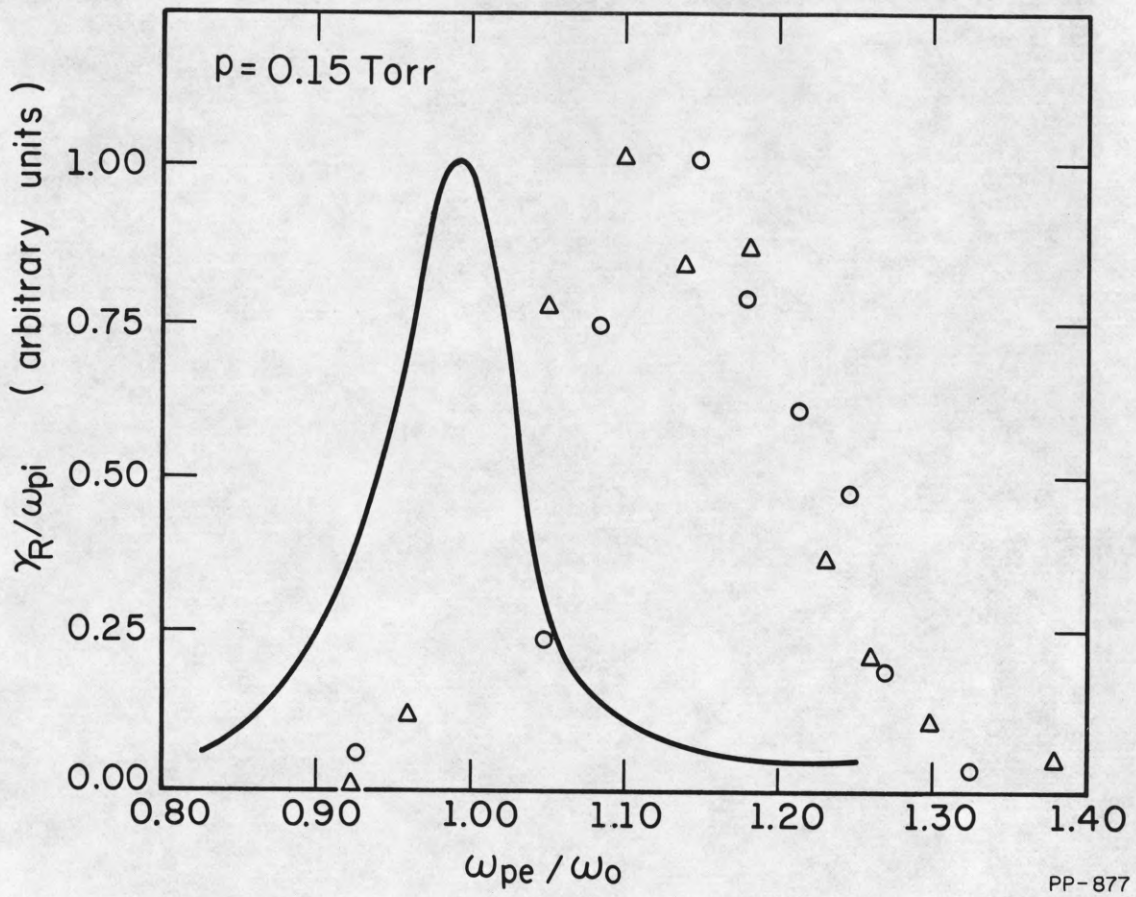

Fig. 21. Observed values and calculated values [solid line] of the relative growth rate versus ω_{pe}/ω_o.

Δ: data of Fig. 16.
o: data of Fig. 17.

The origin of this difference also appears to lie in the radial boundary conditions of the positive column. For $\omega_L << \omega_H$, the frequency matching condition (III-6) implies

$$\omega_H(k_R,k_z) \simeq \omega_o. \qquad \text{(III-7)}$$

But this relationship is not satisfied for the observed values of $\omega_{pe}/\omega_o > 1$ if ω_H corresponds to the electron plasma mode of an unbounded plasma

$$\omega_H \simeq \omega_{pe}\left(1 + \frac{3}{2}\frac{k^2}{k_{De}^2}\right)^{1/2} + \underset{\sim}{k}\cdot\underset{\sim}{v}_{De}$$

However, Nickel, Parker, and Gould[45] show that in the positive column a hierarchy of discreet high frequency radial modes, the Tonks-Dattner resonances, exist due to the combined effects of radial density gradients and thermal velocities. These resonances are the counterpart of electron plasma waves in an unbounded plasma. The lower order resonances have frequencies ω_{TD} sufficiently low that Eq. (III-7) may be satisfied even though $\omega_{pe}/\omega_o > 1$. According to O'Brien, Gould, and Parker[46], the purely radial Tonks-Dattner resonances act as low frequency cutoffs for hybrid radial waves which propagate parallel to the positive column axis with $k_z \neq 0$. Consequently, these hybrid Tonks-Dattner waves satisfy the frequency and wave vector conditions (III-6) for the observed plasma densities. In particular, at the optimum densities of Figs. 20 and 21, the frequency ratio ω_{TD}/ω_o for the second thermal Tonks-Dattner resonance is $\omega_{TD}/\omega_o \simeq .99$.

Thus, the applied pump field enters the plasma with a frequency near the second thermal Tonks-Dattner resonance and parametrically excites hybrid Tonks-Dattner waves with $k_z \neq 0$ in addition to the complementary radial ion-acoustic waves.

The spectra for various applied rf power levels are displayed in Fig. 22. In accord with the theoretical predictions for parametrically excited waves, the frequency of the resonance remains relatively constant during an increase in power by a factor of 10. Above field strengths of the order of 7-8 volts/cm, the frequency decreases sharply with additional power. This sudden frequency shift is probably due to changes in the equilibrium velocity distribution caused by the incident microwave power.

In Fig. 23 the logarithm of the relative intensity is seen to increase linearly with power for moderate field strength, indicating that the spatial growth rate varies linearly with applied power as calculated numerically. No appreciable threshold is observed because the plasma is unstable due to the electron drift velocity. The theoretical estimate of the intensity is obtained by approximating the spatial growth rate β_L

$$\beta_L = \gamma_L / v_{group}$$

and assuming $I = I_o e^{2\beta w}$ where w is the width (10 cm) of the resonant cavity.

The observed parametrically excited waves also show a maximum growth rate as a function of pressure when ω_{pe}/ω_o remains constant. This

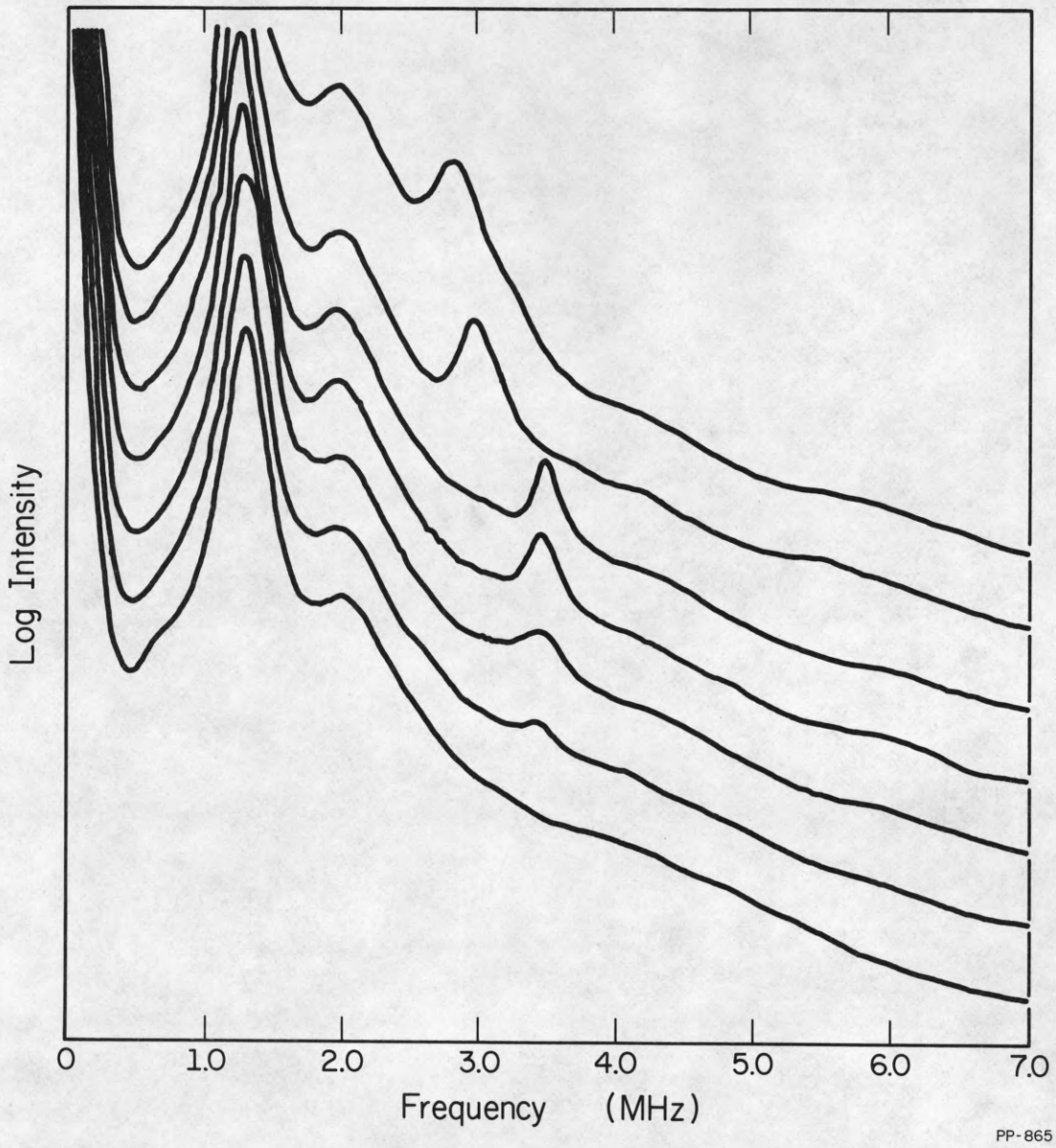

Fig. 22. Low frequency spectra observed with a floating probe in a helium positive column for several applied pump fields with p = .14 torr, ω_{pe}/ω_o = 1.05, and $\omega_o/2\pi$ = 1.5 GHz. Parametrically excited oscillations occur near 3.5 MHz. Approximate values of E_o^2 starting from the top of the figure are: 100, 85, 60, 30, 15, 5, 0 $(V/cm)^2$.

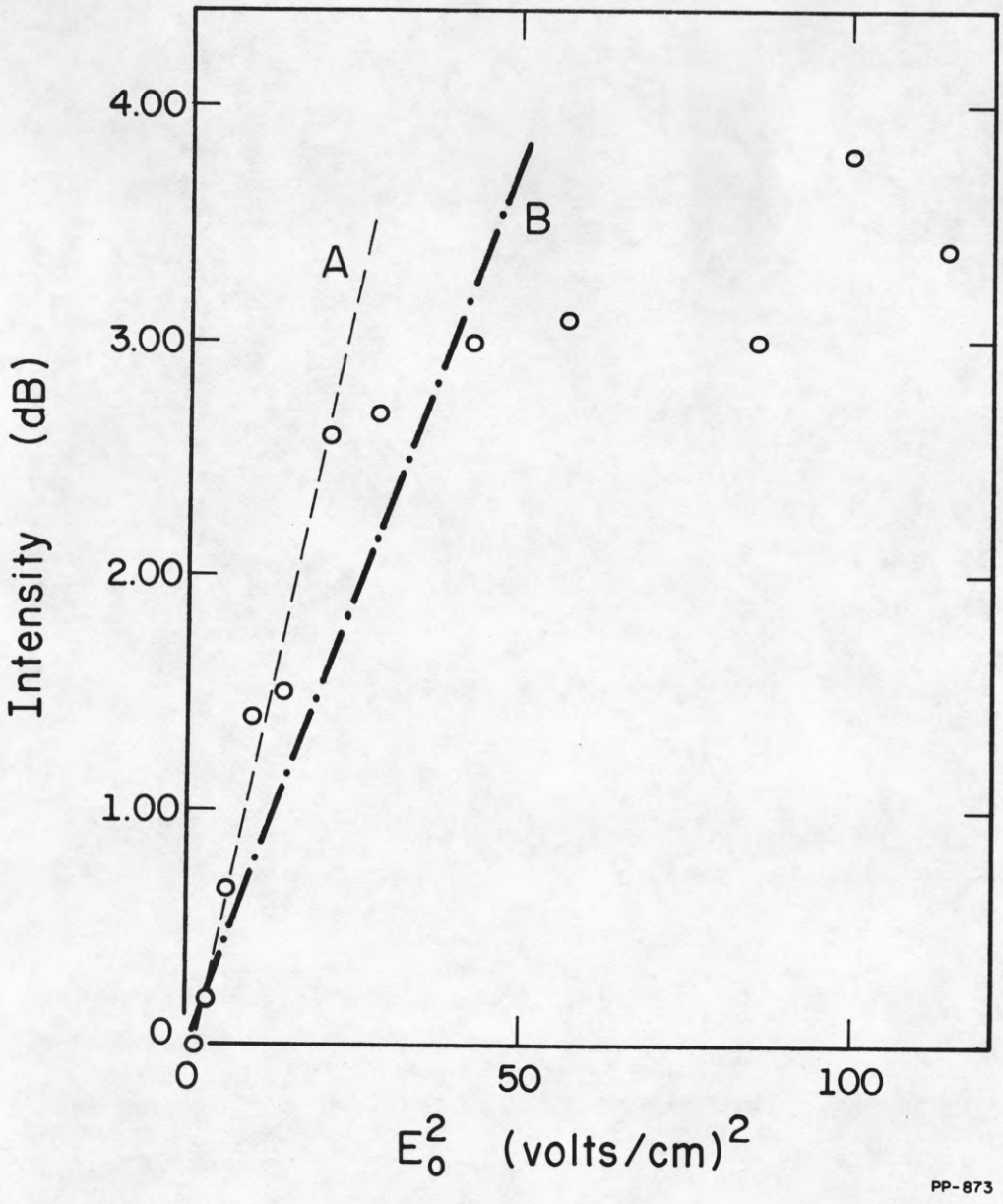

Fig. 23. Observed intensity of the parametrically excited resonance as a function of E_o^2 for the spectra of Fig. 22. The intensity of the resonant oscillations grows linearly with applied power for E_o < 5 V/cm [A] in good agreement with the numerical estimate [B].

dependence is shown in Fig. 24 for a constant value of $\omega_{pe}/\omega_o = 1.14$. The numerical calculations presented in Fig. 11 show that the optimum growth rate increases monotonically with decreasing pressure. However, for a constant value of ω_{pe}/ω_o, the growth rate climbs to a maximum and then declines as the pressure is varied because the effectiveness of the parametric coupling is altered by changes in the electron drift velocity and temperature.

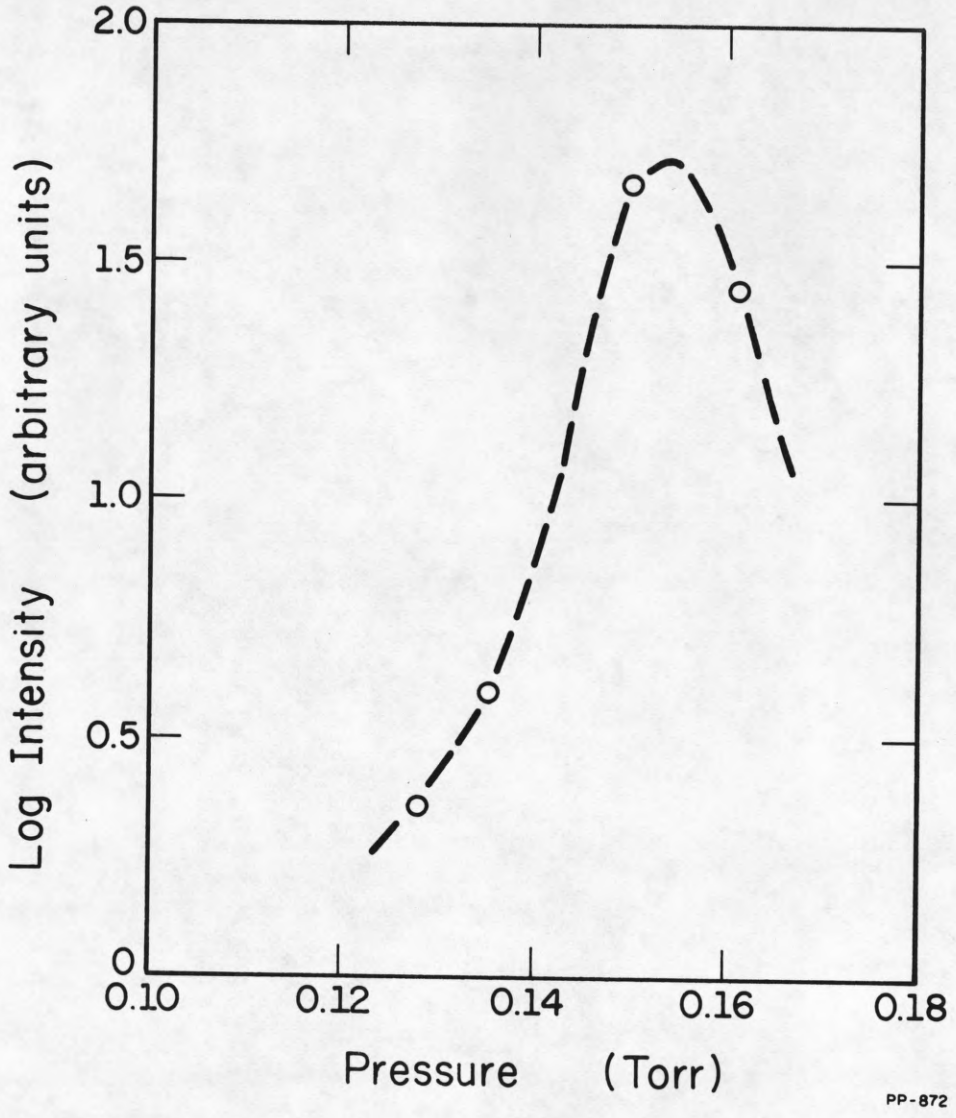

Fig. 24. Peak intensity of parametrically excited oscillations as a function of pressure. Oscillations were observed in a helium positive column with a floating probe for $\omega_{pe}/\omega_o = 1.14$, $E_o \simeq 4$ V/cm, and $\omega_o/2\pi \simeq 1.5$ GHz. Dashed curve represents approximate observed profile. o: experimental points.

IV. ION-ACOUSTIC WAVES IN THE HELIUM POSITIVE COLUMN

Since ion-acoustic waves are actively involved in the parametric excitation process, a brief study of drift-excited ion-acoustic waves in a positive column plasma was undertaken. The results are presented in this section.

A. Ion-Acoustic Theory for the Infinite Plasma

In the absence of an applied rf field, perturbations of the plasma density obey the linearized Vlasov Eq. (II-1) with $\underset{\sim}{E}_o = 0$. The resultant normal modes of oscillation of the plasma are obtained by equating the determinant of the coefficient matrix of Eq. (II-12) to zero for $\underset{\sim}{E}_o = 0$ to give

$$1 + \chi_e(\omega) + \chi_i(\omega) = 0. \tag{IV-1}$$

The effects of plasma-neutral collisions and steady-state drift velocities can be incorporated into the definition of $\chi_\sigma(\omega)$ as in Section II. Analytical expressions for the frequency and growth rate of the ion-acoustic mode are obtained if the susceptibility is expanded according to Eqs. (II-13) and (II-14) for the conditions

$$T_e >> T_i,\ \omega/kv_{Te} << 1,\ \omega/kv_{Ti} >> 1,\ \text{and}\ \gamma << \omega. \tag{IV-2}$$

The approximate expressions for frequency ω, temporal growth rate γ, and spatial growth rate β are:

$$\omega = \underset{\sim}{k}\cdot\underset{\sim}{v}_{Di} + \frac{\omega_{pi}\, k/k_{De}}{(1+k^2/k_{De}^2)^{1/2}}, \tag{IV-3}$$

$$\gamma = \mathrm{Im}\ \omega = -\frac{\nu_i}{2} + \left(\frac{\pi}{8}\right)^{1/2} \frac{\omega_{pi}}{(1+k^2/k_{De}^2)^{3/2}} \frac{k}{k_{De}} \left[\frac{v_{De}}{v_{Te}} - \frac{(m_e/m_i)^{1/2}}{(1+k^2/k_{De}^2)^{1/2}}\right], \tag{IV-4}$$

and

$$\beta = -\mathrm{Im}\ k = -\frac{\nu_i}{2\omega_{pi}} \frac{k_{De}}{(1-\omega^2/\omega_{pi}^2)^{3/2}} + \left(\frac{\pi}{8}\right)^{1/2} k_{De} \frac{\omega}{\omega_{pi}} \left[\frac{v_{De}/v_{Te}}{(1-\omega^2/\omega_{pi}^2)^{1/2}} - \left(\frac{m_e}{m_i}\right)^{1/2}\right]. \tag{IV-5}$$

Ion-acoustic oscillations become unstable when $\gamma = \beta = 0$ which leads to a critical drift velocity

$$\frac{v_c}{v_{Te}} = \left(\frac{2}{\pi}\right)^{1/2} \frac{\nu_i}{\omega_{pi}} \frac{(1+k^2/k_{De}^2)^{3/2}}{k/k_{De}} \tag{IV-6}$$

for $(m_e/m_i)^{1/2} \ll 1$. When $k^2/k_{De}^2 = 1/2$, the critical drift velocity attains a minimum value

$$\frac{v_c}{v_{Te}} = 2.07 \frac{\nu_i}{\omega_{pi}}. \tag{IV-7}$$

This critical condition for instability of ion-acoustic waves is easily attained in a low pressure positive column plasma.

B. Experimental Observations of Ion-Acoustic Waves in the Helium Positive Column

For the plasma conditions described in Section III, the ion-acoustic waves are unstable because the electron drift velocity exceeds the critical velocity (IV-7). However, the observed spectra consist primarily of discreet low frequency radial ion-acoustic and electron oscillations. At higher pressures the low frequency noise decreases appreciably and onset of the characteristic wide band ion-acoustic oscillations is observed. These waves are adequately described by kinetic theory for the infinite plasma because $k_R << k_z$.

A set of typical ion-acoustic spectra are shown in Fig. 25 including onset of the instability near 7MHz. The waves are detected with a floating probe for the experiment arrangement described in Section III. Between successive spectra, the discharge current is increased with a proportionate increase in density. The frequency of maximum spatial growth shifts to higher frequencies with increasing density in agreement with the frequency relation (IV-3). Simultaneously, the intensity of the oscillations grow in accord with (IV-5). The oscillations below 4MHz are presumably ion-acoustic or electron waves with larger radial wave vectors.

For comparison, numerical solutions of the ion-acoustic spatial growth rate were obtained for the plasma conditions of Fig. 25. The calculations include the effects of steady state drift velocities and plasma-neutral collisions in the manner of Bhatnagar, et al.[9]

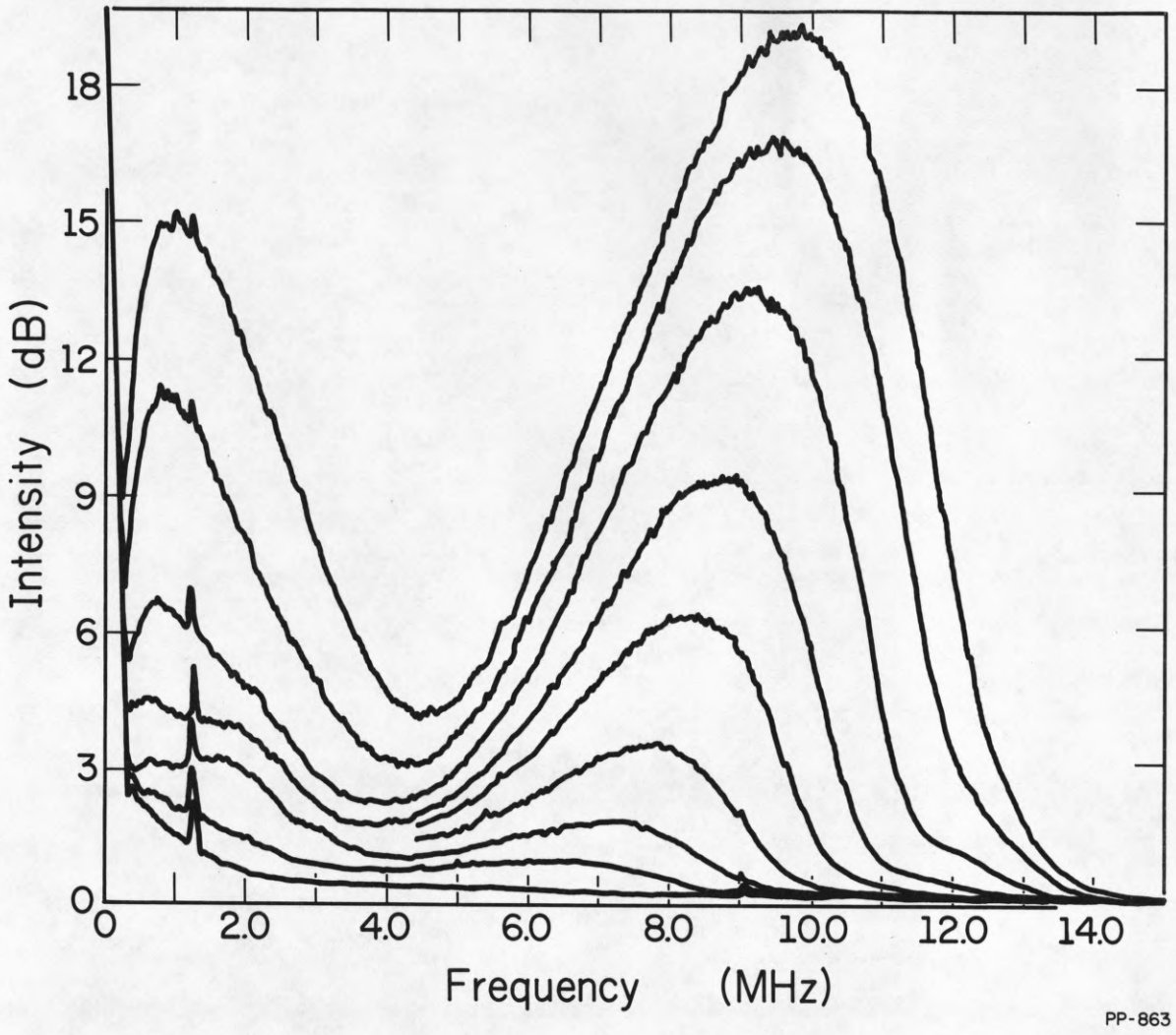

Fig. 25. Electron drift-excited ion-acoustic oscillations observed with a floating probe in a .96 cm diameter helium positive column in the absence of an applied electric field for p = .43 torr. Oscillations below 4 MHz are believed to be radial ion-acoustic waves. The peak plasma density in units of 10^{10} cm^{-3} for each spectrum starting from the top of the figure is: 9.7, 9.5, 8.9, 8.3, 7.8, 7.0, 6.3, 5.6, 4.2.

Experimental and numerical curves for the frequency ratio ω/ω_{pi} at onset are shown as a function of pressure in Fig. 26. The experimental data agree poorly with the numerical results for a He^+ plasma. The observed frequency ratio ω/ω_{pi} is low by a factor of 2 and the pressure dependence of the observed waves is opposite that of a He^+ plasma. A similar trend is evident in the data of Fujiwara, Raether, and Yamada[47] for a helium dc discharge.

As a result, calculations were performed to determine the influence of a more massive helium ion, He_2^+. The numerical results for a plasma mixture of He^+ and He_2^+ are seen to correlate much better with the observed data.

In past studies of the helium positive column, the concentration of He_2^+ was assumed to be negligible. However, in view of the data presented in Fig. 26, the existence of He_2^+ in the positive column of a helium plasma should be investigated. There are two likely processes for the formation of He_2^+ in the positive column. First, molecular helium metastables,[48,49] He_2^*, may be ionized to produce He_2^+ directly

$$He_2^* + e \rightarrow He_2^+ + 2e. \qquad \text{(IV-8)}$$

Molecular ions may also be produced in 3 body collisions; either by the reaction[50]

$$2He + He^+ \rightarrow He_2^+ + He \qquad \text{(IV-9)}$$

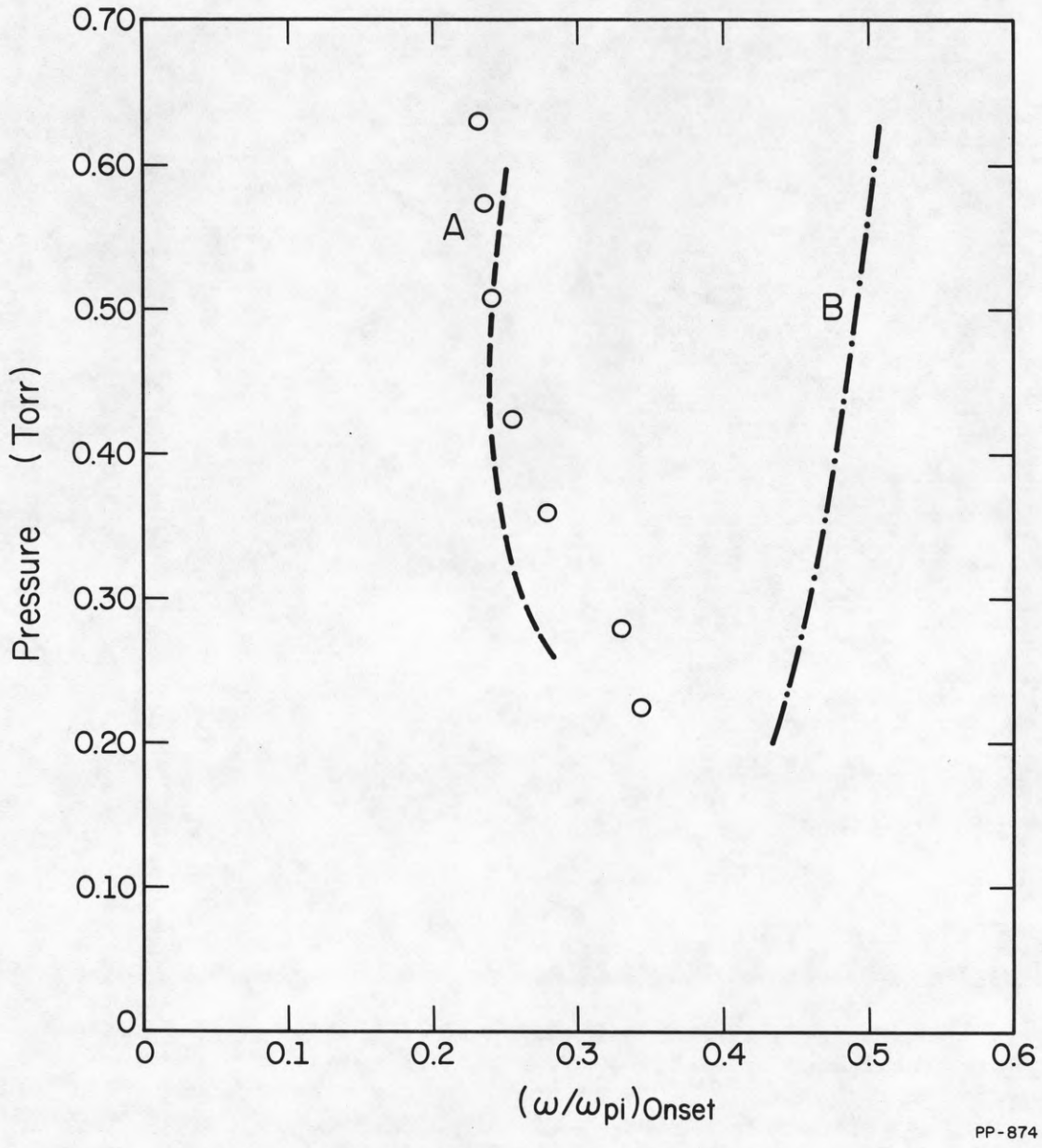

Fig. 26. Pressure dependence of $(\omega/\omega_{pi})_{Onset}$ for electron drift-excited ion-acoustic waves in a .96 cm diameter helium positive column.

o: experimental data.

A: numerical results for a two ion component plasma with $[He_2^+]/[He^+] = 24 \cdot p^2$ (p in torr).

B: numerical results for a pure He^+ plasma.

or by the process

$$He + He^+ + wall \rightarrow He_2^+ + wall. \qquad (IV-10)$$

However, no data is available concerning the effectiveness of the processes (IV-8) and (IV-10). Based on the measurements of Gerber, Sauter, and Oskam,[50] the production of He_2^+ in the reaction (IV-9) is negligible for pressures below several torr.

For the numerical results presented in Fig. 26, the ion concentration ratio, $\alpha = [He_2^+]/[He^+]$, ranges between 1 and 4. In analogy with 3-body formation processes, the concentration ratio is assumed to vary as (pressure),[2] i.e., $\alpha = \alpha_o p^2$, where the coefficient α_o is chosen to provide the best agreement with the observed data. For our choice of α_o, the ion concentrations are equal when p = .205 torr. At the low pressures used in the experimental study of the parametric excitation process, the concentration of He_2^+ should be insignificant.

The addition of He_2^+ decreases the frequency ratio ω/ω_{pi} at constant pressure for several reasons. First, the more massive He_2^+ ion depresses the ion-acoustic frequency by a factor of $1/\sqrt{2}$. Secondly, the mobility μ_2 of He_2^+ is 3 times as large as the mobility μ_1 of He^+. Therefore, ion-acoustic waves in He_2^+ are Doppler shifted a greater amount than similar waves in He^+.

Impurities also lower the ion-acoustic frequency due to their greater mass. However, impurities also tend to be more easily ionized, thus lowering the electron drift velocity in the positive column with a resultant decrease in the ion-acoustic growth rate. Furthermore, the percentage of impurities would have to increase with pressure in order to explain the frequency shift in Fig. 26. Experimentally, identical spectra have been obtained with different sources of helium gas indicating that impurity concentrations are negligible.

The observed variation of density with pressure at onset of the instability (Fig. 27) is approximated by the numerical solutions for a plasma mixture of He^+ and He_2^+. At high pressure the onset density is much lower than predicted for an atomic helium plasma. However, according to our model for the two ion component plasma, He_2^+ becomes the dominant ion species at high pressures. Unlike He^+, He_2^+ has a low charge exchange collision frequency, so the collisional damping rate is low, and instability occurs at lower densities.

As the plasma density is increased above onset, the intensity of the oscillations grows. The intensity of the observed spectrum correlates well with the spatial growth rate as a function of frequency for a $He^+ - He_2^+$ plasma under similar conditions (Fig. 28). The corresponding growth rate curve for an atomic helium plasma is similar in shape but occurs at larger values of ω/ω_{pi}. In Fig. 29 the change in ω/ω_{pi} for densities above onset is shown for experimental and calculated results. Agreement with a two ion component plasma is excellent.

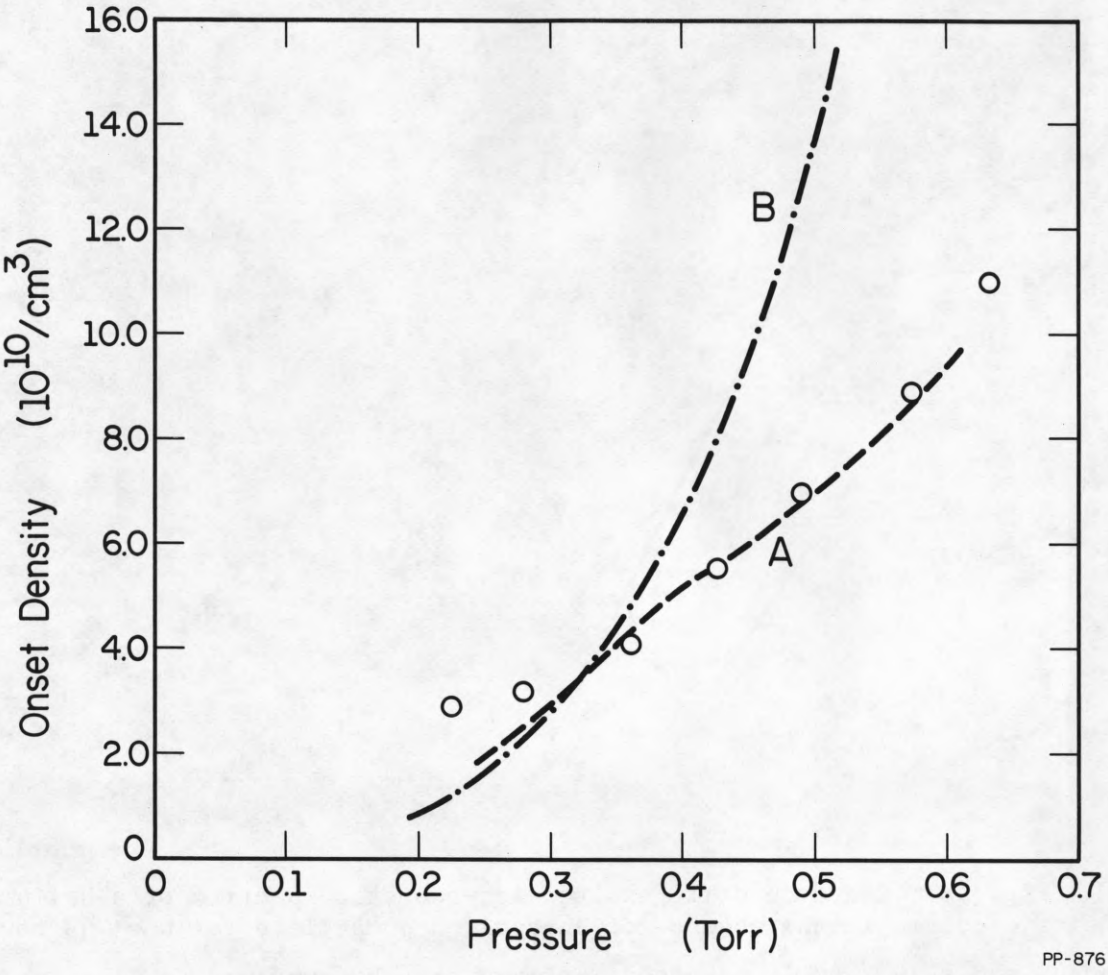

Fig. 27. Onset density as a function of pressure for electron drift-excited ion-acoustic waves in a .96 cm diameter helium positive column.

o: experimental data.

A: numerical results for a two ion component plasma with $[He_2^+]/[He^+] = 24 \cdot p^2$ (p in torr).

B: numerical results for a pure He^+ plasma.

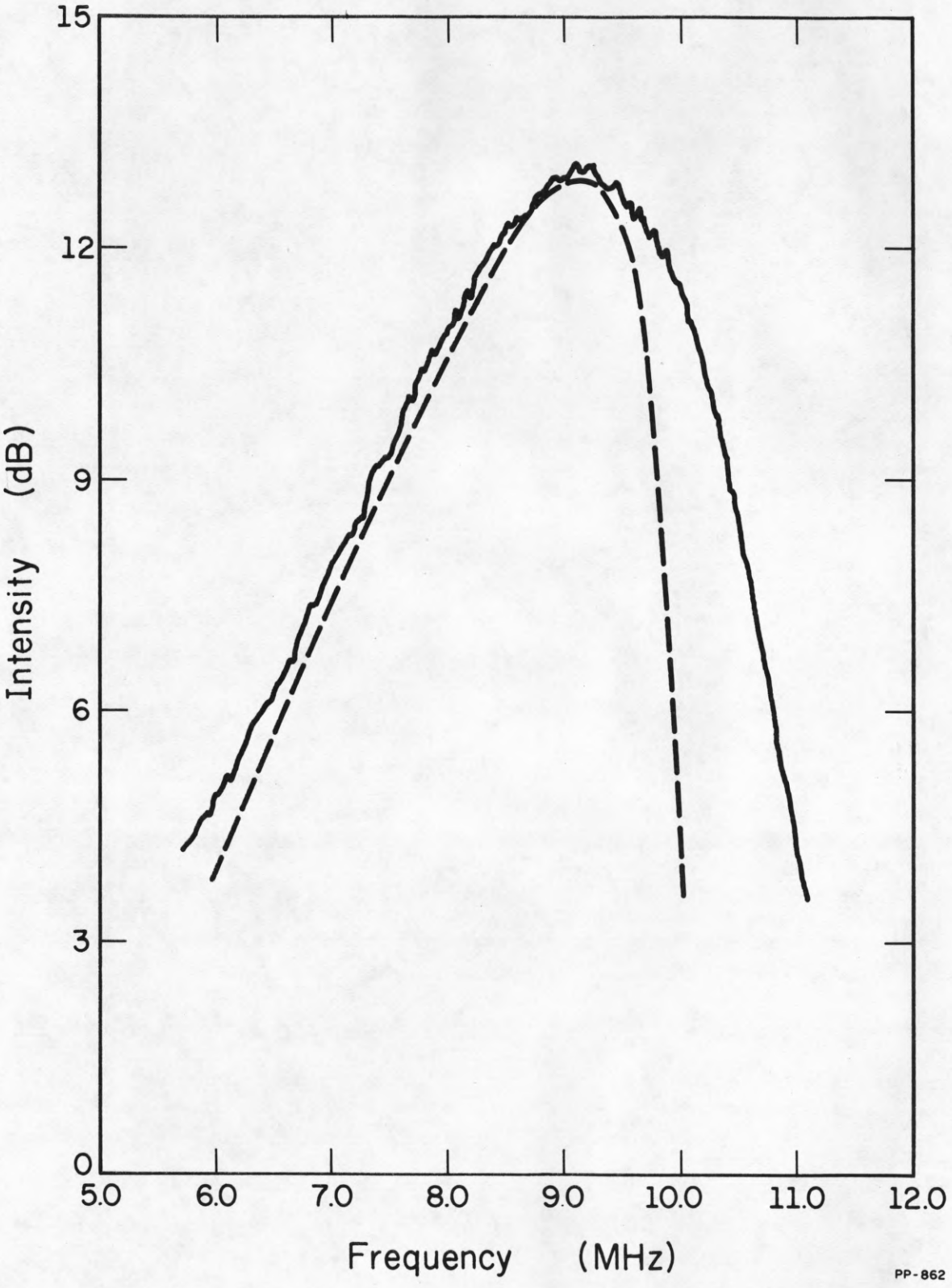
15
12
9
6
3
0
Intensity (dB)
5.0
6.0
7.0
8.0
9.0
10.0
11.0
12.0
Frequency (MHz)
PP-862

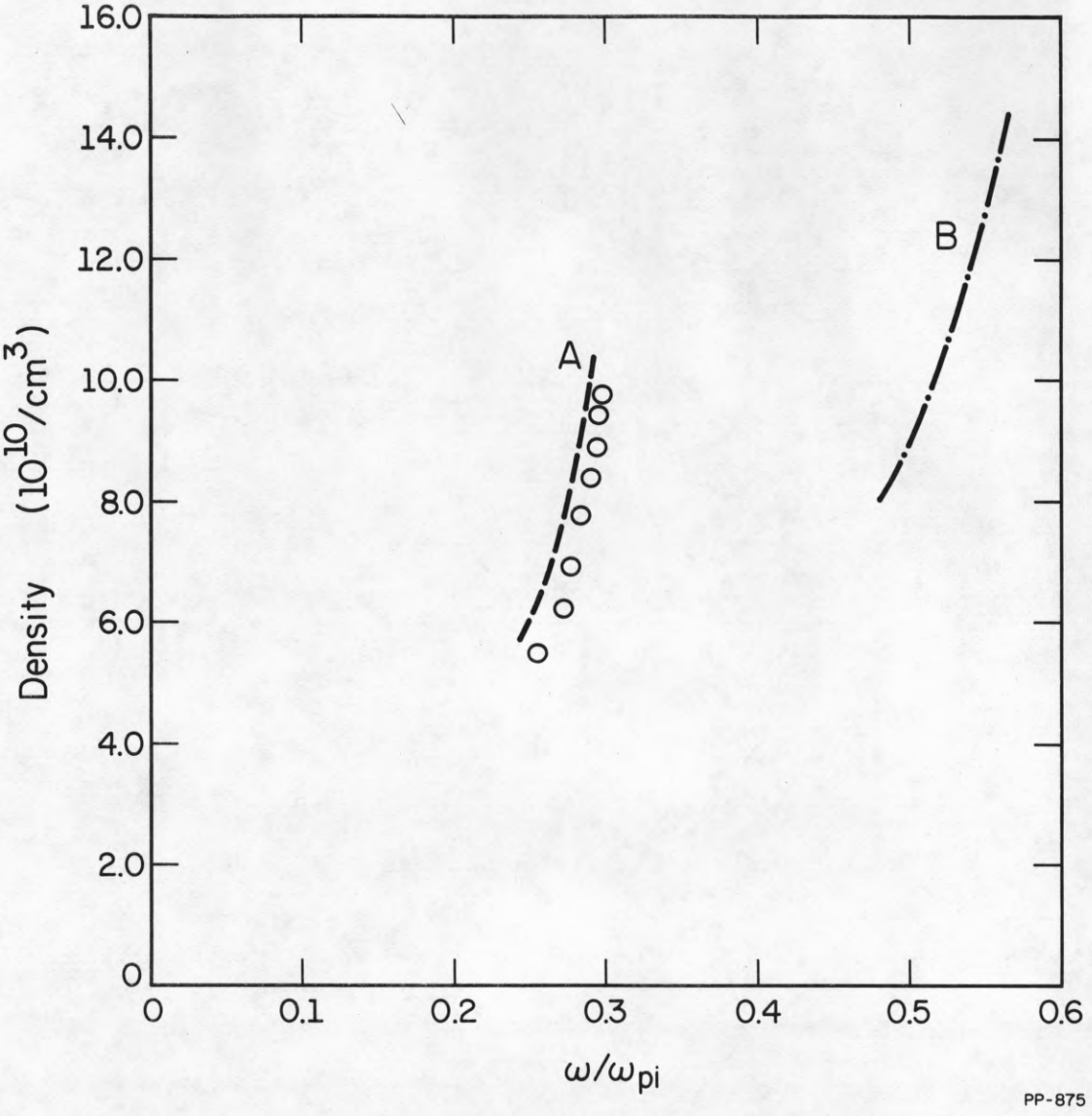

Fig. 29. Variation of ω/ω_{pi} with density for unstable electron drift-excited ion-acoustic waves in a helium positive column with p = .43 torr.

o: experimental data of Fig. 25.

A: numerical results for a two ion component plasma with $[He_2^+]/[He^+] = 4.4$.

B: numerical results for a pure He^+ plasma.

V. SUMMARY OF RESULTS

Numerical calculations of the growth rate for parametric coexcitation of electron plasma and ion-acoustic waves have been performed based on the kinetic treatment of Jackson[2] and Sanmartin[3]. The effect of steady state drift velocity and plasma-neutral collisions are included for plasma conditions simulating a low pressure helium dc discharge.

It is found that electron drift velocity tends to reduce the threshold field strength required for parametric excitation by decreasing the stability of ion-acoustic waves in the undisturbed plasma. If the ion-acoustic waves become intrinsically unstable due to the electron drift velocity, no minimum field strength is required for parametric excitation. The electron drift velocity also causes a further separation of the resonances occurring when $\omega_H \pm \omega_L \simeq \omega_o$, thus eliminating destructive interference between the resonances. The predominant effect of the ion drift velocity is the Doppler decrease in frequency of the low frequency mode as observed in the laboratory.

Collisional damping is seen to increase the requisite threshold field strength in two ways. First, collisions increase the damping rates of the high and low frequency modes in an undisturbed plasma, and secondly, the actual effectiveness of the parametric coupling between the excited modes appears to be reduced. Collisional broadening of the resonances also occurs.

Parametric excitation of ion-acoustic waves is also observed experimentally. The excited oscillations show the proper dependence of frequency with ω_{pe}/ω_o and the proper dependence of growth rate with ω_{pe}/ω_o,

power, and pressure. Differences between the observations and theoretical predictions are believed to arise from the modification of the infinite plasma modes due to the radial boundary restrictions of the positive column. In particular, the discreet nature of the modes allows the possibility of simultaneous parametric excitation of several modes.

The numerical and experimental results indicate that ion-acoustic waves in a weakly damped plasma are readily excited by an appropriate rf field, suggesting that the mechanism of parametric excitation is a feasible means of coupling energy into a plasma.

A brief separate study shows that ion-acoustic waves in a helium dc discharge can become unstable due to steady state electron drift velocities. Experimental results agree well with numerical calculations for a plasma consisting of two ion species, He^+ and He_2^+, when the mixture ratio of the species, $[He_2^+]/[He^+]$ is assumed proportional to $(\text{pressure})^2$.

APPENDIX

TERMINOLOGY AND DEFINITIONS

All mathematical expressions in the text and Appendix are in cgs units.

$A_{Dis} = \pi R^2$ — Cross-sectional area of discharge

$A^m_{\sigma \underset{\sim}{k}} = q_\sigma \int f^m_{\sigma \underset{\sim}{k}} d\underset{\sim}{u}_\sigma$

c — Speed of light

D — Microwave cavity diameter

$\underset{\sim}{E}$ — Self-consistent electric field in plasma

$\underset{\sim}{E}_o$, $\underset{\sim}{E}_o \cos\omega_o t$ — Externally applied electric field

E_{pc} — DC electric field in positive column

$F_\sigma(\underset{\sim}{r}, \underset{\sim}{v}, t)$ — Particle distribution function

$f_{o\sigma}$ — Equilibrium distribution function

f_σ — Perturbed distribution function

$f_{\sigma \underset{\sim}{k}} = \int f_\sigma \, e^{-i\underset{\sim}{k}\cdot\underset{\sim}{\rho}_\sigma} \, d\underset{\sim}{\rho}_\sigma$ — Spatial Fourier transform of f_σ

$f^m_{\sigma \underset{\sim}{k}} = \int_o^\infty dt \, f_{\sigma \underset{\sim}{k}} \exp(i(\omega + m\omega_o)t)$ — Laplace transform of $f_{\sigma \underset{\sim}{k}}$

I_{Dis} — Discharge current

Im — Imaginary part of

K — Boltzmann constant (3/2 KT is the thermal energy per particle)

$\underset{\sim}{k}$ — Wave vector of plasma wave

$\underset{\sim}{k}_o$	Wave vector of applied field $\underset{\sim}{E}_o$
$k_{D\sigma} = (4\pi n_\sigma q_\sigma^2/(KT_\sigma))^{1/2} = \omega_{p\sigma}/v_{T\sigma}$	Debye wave number
m_σ	Mass
n, n_σ, $n(\underset{\sim}{r})$, $n(\underset{\sim}{r},t)$	Number density of plasma particles
n_o	Maximum number density in profile $n(r) = n_o J_o(2x_{01}r/D)$
p	Pressure (torr)
$Q = \omega/\Delta\omega$	Measure of sharpness of microwave cavity response
q_σ	Magnitude and sign of charge
R	Plasma radius
$\underset{\sim}{r}$	Position vector
Re	Real part of
T_σ	Temperature (^oK)
TM_{010}, TM_{020}	Microwave cavity transverse magnetic field modes
$\underset{\sim}{u}_\sigma = \underset{\sim}{v} - (q_\sigma \underset{\sim}{E}_o/(m_\sigma\omega_o))\sin\omega_o t$	Velocity vector in reference frame oscillating with σth component
$\underset{\sim}{v}$	Velocity vector
$v_{T\sigma} = (KT_\sigma/m_\sigma)^{1/2}$	Thermal velocity
$v_{D\sigma}$	Drift velocity
$v_{ia} = (KT_e/m_i)^{1/2}$	Ion-acoustic phase velocity

$v_c = 2.07\ \nu_i v_{Te}/\omega_{pi}$ — Critical drift velocity for ion-acoustic instability

v_{ph} — Phase velocity = ω/k

W — Plasma dispersion function Eq. (II-14)

w — Height of microwave cavity

$x_{\ell m}$ — Argument at mth zero of ℓth Bessel function

$\alpha = \alpha_o p^2 = [He_2^+]/[He^+]$ — Ion concentration ratio

$\alpha_o = \alpha/p^2$

β — Ion-acoustic spatial growth rate Eq. (IV-5)

γ — Ion-acoustic temporal growth rate Eq. (IV-4)

γ_L — Temporal growth rate of low frequency mode

$$\gamma_{L\sigma}(\omega) = \left(\frac{\pi}{8}\right)^{1/2} \omega \left(\frac{\omega}{kv_{T\sigma}}\right)^3 \exp\left(-\frac{\omega^2}{2k^2 v_{T\sigma}^2}\right)$$ — Linear Landau damping rate

$\gamma_R = \gamma_L\big|_{\text{Field applied}} - \gamma_L\big|_{\text{Field off}}$ — Relative growth rate

$\epsilon_\sigma(\omega) = 1 + \chi_\sigma(\omega)$

$\underset{\sim}{\varepsilon}_\sigma = q_\sigma \underset{\sim}{E}_o/(m_\sigma \omega_o^2)$

$\underset{\sim}{\varepsilon}_{\sigma\tau} = \underset{\sim}{\varepsilon}_\sigma - \underset{\sim}{\varepsilon}_\tau = -\underset{\sim}{\varepsilon}_{\tau\sigma}$

$\mu_\sigma = q_\sigma/(m_\sigma \nu_\sigma)$ — Mobility

ν_σ — Effective plasma-neutral collision frequency for momentum transfer

$\underset{\sim}{\rho}_\sigma = \underset{\sim}{r} + \underset{\sim}{\varepsilon}_\sigma \cos\omega_o t$ — Position vector in reference frame oscillating with σth component

$\sum$ — Summation symbol

φ — Self-consistent potential

$\varphi_{\underset{\sim}{k}} = \int \varphi(\underset{\sim}{r}) e^{-i\underset{\sim}{k}\cdot\underset{\sim}{r}} \, d\underset{\sim}{r}$ — Spatial Fourier transform of φ

$\chi_\sigma(\omega) = \frac{k_{D\sigma}^2}{k^2} W\left(\frac{\omega}{kv_{T\sigma}}\right)$ — Linear dielectric susceptibility

ω — Angular frequency of plasma wave

ω_H, ω_L — Angular frequency of high and low frequency plasma modes

ω_o — Angular frequency of applied field $\underset{\sim}{E}_o$

$\omega_{p\sigma} = (4\pi n q_\sigma^2/m_\sigma)^{1/2}$ — Angular plasma frequency

$\omega_{k\sigma} = (\omega_{p\sigma}^2 + 3k^2 v_{T\sigma}^2)^{1/2}$

$\omega_{c\sigma} = q_\sigma B/(m_\sigma c)$ — Angular cyclotron frequency

ω_{TD} — Angular frequency of the Tonks-Dattner resonances

SUBSCRIPTS

c	Cyclotron
D	Debye, drift
Dis	Discharge
e	Electron
H	High mode
i	Ions
$\underset{\sim}{k}$	Wave vector
L	Low mode, Landau
N	Neutral
Onset	Value of parameter at onset of ion-acoustic instability
Opt	Value of parameter at maximum relative growth rate
o	Applied field, equilibrium, maximum
p	Plasma
R	Radial
z	z-direction, parallel to discharge axis
σ	Plasma species
τ	Plasma species

LIST OF REFERENCES

1. N. W. McLachlan, Theory and Application of Mathieu Function, (Clarendon, London, 1947), pp. 2-9.
2. E. A. Jackson, Phys. Rev. 153, 235 (1967).
3. J. R. Sanmartin, Phys. Fluids 13, 1533 (1970).
4. D. F. DuBois and M. V. Goldman, Phys. Rev. Letters 14, 544 (1965).
5. M. V. Goldman, Ann. Phys. (N. Y.), 38, 95 (1966).
6. D. F. DuBois and M. V. Goldman, Phys. Rev. 164, 207 (1967).
7. R. R. Ramazashvili, Sov. Phys. JETP. 26, 1225 (1968).
8. T. Amano and M. Okamoto, J. Phys. Soc. Jap. 26, 529 (1969).
9. P. L. Bhatnager, E. P. Gross, and M. Krook, Phys. Rev. 94, 511 (1954).
10. J. D. Jackson, J. Nucl. Energy, Part C: Plasma Physics 1, 171 (1960).
11. S. Ichimaru, Ann. Phys. 20, 78 (1962).
12. J. H. Krenz and G. S. Kino, J. App. Phys. 36, 2387 (1965).
13. V. P. Silin, Sov. Phys. JETP. 21, 1127 (1965).
14. Y. C. Lee and C. H. Su, Phys. Rev. 152, 129 (1966).
15. K. Nishikawa, J. Phys. Soc. Jap. 24, 916 (1968).
16. K. Nishikawa, J. Phys. Soc. Jap. 24, 1152 (1968).
17. A. Sjölund and L. Stenflo, J. App. Phys. 38, 2676 (1967).
18. J. Okutani, J. Phys. Soc. Jap. 23, 110 (1967).
19. A. Takeo, J. Phys. Soc. Jap. 22, 1282 (1967).
20. D. Montgomery and R. C. Harding, Phys. Letters 23, 670 (1966).
21. R. A. Stern and N. Tzoar, Phys. Rev. Letters 17, 903 (1966).
22. C. W. Mendel, Jr. and R. A. Stern, J. App. Phys. 41, 734 (1970).

23. A. M. Messiaen and P. E. Vandenplas, Phys. Letters 25A, 339 (1967).

24. M. M. Widner, H. E. S. Hsuan, and K. E. Lonngren, Phys. Letters 26A, 553 (1968).

25. K. Kato and K. Yamagiwa, J. Phys. Soc. Jap. 26, 1330 (1969).

26. A. Y. Wong, M. V. Goldman, F. Hai and R. Rowberg, Phys. Rev. Letters 21, 518 (1968).

27. E. J. Yadlowsky, R. H. Abrams, Jr., T. Ohe, and H. Lashinsky, Phys. Fluids 14, 1584 (1971).

28. H. Dreicer, D. Henderson, and J. Ingraham, Los Alamos Sci. Lab. LA-DC 12569, U. of Calif., Los Alamos, N. Mex.

29. K. Kato, M. Yoseli, S. Kiyama, and S. Watanabe, J. Phys. Soc. Jap. 20, 2097 (1965).

30. M. Yoseli, J. Phys. Soc. Jap. 23, 611 (1967).

31. N. W. McLachlan, op. cit., p. 20.

32. S. Hiroe and H. Ikegami, Phys. Rev. Letters 19, 1414 (1967).

33. A. Y. Wong and R. J. Taylor, Phys. Rev. Letters 27, 644 (1971).

34. D. C. Montgomery and D. A. Tidman, Plasma Kinetic Theory, (McGraw Hill, N. Y., 1964), pp. 27-28.

35. S. C. Brown, Basic Data of Plasma Physics, (J. Wiley and Sons, Inc., N. Y., 1959), p. 37.

36. N. A. Karelina, J. Phys. VI, 218 (1942).

37. J. A. Hornbeck, Phys. Rev. 84, 615 (1951).

38. J. P. Freidberg and B. M. Marder, Los Alamos Sci. Lab. LA-DC 12461, U. of Calif., Los Alamos, N. Mex.

39. M. A. Heald and C. B. Wharton, Plasma Diagnostics with Microwaves, (J. Wiley and Sons, Inc., N. Y., 1956), pp. 159-160.

40. R. H. Huddlestone and S. L. Leonard, Plasma Diagnostic Techniques, (Academic Press, N. Y., 1965), pp. 135-136.

41. F. W. Crawford, Phys. Rev. Letters 6, 663 (1961).

42. H. N. Ewald, F. W. Crawford, and S. A. Self, Phys. Fluids 12, 303 (1969).

43. S. A. Self, F. W. Crawford, and H. N. Ewald, Phys. Fluids 12, 316 (1969).

44. F. W. Crawford, Studies of Plasma Oscillations, SUIPR Report 411, Stanford University, Stanford, Calif. (1971)

45. J. C. Nickel, J. V. Parker, and R. W. Gould, Phys. Rev. Letters 11, 183 (1963).

46. B. O'Brien, R. W. Gould, and J. Parker, Phys. Rev. Letters 14, 630 (1965).

47. M. Fujiwara, M. Raether, and M. Yamada, J. Phys. Soc. Jap. 27, 758 (1969).

48. A. V. Phelps, Phys. Rev. 99, 1307 (1955).

49. E. E. Benton, E. E. Ferguson, F. A. Matsen, and W. W. Robertson, Phys. Rev. 128, 206 (1962).

50. R. A. Gerber, G. F. Sauter, and H. J. Oskam, Physica 32, 2173 (1966).

VITA

David William Stowe was the New Year's Baby of Three Rivers, Michigan, in 1944, the son of John H. and Marion R. Stowe. He received his elementary and secondary education in the public school system of Wauwatosa, Wisconsin, graduating from Wauwatosa West Senior High School in June 1962. The following fall he enrolled in the University of Wisconsin, Madison, majoring in physics. During the summer of 1965, he was a research assistant at the National Radio Astronomy Observatory in Green Bank, West Virginia. He married the former Diana Gay Kuckuck during the summer of 1966 following his graduation from the University of Wisconsin.

In the fall of 1966, graduate work in physics at the University of Illinois was begun. During the summer of 1967, he was employed at Lawrence Radiation Laboratory, Livermore, California, and in December, 1967, he became the proud father of Lisa Ruth Stowe. After receiving his Master's Degree in physics in January, 1968, he commenced study of ionospheric physics with Dr. Sidney A. Bowhill at the University of Illinois Aeronomy Laboratory. Intrigued by plasma physics, he undertook graduate research with Dr. Manfred Raether and Dr. Heinrich Böhmer in the Coordinated Science Laboratory at the University of Illinois, in September, 1968. In November of 1970, he became the father of a second daughter, Laura Renee Stowe.

Security Classification

DOCUMENT CONTROL DATA - R & D

(Security classification of title, body of abstract and indexing annotation must be entered when the overall report is classified)

1. ORIGINATING ACTIVITY *(Corporate author)*

Coordinated Science Laboratory
University of Illinois
Urbana, Illinois 61801

2a. REPORT SECURITY CLASSIFICATION

UNCLASSIFIED

2b. GROUP

3. REPORT TITLE

PARAMETRIC COEXCITATION OF ION-ACOUSTIC WAVES AND ELECTRON PLASMA WAVES BY A HIGH FREQUENCY ELECTRIC FIELD

4. DESCRIPTIVE NOTES *(Type of report and inclusive dates)*

5. AUTHOR(S) *(First name, middle initial, last name)*

David William Stowe

6. REPORT DATE

September, 1971

7a. TOTAL NO. OF PAGES

93

7b. NO. OF REFS

50

8a. CONTRACT OR GRANT NO.

DAAB-07-67-C-0199

b. PROJECT NO.

c.

d.

9a. ORIGINATOR'S REPORT NUMBER(S)

R-534

9b. OTHER REPORT NO(S) *(Any other numbers that may be assigned this report)*

UILU-ENG 71-2237

10. DISTRIBUTION STATEMENT

This document has been approved for public release and sale; its distribution is unlimited.

11. SUPPLEMENTARY NOTES

12. SPONSORING MILITARY ACTIVITY

Joint Services Electronics Program through U.S. Army Electronics Command, Fort Monmouth, New Jersey

13. ABSTRACT

The basic theory of parametric coexcitation of ion-acoustic and electron plasma waves by a high frequency electric field is reviewed. Numerical calculations show that plasma-neutral collisions and steady state drift velocities have a significant influence on the interaction. Parametric excitation of ion-acoustic waves is observed experimentally in a helium dc discharge. The observations indicate that the radial density profile of the dc discharge modifies the parametric effect. In the absence of an applied field, unstable electron drift-excited ion-acoustic waves are experimentally observed. These waves are found to satisfy the dispersion relation for a plasma consisting of He^+ and He_2^+.

DD FORM 1 NOV 65 1473

Security Classification

14 KEY WORDS	LINK A		LINK B		LINK C	
	ROLE	WT	ROLE	WT	ROLE	WT
Parametric Excitation						
Microwave Excitation						
Ion-Acoustic Waves						